DENSITY-FUNCTIONAL THEORIES FOR SOLVENT-FREE NANOPARTICLE–ORGANIC HYBRID MATERIALS

A Dissertation

Presented to the Faculty of the Graduate School

of Cornell University

in Partial Fulfillment of the Requirements for the Degree of

Doctor of Philosophy

by

Hsiu-Yu Yu

May 2012

DENSITY-FUNCTIONAL THEORIES FOR SOLVENT-FREE NANOPARTICLE–ORGANIC HYBRID MATERIALS

Hsiu-Yu Yu, Ph.D.

Cornell University 2012

Density-functional theories are developed to address the equilibrium structure, solvent behavior, disordered-fluid–fcc-solid transitions, and the transport properties of solventless nanoparticle–organic hybrid materials (NOHMs) consisting of nanoparticles with tethered oligomers with no solvents. The coarse-grained model of hard spheres and attached bead chains combined with the assumptions of incompressible oligomers, faster relaxation of oligomers than core particles, and large ratio of the oligomer radius of gyration to the core radius that is useful to make a weak oligomeric-field approximation allows quasi-analytic determination of the equilibrium distribution function of the cores and the concentration field of oligomers, which then determine the system free energy. The static structure factor for monodisperse NOHMs shows zero value at zero wave number, indicating that each core carries the same amount of the fluid. Including bidispersity in the system leads to non-zero structure factor at zero wave number with stronger effects resulted from bidispersity in the oligomer grafting density than bidispersity in the core size. When the oligomers are short compared with the interparticle spacing, the entropic frustrations due to limited oligomer configurations yield stronger oligomer-mediated particle–particle correlations characterizing the entropic attraction among the cores. Meanwhile, higher solvent capacity is predicted as the solute releases the entropic penalty of oligomers. This thermodynamic driving force for solute uptake yields good CO_2

selectivity over N_2 and CH_4 in NOHMs compared with unattached PEG melts or ionic liquids because the lower affinity of CO_2 for oligomers make the chains retract and reduce more of the free energy. Since many neighboring particles co-operate in filling the space, solventless NOHMs can remain disordered even if the core volume fraction is above the freezing transition point of hard-sphere suspensions. Transport properties such as the long-time self-diffusivity and linear viscoelastic behavior are determined by solving for the non-equilibrium probability density function for pairs of particles subjected to a weak applied flow and many-body intercore potential of mean force without hydrodynamic interactions. Again, the theory predicts hindered particle dynamics as the stiffer oligomers feel more entropic penalty to fill the space.

BIOGRAPHICAL SKETCH

Hsiu-Yu Yu was born to parents Chi-Fu Yu and Chin-Hsiu Chen in Hsinchu County, Taiwan on December 6th, 1981. After graduating from Taipei Municipal First Girls' Senior High School, she passed the Joint College Entrance Exam and was admitted to National Taiwan University in the field of Chemical Engineering. In her undergraduate studies, she won five times of Presidential Award and was first exposed to the field of colloidal science. After obtaining her degree of Bachelor of Science in Chemical Engineering with honors in 2004, she was admitted to the Master's degree program at National Taiwan University in the field of Chemical Engineering. In her Master research, she studied interactions between two charged colloidal particles in a salt-free medium and predicted the stability criteria of salt-free colloidal suspensions. She obtained her degree of Master of Science in Chemical Engineering with honors in 2006. In the same year Hsiu-Yu accepted an offer to enter the Ph.D. degree program at Cornell University in the field of Chemical Engineering. Her strong interest in colloidal science and theory urged her to join the Koch group since the spring of 2007.

To my parents, my brother, and Ming-Tsung

ACKNOWLEDGEMENTS

I would like to show my utmost gratitude to my thesis advisor, Professor Donald L. Koch. Without his guidance, I would not have gone this far. His knowledge and intuition inspired me and helped me understand the project in different ways. His patience allowed me to try N versions of derivation just to find the one that really makes things work (sometimes $N \approx 10$). He is such an approachable person that no matter how small the question is, I can always find an answer from him. I am grateful to have Professor Lynden A. Archer serve on my committee. His expertise in polymer physics and material science broadened my view of nanocomposites. I would not have learned how to communicate with experimentalists without those valuable discussions with him. It is a great honor for me to meet Professor Benjamin Widom at Cornell. He has shown me the beauty of statistical mechanics and I will never forget how inspired I was when I was in his class. This thesis would not have been possible without these three committee members.

It is my pleasure to have Professor Athanassios Z. Panagiotopoulos and Dr. Alexandros Chremos at Princeton University as close collaborators. The experience of writing a joint paper with them is priceless. I would like to show my sincere acknowledgement to them.

Furthermore, I am very lucky to have had some meaningful discussions with Professor Fernando A. Escobedo and Professor Claude Cohen. Their valuable feedback made this thesis better and I would also like to show my gratitude to them.

I would like to acknowledge some former and current members of the Koch group (including joint members), especially Dr. John Singh, Dr. Arijit Sarkar, Kaysap Thottasserymana Vasudevan, Rajesh Mallavajula, Dr. Vikram Singh,

and Pavithra Sundararajan, not only for stimulating discussions but also for their friendship. They made me love Indian foods.

I would like to thank Praveen Agarwal and Samanvaya Srivastava from the Archer group, Dr. Robert Rodriguez (formerly Giannelis Group), and Andrew Lin from the Park group at Columbia University for kindly helping me understand NOHMs experiments better. I would also like to thank Sushmit Goyal from the Escobedo group for enthusiastically sharing his thoughts of NOHMs simulations.

I am indebted to my best friend since junior high, Ya-Hui Yeh, and my best friend as a graduate student, Dr. Danielle Tan, for all the emotional support and joy they provided.

Finally, and most importantly, I wish to thank my parents, Chi-Fu Yu and Chin-Hsiu Chen, and my brother, Cheng-Hsuan Yu, for always being there from the beginning to the end. I wish to thank my husband, Ming-Tsung Lee, for his support and all the sacrifices he made for me.

This work is funded by the KAUST-Cornell Center for Energy and Sustainability (KAUST-CU).

TABLE OF CONTENTS

LIST OF TABLES

LIST OF FIGURES

CHAPTER 1

INTRODUCTION

Solvent-free nanoparticle–organic hybrid materials (NOHMs) are a new type of nanoparticle fluid composed of hard, inorganic nanocores with oligomeric chains covalently grafted to the surface of the core in the absence of any intervening solvent. The cores are self-suspended by the attached oligomers, which in turn mediate the interparticle forces and affect the equilibrium properties and dynamic behavior of the bulk system. Experimentally, it is shown that NOHMs show liquid-like behavior and provide a homogeneous nanoscale mixture of organic oligomers and inorganic cores [1–4], which reveals that these surface-functionalized nanostructures can relax to an equilibrium state. Noting that there are many ($O(500)$) oligomers per nanoparticle, the free energy associated with the oligomer configuration is much larger than the van der Waals attraction among the cores and prevents aggregation. If we define a dimensionless number, $X = (\chi_T n_\mathrm{b})^{-1}/k_\mathrm{B}T$, to be the ratio between the energy to compress the oligomers and the thermal energy associated with the translation of the cores, where χ_T is the isothermal compressibility of oligomers, n_b is the particle number density, k_B is the Boltzmann constant, and T is the temperature, then for a test suspension of 5 nm radius cores with tethered polyethylene chains with $\chi_T \approx 5 \times 10^{-10} Pa^{-1}$ calculated from a *Padé* equation of state [5] and a core volume fraction of 0.3, we obtain $X \approx 10^6$ at 301 K. This indicates that the intervening oligomeric fluid is incompressible. Therefore, the absence of a solvent, the small size of the nanocores and oligomers (with the radius of gyration also of O(5 nm)), and the incompressibility of the tethered oligomeric fluid make

Adapted in part with permission from (H.-Y. Yu and D. L. Koch, *Langmuir* **2010** *26*(22), 16801–16811). Copyright (2010) American Chemical Society.

the oligomer-mediated interactions non-pairwise-additive since oligomers from many neighboring cores compete to uniformly fill the interstitial space.

The goal of this study is to develop a theoretical description of the equilibrium properties (structure, solvent capacity, and disorder–order phase transition) and the transport properties of solventless, pure NOHMs. The non-pairwise-additive interparticle forces in such a homogeneous nanoscale suspension need a new type of theoretical treatment. Therefore, previous self-consistent field theories (SCFT) [6–9] and scaling analyses [10–12] for particles with tethered molecules are not feasible for solvent-free NOHMs since these theories have emphasized attached polymers whose molecular weight was large under conditions where the particle interactions are pairwise additive. The condition of incompressibility for the space-filling oligomers adds other difficulties to the application of these approaches. Another type of theoretical study for nanoparticles with tethered chains is the polymer reference interaction site model (PRISM) [13, 14], in which one solves a multi-component Ornstein–Zernike-like equation [15] for different site–site interactions with a chosen closure. However, so far the studies have been focused on a situation where the tethered oligomers are in a phantom solvent that merely fills the rest of the fluid space and have not addressed the space-filling effects due to the tethered chains. While molecular dynamics (MD) simulations provide a powerful tool for investigating nanoparticles with tethered branches at various solvent conditions [16–18], the present study will seek a more analytical treatment that can directly incorporate the space-filling requirement in pure NOHMs.

In this thesis, a classical density-functional approach is formulated for model hard spheres with tethered bead-spring oligomers. The simple model allows

one to have a direct description of the system free energy as a functional of the probability densities of cores and oligomers. Since the number of oligomers per particle is large, a continuum description of the oligomer concentration can be adopted such that the concentration field is at an equilibrium based on the minimization of the free energy subject to a constraint of uniform concentration of monomers in the interstitial space. While the compression of oligomer brushes when two particles approach one another yield steric repulsion as is typically found in hairy particles, this constraint of incompressibility leads to unusual "entropic attraction" forces that prevent the formation of large regions of free volume between the core particles and result in deviations of the equilibrium structure and transport properties from those of hard sphere suspensions.

To visualize the oligomer-mediated interparticle potential, in Chapter 2, the problem is first simplified to a conventional, pair level, in which two models of parallel hard walls with tethered bead-spring oligomers are presented. The oligomer free energy is calculated as a function of interwall separation. In Chapter 3, two models of the solvent-free, monodisperse NOHMs suspension are proposed: one in which the cores are points and a second in which the finite hard-sphere radius of the core is taken into account. The radial distribution function and the static structure factor of the particles are solved semi-analytically based on a regular perturbation analysis valid for large ratio of the oligomer radius gyration (R_g) to the core radius (a). The qualitative predictions of the theory are confirmed by the MD simulations in Ref. [18], a paper I coauthored with Dr. Alexandros Chremos, a postdoc of Professor Athanassios Z. Panagiotopoulos, which is not included in this thesis. In Ref. [18] a Lennard-Jones potential among the monomers is considered and the incompressibility condition is achieved when $k_B T/\varepsilon_{LJ} = 1$ with ε_{LJ} being the attraction well depth.

Although the theory is formulated for $R_g/a \gg 1$, the qualitative agreement between the theory and simulations in the radial distribution function, static structure factor, and root-mean-square chain stretching at R_g/a as small as 0.54 provides one with confidence in the applicability of the theory. The zero structure factor at zero wave number predicted for a monodisperse NOHMs may deviate in real polydisperse systems. In Chapter 4, the theory presented in Chapter 3 is generalized to consider a solvent-free, bidisperse NOHMs mixture to address possible polydispersity effects in experiments. The deviations in the static structure factor from a monodisperse system due to different bidispersities are predicted.

In the absence of an unattached fluid, the oligomers are frustrated as their conformational space is limited. This "entropic frustration" may lead to a thermodynamic driving force for solute uptake if the solute can reduce the system free energy. In Chapter 5, the monodisperse pure NOHMs system is considered as a solvent capturing a target gas solute. A theory for a mixture of NOHMs and added solute is formulated with the affinity of the solute for the oligomers being modeled using a Flory–Huggins parameter. The equilibrium configurations of the cores, oligomers, and solute molecules are again obtained semi-analytically. The solvent capacity of NOHMs is governed not only by the enthalpic interactions between the oligomers and a solute, but also by the changes in the configurational entropy of the oligomers upon uptake of the solute. The application of CO_2 capture using NOHMs is addressed. In Chapter 6, the transition from disordered fluid to face-centered-cubic solid of solvent-free NOHMs is predicted based on the liquid state theory in Chapter 3 and the proposed solid state theory. The phase boundary is determined by comparing the free energies of the two phases. Finally, in Chapter 7, the non-equilibrium pair probability is formu-

lated. Theoretical predictions for pure NOHMs transport properties including the long-time diffusivity of the cores, the low shear rate viscosity, and the linear elastic properties are developed by analyzing the interactions of pairs of cores subjected to a weak applied force and a potential of mean force derived from the radial distribution function shown in Chapter 3.

BIBLIOGRAPHY

[1] A. B. Bourlinos, R. Herrera, N. Chalkias, D. D. Jiang, Q. Zhang, L. A. Archer, and E. P. Giannelis, Adv. Mater. **17**, 234 (2005).

[2] R. Rodriguez, R. Herrera, L. A. Archer, and E. P. Giannelis, Adv. Mater. **20**, 4353 (2008).

[3] P. Agarwal, H. Qi, and L. A. Archer, Nano Lett. **10**, 111 (2010).

[4] J. L. Nugent, S. S. Moganty, and L. A. Archer, Adv. Mater. **22**, 3677 (2010).

[5] I. C. Sanchez and J. Cho, Polymer **36**, 2929 (1995).

[6] C. M. Wijmans and E. B. Zhulina, Macromolecules **26**, 7214 (1993).

[7] E. K. Lin and A. P. Gast, Macromolecules **29**, 390 (1996).

[8] C. Singh, G. T. Pickett, E. B. Zhulina, and A. C. Balazs, J. Phys. Chem. B **101**, 10614 (1997).

[9] M. Surve, V. Pryamitsyn, and V. Ganesan, Langmuir **22**, 969 (2006).

[10] T. A. Witten and P. A. Pincus, Macromolecules **19**, 2509 (1986).

[11] P. A. Pincus, Macromolecules **24**, 2912 (1991).

[12] M. Badia, M. Benhamou, A. Derouiche, and J. L. Bretonnet, Colloid Polym. Sci. **279**, 763 (2001).

[13] A. Jayaraman and K. S. Schweizer, J. Chem. Phys. **128**, 164904 (2008).

[14] A. Jayaraman and K. S. Schweizer, Langmuir **24**, 11119 (2008).

[15] J.-P. Hansen and I. R. McDonald, *Theory of Simple Liquids*, Academic Press, London, 3 edition, 2006.

[16] M. R. Wilson, A. B. Thomas, M. Dennison, and A. J. Masters, Soft Matter **5**, 363 (2009).

[17] B. Bozorgui, M. Sen, W. L. Miller, J. C. Pàmies, and A. Cacciuto, J. Chem. Phys. **132**, 014901 (2010).

[18] A. Chremos, A. Z. Panagiotopoulos, H.-Y. Yu, and D. L. Koch, J. Chem. Phys. **135**, 114901 (2011).

CHAPTER 2

OLIGOMER-MEDIATED INTERPARTICLE POTENTIAL

The thermodynamics and the transport properties of solvent-free NOHMs are governed by the requirement that the tethered incompressible oligomeric fluid must fill the interstitial space. In solventless condition, the tethered oligomers conform to the local interparticle spacing and their conformational space is limited. As the interparticle spacing changes, variation of the oligomer configuration results in changes in the oligomer free energy, which in turn influences the distribution of the cores and the macroscopic properties of the material. While the space-filling constraint leads to many-body interactions as mentioned in Introduction, to visualize the oligomer-mediated interparticle potential in a straightforward way and help future development of Brownian Dynamics (BD) simulations, we first simplify the problem down to a conventional, pair level.

In section 2.1, a model of surface-tethered bead-spring oligomers between two semi-infinite parallel plates is presented. In section 2.2, we modify the flat-wall model to the one with two semi-infinite sinusoidal walls to capture the effect of non-uniform interparticle spacing. In both models, we formulate the oligomer free energy as a functional of the probability density of the oligomer at $\mathbf{r}$ in space between the walls given that the tethered point is $\mathbf{r}_t$ on the wall. At equilibrium, for a given wall-to-wall separation, the probability density minimizes the free energy subject to the constraints of normalization and incompressibility of oligomers. The interwall potential corresponds to the free energy determined from the equilibrium probability density and provides us with some insight into the bulk properties of pure NOHMs.

2.1 Interactions between Parallel Plane Walls

We consider a tethered oligomeric fluid confined between two semi-infinite parallel plane walls separated with a distance H. As depicted in Fig. 2.1(a), the oligomers with radius of gyration R_g are modeled as bead-springs grafted to the surfaces. Each oligomer has one monomer bead and the springs are linear, massless, and have a rest length of zero. For unattached, ideal chains, the spring constant ξ is related to R_g via $\xi = k_B T/2R_g^2$ with k_B being the Boltzmann constant, T being the temperature, and the mean-square end-to-end distance of oligomers is $6R_g^2$ [1]. The oligomers are assumed to be uniformly grafted to the surface with the number of oligomers per unit area being n_a. Since the system is axisymmetric about the z axis and infinite in the x-y plane, we define the probability density of finding a monomer at (ρ, z) given that the spring is tethered to the origin as $P(\rho, z)$ with $\rho = \sqrt{x^2 + y^2}$. The probability density is normalized,

$$2\pi \int_0^\infty \int_0^H P(\rho, z) \mathrm{d}z \rho \mathrm{d}\rho = 1, \tag{2.1}$$

and the monomer number density is a constant across the gap,

$$n(z) = 2\pi n_a \int_0^\infty \int_0^H P(\rho, \bar{z}) \left[\delta(\bar{z} - z) + \delta(\bar{z} - H + z)\right] \mathrm{d}\bar{z} \rho \mathrm{d}\rho = n_0 \tag{2.2}$$

with n_0 being the monomer number density and $\delta(\bar{z})$ being the Dirac delta function. $n_0 = 2n_a/H$ because oligomers from both surfaces contribute to the number density at (ρ, z).

To obtain the interwall potential we need to calculate the change in oligomer free energy as a function of H. If we neglect the constant thermal de Broglie wavelength, the free energy of one oligomer is

$$\frac{F}{k_B T} = 2\pi \int_0^\infty \int_0^H P(\rho, z) \left[\ln 2\pi P(\rho, z) R_g^3 - 1\right] + \frac{1}{4R_g^2}(\rho^2 + z^2) P(\rho, z) \mathrm{d}z \rho \mathrm{d}\rho. \tag{2.3}$$

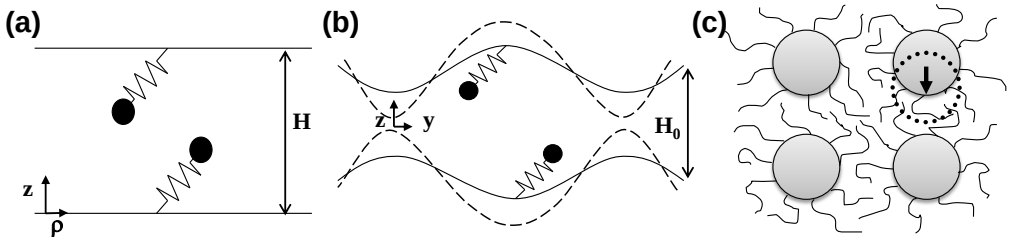

Figure 2.1: (a) Schematic of bead-spring oligomers tethered to two semi-infinite parallel plates separated by a distance H. (b) Schematic of bead-spring oligomers tethered two semi-infinite sinusoidal walls with a mean separation of H_0. The gap thickness is a function of y written as $H(y) = H_0[1 + \varepsilon \sin(ky)]$. The dashed curves represent the deformed gap thickness that mimics the effect of particle displacement. In our model, the oligomers are densely and uniformly grafted to the two surfaces but for simplicity we only plot one oligomer from each surface. (c) A particle array showing that the oligomers fill the interparticle space. The arrow and the dotted circle show that as one particle moves in a given direction it deforms the nearby fluid volume.

Making use of Lagrange undetermined multipliers [2] allows us to find the minimum of a function subject to constraints. Therefore at equilibrium F is determined by the minimization of the following Lagrange function,

$$L_0[P(\rho,z)] = \frac{F}{k_B T} - \lambda\left\{2\pi\int_0^\infty\int_0^H P(\rho,z)\mathrm{d}z\rho\mathrm{d}\rho - 1\right\} - \frac{1}{n_a}\int_0^H \beta(z)\left\{n(z) - n_0\left[U(z) - U(z-H)\right]\right\}\mathrm{d}z, \tag{2.4}$$

where the constant multiplier λ enforces the normalization, the functional multiplier $\beta(z)$ accounts for the constraint that $n(z)$ must be a constant for all z, and $U(z)$ is the unit step function used to constrain the monomers to be within the gap. The minimization $\delta L_0/\delta P(\rho,z)$ yields

$$P(\rho,z) = \frac{1}{2\pi R_g^3}\exp\left\{\beta(z) + \beta(H-z) + \lambda - \frac{\rho^2+z^2}{4R_g}\right\}, \tag{2.5}$$

where $\beta(z) = \beta(H - z)$ from the symmetry of the two plates. Substituting this expression into Eqs. 2.1 and 2.2 leads to the probability density

$$P(\rho, z) = \frac{1}{2\pi R_g^2 H} \frac{e^{-\frac{\rho^2+z^2}{4R_g^2}}}{e^{-\frac{z^2}{4R_g^2}} + e^{-\frac{(H-z)^2}{4R_g^2}}} \tag{2.6}$$

and the equilibrium free energy per chain is

$$\frac{F}{k_B T} = \frac{2}{H} \int_0^H \left[\frac{e^{-\frac{z^2}{4R_g^2}}}{e^{-\frac{z^2}{4R_g^2}} + e^{-\frac{(H-z)^2}{4R_g^2}}} \right] \ln \left[\frac{\frac{R_g}{H}}{e^{-\frac{z^2}{4R_g^2}} + e^{-\frac{(H-z)^2}{4R_g^2}}} \right] dz - 1. \tag{2.7}$$

We may also consider a test problem in which the tethered oligomers are immersed in a theta solvent such that the volume not occupied by the oligomers is easily filled with the unattached solvent molecules. In this case the oligomer configuration satisfies the normalization of probability density but the incompressibility constraint disappears. Therefore from Eqs. 2.1, 2.3, and 2.5 with $\beta(z) = 0$ we arrive at the following probability density and free energy per chain for tethered oligomers in a theta solvent:

$$P_\theta(\rho, z) = \frac{1}{4\pi^{\frac{3}{2}} R_g^3 \mathrm{erf}\left(\frac{H}{2R_g}\right)} e^{-\frac{\rho^2+z^2}{4R_g^2}} \tag{2.8}$$

and

$$\frac{F_\theta}{k_B T} = -\ln \left[2\sqrt{\pi} \mathrm{erf}\left(\frac{H}{2R_g}\right) \right] \tag{2.9}$$

with $\mathrm{erf}(x)$ being the error function.

In Fig. 2.2, we calculate the free energy per oligomer at different interwall separations by numerical integration of Eq. 2.7 using an extended trapezoidal method [3]. At small separations, restricted oligomer-conformational space leads to a divergence of the free energy at $H = 0$, which characterizes a steric repulsion similar to interactions between polymer brushes in a solvent. Roughly as $H > 2\sqrt{6}R_g$, two times the unperturbed end-to-end distance of oligomers, the

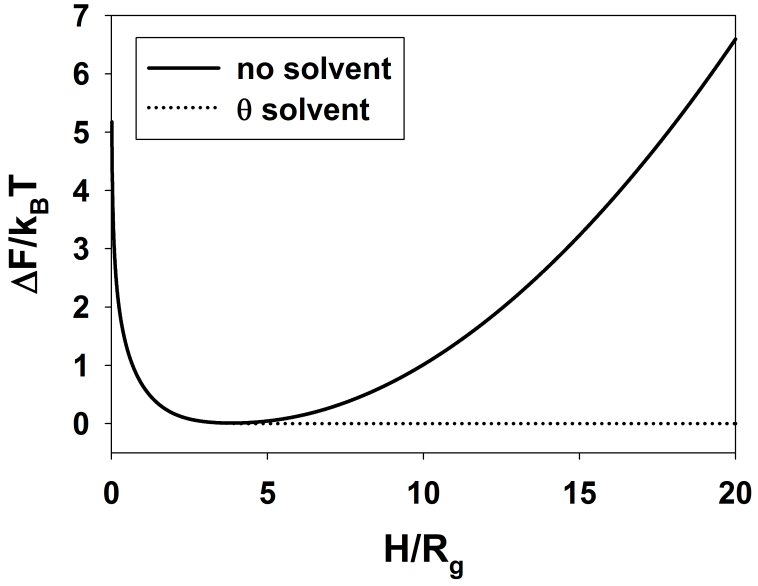

Figure 2.2: Change in the free energy of one bead-spring oligomer non-dimensionalized by the thermal energy, $\Delta F/k_{\mathrm{B}}T$, as a function of the interwall separation non-dimensionalized by the radius of gyration, H/R_{g}, for the plane-wall model in the absence of an unattached solvent. The corresponding free energy in the presence of a theta solvent is shown for comparison. At small H/R_{g} the two free energies are indistinguishable at the scale of the graph.

free energy increases with H because the chains have to stretch out to uniformly fill the interwall space. This "entropic attraction" is purely induced by the tethered oligomers in the absence of solvent, and is a unique feature of solvent-free oligomer-stabilized particles. For comparison, the corresponding free energy curve for tethered oligomers in a theta solvent shows a monotonic decay with H. The entropic attraction obtained for large separations is consistent with the enhanced peaks in core–core correlations [1, 4] and hindered particle diffusion [5] in pure NOHMs when the oligomer radius of gyration is smaller than the average interparticle spacing; meanwhile, the potential minimum around

$H = 2\sqrt{6}R_g$ also explains the predicted smaller viscosity of NOHMs compared with hard spheres when the average interparticle separation is about $2R_g$ and the tethered hairs yield less resistivity [5].

2.2 Interactions between Wavy Walls

In a particle array, the interparticle spacing is non-uniform. To mimic the variations in the interparticle spacing, we consider the model of tethered oligomers within two semi-infinite wavy walls, as shown in Fig. 2.1(b). The walls are sinusoidal in the y direction with wave number k and wavelength $l_0 = 2\pi/k$. As in section 2.1, the oligomers have a radius of gyration R_g and a constant surface grafting density n_a. Since the system is symmetric about the mid plane and unchanged along the x direction, we choose the mid plane as $z = 0$ and define the probability density of finding a monomer at (x, y, z) given that the spring is tethered to $(0, y_t, z_t)$ as $P_{l_0}(x, y, z|y_t)$ with $z_t = \pm\frac{1}{2}H_0\left[1 + \varepsilon\sin(ky)\right]$ ("$-$" for the lower wall and "+" for the upper wall). ε is the magnitude of waviness varying from 0 to 1. When $\varepsilon = 0$ we obtain two plane walls; when $\varepsilon = 1$ the trough of the upper wall touches the peak of the lower wall. H_0 is the mean gap thickness. As a particle moves in the array, it deforms the interparticle spacing and creates regions with increased and decreased fluid space such that the overall fluid space remains unchanged, as depicted in Fig. 2.1(c). To capture this effect, for a given H_0 we change ε and estimate how the oligomer free energy varies with the deformation.

Similar to section 2.1, the probability density is normalized,

$$\int_{-\infty}^{\infty}\int_{-\infty}^{\infty}\int_{-\frac{H(y)}{2}}^{\frac{H(y)}{2}} P_{l_0}(x, y, z|y_t)\mathrm{d}z\mathrm{d}y\mathrm{d}x = 1 \tag{2.10}$$

with $H(y) = H_0\left[1 + \varepsilon \sin(ky)\right]$, and incompressibility of oligomers leads to a constant monomer density throughout the interwall space such that for any given x

$$n(y,z) = n_\mathrm{a} \int_{-\infty}^{\infty}\int_{-\infty}^{\infty}\int_{-\infty}^{\infty}\int_{-\frac{H(y)}{2}}^{\frac{H(y)}{2}} P_{l_0}(x,\bar{y},\bar{z}|y_\mathrm{t})\delta(\bar{y}-y)\left[\delta(\bar{z}-z)+\delta(\bar{z}+z)\right]\mathrm{d}\bar{z}\mathrm{d}\bar{y}\mathrm{d}x\mathrm{d}y_\mathrm{t} = n_0 \tag{2.11}$$

with $n_0 = 2n_\mathrm{a}/H_0$. The free energy per oligomer averaged over a wavelength is

$$\begin{aligned}\frac{F_{l_0}}{k_\mathrm{B}T} = \frac{1}{l_0}\int_0^{l_0}\int_{-\infty}^{\infty}\int_{-\infty}^{\infty}\int_{-\frac{H(y)}{2}}^{\frac{H(y)}{2}} P_{l_0}(x,y,z|y_\mathrm{t})\left[\ln 2\pi P_{l_0}(x,y,z|y_\mathrm{t})R_\mathrm{g}^3 - 1\right] \\ + \frac{1}{4R_\mathrm{g}^2}\left[x^2+(y-y_\mathrm{t})^2+(z-z_\mathrm{t})^2\right]P_{l_0}(x,y,z|y_\mathrm{t})\mathrm{d}z\mathrm{d}y\mathrm{d}x\mathrm{d}y_\mathrm{t}\end{aligned} \tag{2.12}$$

and the Lagrange function takes the form

$$\begin{aligned}L[P_{l_0}(x,y,z|0,y_\mathrm{t})] = \frac{F_{l_0}}{k_\mathrm{B}T} - \frac{1}{l_0}\int_0^{l_0}\lambda(y_\mathrm{t})\left\{\int_{-\infty}^{\infty}\int_{-\infty}^{\infty}\int_{-\frac{H(y)}{2}}^{\frac{H(y)}{2}} P_{l_0}(x,y,z|y_\mathrm{t})\mathrm{d}z\mathrm{d}y\mathrm{d}x - 1\right\}\mathrm{d}y_\mathrm{t} \\ - \frac{1}{l_0 n_\mathrm{a}}\int_0^{l_0}\int_{-\frac{H(y)}{2}}^{\frac{H(y)}{2}}\beta(y,z)\left\{n(y,z) - n_0\left[U\left(z+\frac{H(y)}{2}\right) - U\left(z-\frac{H(y)}{2}\right)\right]\right\}\mathrm{d}z\mathrm{d}y,\end{aligned} \tag{2.13}$$

where the functional Lagrange multiplier $\lambda(y_\mathrm{t})$ enforces the normalization of oligomers tethered to y_t and the functional Lagrange multiplier $\beta(y,z)$ enforces the incompressibility constraint for any x. Both $\lambda(y_\mathrm{t})$ and $\beta(y,z)$ are periodic functions with a wavelength of $2\pi/k$. The minimization $\delta L/\delta P_{l_0}(x,y,z|0,y_\mathrm{t})$ yields

$$P_{l_0}(x,y,z|y_\mathrm{t}) = \frac{1}{2\pi R_\mathrm{g}^3}\exp\left\{\beta(y,z)+\beta(y,-z)+\lambda(y_\mathrm{t}) - \frac{1}{4R_\mathrm{g}^2}\left[x^2+(y-y_\mathrm{t})^2+(z-z_\mathrm{t})^2\right]\right\} \tag{2.14}$$

with $\beta(y,z) = \beta(y,-z)$. First substituting this expression into Eq. 2.11 to relate $\beta(y,z)$ to $\lambda(y_\mathrm{t})$ allows us to write $P(x,y,z|y_\mathrm{t})$ in terms of $\lambda(y_\mathrm{t})$ only. If we then substitute the new expression for $P(x,y,z|y_\mathrm{t})$ into Eq. 2.10 we obtain a nonlinear integral equation with respect to $\lambda(y_\mathrm{t})$:

$$\frac{2}{H_0}e^{\lambda(y_\mathrm{t})}\int_{-\infty}^{\infty}\int_{-\frac{H(y)}{2}}^{\frac{H(y)}{2}}\frac{e^{-\frac{1}{4R_\mathrm{g}^2}\left[(y-y_\mathrm{t})^2+(z-z_\mathrm{t})^2\right]}}{\int_{-\infty}^{\infty}e^{\lambda(y_\mathrm{t})-\frac{(y-y_\mathrm{t})^2}{4R_\mathrm{g}^2}}\left[e^{-\frac{(z-z_\mathrm{t})^2}{4R_\mathrm{g}^2}}+e^{-\frac{(z-z_\mathrm{t})^2}{4R_\mathrm{g}^2}}\right]\mathrm{d}y_\mathrm{t}}\mathrm{d}z\mathrm{d}y = 1. \tag{2.15}$$

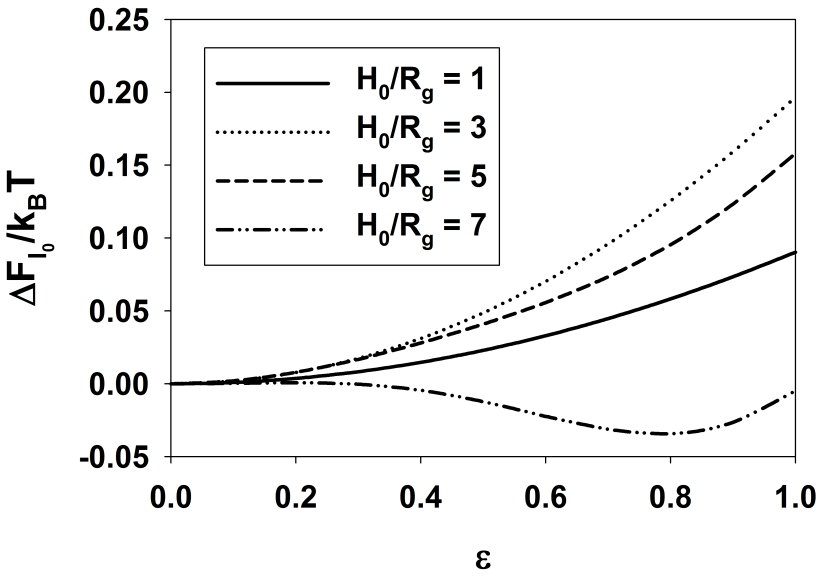

Figure 2.3: Changes in the free energy of one bead-spring oligomer for the wavy-wall model relative to the plane-wall model non-dimensionalized by the thermal energy, $\Delta F_{l_0}/k_{\mathrm{B}}T$, as a function of the magnitude of waviness, ε, for various dimensionless mean interwall separations H_0/R_{g} at $l_0 = 2\pi R_{\mathrm{g}}$.

Making use of a finite-difference discretization in y_{t} and an extended multidimensional trapezoidal method as the integrator, we solve for $\lambda(y_{\mathrm{t}})$ numerically by applying a globally convergent method with line searches and backtracking for a nonlinear system of equations [3]. In this algorithm, the full Newton step is tried and the reduction in the targeted numerical minimization function is checked at each iteration. Backtracking along the Newton direction is performed until an acceptable step is found. Once the function $\lambda(y_{\mathrm{t}})$ is obtained, we substitute the resulting $P_{l_0}(x, y, z|y_{\mathrm{t}})$ into Eq. 2.12 and again calculate the free energy by numerical integration.

The change in the average free energy per oligomer relative to the plane-wall result is compared in Fig. 2.3 for different waviness ε and mean gap thickness

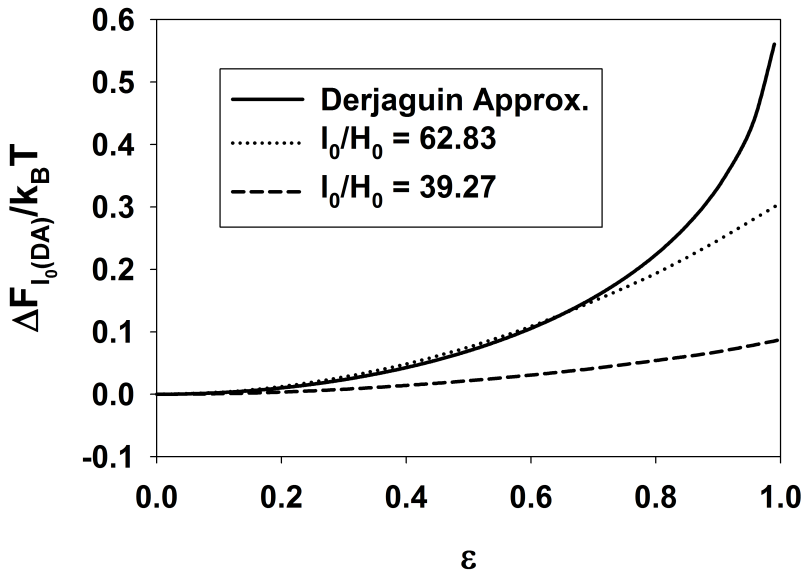

Figure 2.4: Comparison between the changes in the dimensionless free energy of one bead-spring oligomer for the wavy-wall model relative to the plane-wall model, $\Delta F_{l_0}/k_BT$, as a function of the magnitude of waviness, ε, for various aspect ratios l_0/H_0 and the estimate using the Derjaguin approximation at $H_0/R_g = 0.2$.

H_0 at $l_0 = 2\pi R_g$. The introduced sinusoidal shape for the walls yield varying gap thickness such that as ε changes there is a combined effect of compression, relaxation, and stretching for different regions of fluid. When $H_0 < 2\sqrt{6}R_g$, for a given H_0 the oligomer free energy between wavy walls increases monotonically with ε and larger H_0 leads to more increase in the free energy. As $H_0 \approx 2\sqrt{6}R_g$ the combined effect of steric repulsion and entropic attraction yields the most increase in the free energy. This most substantial increase in the free energy with increasing ε indicates that the particles are prone to retain the configuration that minimizes the variations in the interparticle spacing. When $H_0 > 2\sqrt{6}R_g$, the increase in the free energy subsides. When $H_0 = 7R_g$ the substantial variation of the gap thickness as $\varepsilon > 0.5$ crosses the broad free energy minimum region

around $H_0 \approx 2\sqrt{6}R_g$ and the entropic attraction region, therefore the free energy remains almost unchanged at small ε and a minimum is observed at larger ε.

The Derjaguin approximation [6, 7] can be made when the minimum separation and the range of the interaction are both small compared with the radii of curvature of the surfaces such that the total interaction energy of curved surfaces 1 and 2 can be approximated as $\tilde{F}_{\text{curve}}(D) = \int_{S_1} f_{\text{plane}}(H)\mathrm{d}A$ with D being the minimum separation of the curved surfaces, f_{plane} being the interaction energy per unit area between two parallel plates separated by H, and S_1 being the surface of 1. Applying this approximation, we may simply calculate

$$F_{\text{DA}}(H_0) = \frac{1}{l_0}\int_0^{l_0} F(H(y_t))\mathrm{d}y_t \tag{2.16}$$

as the approximated wavy-wall free energy per oligomer obtained from averaging the plane-wall free energy over one wavelength, and compare F_{DA} with the full numerical result of F_{l_0}. As shown in Fig. 2.4 for a given separation, as the aspect ratio l_0/H_0 increases F_{DA} is a good approximation up to $\varepsilon \approx 0.7$. This observation justifies the applicability of the Derjaguin approximation in the long wavelength limit where the undulation is gentle. For more complex surface geometries full numerical calculation is unavoidable to obtain the free energy of surface-tethered oligomers without a solvent.

BIBLIOGRAPHY

[1] H.-Y. Yu and D. L. Koch, Langmuir **26**, 16801 (2010).

[2] D. A. McQuarrie, *Statistical Mechanics*, University Science Books, Sausalito, 2000.

[3] W. H. Press, S. A. Teukolsky, W. T. Vetterling, and B. P. Flannery, *Numerical Recipes in Fortran 77*, Cambridge University Press, Cambridge, 2 edition, 1992.

[4] A. Chremos, A. Z. Panagiotopoulos, H.-Y. Yu, and D. L. Koch, J. Chem. Phys. **135**, 114901 (2011).

[5] H.-Y. Yu and D. L. Koch, Prepared for submission to J. Rheol. .

[6] W. B. Russel, D. A. Saville, and W. R. Schowalter, *Colloidal Dispersions*, Cambridge University Press, New York, 1989.

[7] R. J. Hunter, *Foundations of Colloid Science*, Oxford University Press, New York, 1986.

CHAPTER 3

STRUCTURE OF SOLVENT-FREE NANOPARTICLE–ORGANIC HYBRID MATERIALS

3.1 Abstract

We derive the radial distribution function and the static structure factor for the particles in model nanoparticle–organic hybrid materials composed of nanoparticles and attached oligomeric chains in the absence of an intervening solvent. The assumption that the oligomers form an incompressible fluid of bead-chains attached to the particles that is at equilibrium for a given particle configuration allows us to apply a density functional theory for determining the equilibrium configuration of oligomers as well as the distribution function of the particles. A quasi-analytic solution is facilitated by a regular perturbation analysis valid when the oligomer radius of gyration R_g is much greater than the particle radius a. The results show that the constraint that each particle carries its own share of the fluid attached to itself yields a static structure factor that approaches zero as the wave number approaches zero. This result indicates that each particle excludes exactly one other particle from its neighborhood.

3.2 Introduction

Solvent-less nanoparticle–organic hybrid materials (NOHMs) are a new type of complex fluid composed of hard, inorganic nanocores with oligomeric chains

Reprinted with permission from (H.-Y. Yu and D. L. Koch, *Langmuir* **2010** *26*(22), 16801–16811). Copyright (2010) American Chemical Society.

covalently grafted to the surface of the core and with no other solvent molecules. The cores are self-suspended in a fluid phase of the attached oligomers, which in turn mediate the intercore forces. For typical polymer-stabilized micron-sized colloidal particles, the polymer mediated forces can be described using a pair interparticle potential. However, the absence of a solvent and the small size of the nanocores in NOHMs make their oligomer-mediated interactions non-pairwise-additive. To get insight into the thermodynamic, transport, and rheological properties of such a system, it is essential to first understand the structure and interparticle forces at equilibrium. The purpose of this paper is to formulate a theory that can estimate the equilibrium structure of homogeneous, liquid phase, solvent-free NOHMs without assuming a pairwise-additive interparticle potential.

NOHMs are a promising new class of materials whose unique physicochemical and transport properties have been demonstrated experimentally [1–5]. They provide a homogeneous nanoscale mixture of organic oligomers and inorganic cores. Unlike most nanoparticle systems which aggregate irreversibly due to strong van der Waals attraction, these surface functionalized nanostructures can relax to an equilibrium state and show liquid-like behavior in the absence of a solvent. One can calculate the van der Waals interaction between two equal spheres of radius a at a center-to-center separation r using $\Phi_{\mathrm{vdW}} = -\frac{1}{6}A\left(\frac{2a^2}{r^2-4a^2} + \frac{2a^2}{r^2} + \ln\frac{r^2-4a^2}{r^2}\right)$ with A being the Hamaker constant [6]. Since the intercore potentials arising from the entropy associated with the oligomer configurations are of $O(k_{\mathrm{B}}T)$ with k_{B} being the Boltzmann constant and T being the temperature, the dimensionless number $W = \Phi_{\mathrm{vdW}}/k_{\mathrm{B}}T$ characterizes the magnitude of the van der Waals attraction relative to the oligomer free energy. For a typical solventless NOHMs system of silica cores with tethered polyethy-

lene chains, the estimated non-retarded Hamarker constant would be about 0.1 $k_{\mathrm{B}}T$ at 301 K given that the approximate dielectric constant and the refractive index are 3.91 and 1.45 for silica [7]; 2.26 and 1.482 for polyethylene [8]. For 10 nm diameter cores with a volume fraction of 0.3, the average interparticle spacing would be approximately the core radius and we obtain $W \approx 6 \times 10^{-4}$ at 301 K, indicating that the van der Waals interaction is much smaller than the oligomer-configurational entropy in such NOHMs systems. The goal of our study is to develop a theory of the many-core interactions arising from the entropy penalty incurred as the oligomers attempt to uniformly fill the space between the cores. We will see that the distribution of the cores arising from these interactions is more evenly spaced than a random hard sphere distribution. Such a uniform distribution occurs in ordered phases where each unit cell has a particle and its share of fluid space. However, here we have a disordered system that can act as a fluid but still has each particle surrounded by its share of the fluid, which is in fact attached to its surface. These features of NOHMs motivate the theoretical understanding of the intrinsic forces governing the equilibrium nanostructure of the system. We believe that NOHMs constitute an important new class of complex materials and the present study is an initial attempt to develop a theory for their unique interactions and equilibrium structure.

Previous self-consistent field theories (SCFT) [9–12] and scaling analyses [13–15] for particles with tethered molecules have emphasized attached polymers whose molecular weight was large under conditions where the particle interactions are pairwise additive. The tethered molecules are typically in a solution of added solvent or a melt of unattached polymers. In contrast, the attached molecules in NOHMs are oligomeric with typical lengths of 3–10 nm that are only a few times larger than the molecules' persistence length. In

addition, the small O(5–10 nm) diameters of the cores and the absence of an added solvent imply that the oligomers from several neighboring cores will compete to fill the local interstitial space, leading to non-pairwise-additive intercore potentials. SCFT and scaling analyses exploit a limit where the grafted polymers' contour length is large compared with the persistence length. In addition, monomer–monomer interactions are typically either neglected or incorporated only through a free energy penalty based on a virial expansion that is accurate when the attached molecules have a low volumetric concentration in a sea of added solvent. It would be difficult to accurately incorporate within these theories the constraint that the oligomers from several neighboring particles must form a nearly constant density fluid in the interstitial space. An attempt to accomplish this goal using SCFT would lead to the need to solve a stiff set of integrodifferential equations in a complex interstitial geometry. The Daoud–Cotton (DC) model uses scaling concepts to provide a more analytical treatment of polymer chains grafted on convex surfaces and star polymers in good and theta solvents [16]. However, this theory again does not account for the space-filling nature of the chains. It has also been argued that the DC model does not correspond to a true minimum of the free energy of a curved brush [17].

Several computational studies have considered nanoparticles with tethered oligomers in added phantom solvents. For instance, the polymer reference interaction site model (PRISM) has been applied to determine the effects of a single tether [18] or multiple tethers [19] on the structure of nanoparticles. In this approach, one solves an Ornstein–Zernike-like equation [20] for different site–site interactions with a chosen closure. The connected monomers within a chain are freely jointed. The colloid–colloid interaction is modeled as a Lennard-Jones-like pair potential and only the hard sphere repulsion is as-

sumed for colloid–monomer and monomer–monomer interactions. The hard-core monomer–monomer interactions can be considered to be applicable to a situation where the tethered oligomers are in a phantom solvent of monomers with the same chemical structure. Therefore non-pairwise-additive space-filling effects are not addressed. The pair correlation function and the structure factor obtained depend on the intercore attraction, positions and number of tethers, chain length, and particle volume fraction. Molecular dynamics simulations [21, 22] for nanoscale colloids with a single tethered polymer have shown interesting phase behavior driven by the change in the chain configuration, polymer–colloid size ratio, and particle volume fraction. In these studies, a repulsive, truncated, and shifted Lennard-Jones pair potential is used for colloid–colloid interactions and bead–bead interactions. The neighboring beads within a polymer are either freely-jointed or connected by harmonic springs. Again these studies correspond to colloids suspended in a phantom solvent. While these computational studies provide an initial indication of the interactions of nanoparticles with tethered branches, we will seek a more analytical treatment and one appropriate to a system without added solvent.

In the present study, we will treat the tethered oligomers as an incompressible fluid. That is to say that the concentration of monomers contributed by oligomers attached to all neighboring particles must be independent of position in the interstitial space. A test of the validity of this assumption can be made by comparing the entropic free energy associated with the translation of the cores to the work required to compress the oligomeric fluid. The isothermal compressibility χ_T (Pa^{-1}) of a fluid defined by $\chi_T = -(\frac{1}{v})(\frac{\partial v}{\partial p})_T$ with v being the molar volume of the fluid or mediate oligomers and p being the pressure, can be considered the inverse of the energy per unit volume required to com-

press the medium by an amount comparable with the system's current density. Thus, the reciprocal of the product of the compressibility and the number density of the particles (n_b^*) in the suspension characterizes the energy per particle required to compress the surrounding oligomers. A dimensionless number, $X = (\chi_T n_b^*)^{-1}/k_B T$, is the ratio of the energy to compress the oligomers and the thermal energy associated with the translation of the cores. For a suspension of 10 nm diameter cores with tethered polyethylene chains with $\chi_T \approx 5 \times 10^{-10} Pa^{-1}$ calculated from a *Padé* equation of state [23] and a core volume fraction of 0.3, $X \approx 10^6$ at 301 K. This indicates that the particle's thermal energy is insufficient to compress the intervening oligomeric fluid, which may then be considered incompressible.

The application of a hard incompressibility constraint using a Lagrange multiplier that we adopt in the present study is unusual in statistical mechanics. The typical procedure would be to specify the pairwise potential interactions among the monomers that make up the oligomers and deduce the configuration of the oligomers on this basis. In a liquid, however, the attractive interactions among the monomers along with their short-range repulsive forces lead to a monomer concentration that is very insensitive to pressure. It may be expected that the incompressibility condition would be approximated by conventional simulations and theories in the limit in which the attractive energy of the monomers becomes large compared with the thermal energy.

Polymers or oligomers tethered to particle surfaces in a good or theta solvent would typically be expected to yield a repulsive (steric) interaction between the particles. This interaction arises because the brush on one particle must be deformed due to the close proximity of the surface of the other particle. The in-

compressibility constraint on the total monomer concentration contributed by the molecules attached to all particles in the absence of an unattached solvent will be seen to yield a qualitatively new type of interparticle interaction. The absence of an unattached solvent and the incompressibility of the fluid phase imply that the space occupied by each particle and its attached oligomers must exclude exactly one neighboring particle with its attached oligomers. This constraint is equivalent to the statement that the static structure factor at zero wave number, which is related to the integral of the deviation of the conditional probability for finding a neighboring particle from the bulk number density, is zero, i.e., $S(k^* = 0) = 1 + n_{\mathrm{b}}^* \int_{V^*} [g(r_{\mathrm{p}}^*) - 1] \mathrm{d}\mathbf{r}_{\mathrm{p}}^* = 0$. Here S is the static structure factor, k^* is the wave number, r_p^* is the interparticle distance, V^* is the suspension volume, $g(r_{\mathrm{p}}^*)$ is the radial distribution function, and n_{b}^* is the bulk number density. It is well known that $S(k^* = 0) = 0$ in an *incompressible single-component fluid* [20]. However, $S(k^* = 0)$ is a finite value between zero and one in a disordered hard-sphere colloidal suspension and in typical disordered suspensions of particles with short-range repulsive forces such as those due to steric brush interactions. The facts that the incompressible fluid suspending the nanocores in NOHMs is attached to the cores and that each particle carries its own share of this fluid on its back imply that the system may be viewed as an *incompressible single-component fluid* with the component consisting of a particle plus its attached oligomers. As a result the static structure factor for the *cores*, a quantity often observed in scattering experiments, will satisfy $S(k^* = 0) = 0$.

The static structure factor and the pair distribution function are interrelated. Thanks to Percus' observation [24, 25], the pair distribution function, i.e. the radial distribution function, in a uniform classical fluid can be calculated from the one-body density profile when one fluid particle is fixed, i.e.

$n^*(\mathbf{r}_2^* - \mathbf{r}_1^*) = n_b^* g(\mathbf{r}_2^* - \mathbf{r}_1^*)$, where $n^*(\mathbf{r}_2^* - \mathbf{r}_1^*)$ is the density of fluid particles at $\mathbf{r}_2^*$ in a subensemble in which a particle is centered at $\mathbf{r}_1^*$. This concept has been widely used in the density functional theory, which successfully describes the structure of inhomogeneous simple fluids around a fixed entity [26].

In this article, we formulate a density functional theory for two simple coarse-grained models for pure NOHMs with bead-spring oligomers attached in the absence of other solvent molecules, one in which the cores are points and a second in which the finite hard-sphere radius of the core is taken into account. We first define the free energy of the oligomers for a given particle configuration. The equilibrium concentration field of the oligomers attached to a core is obtained by minimizing the oligomer free energy subject to the constraints that the field produced by the oligomers attached to an i^{th} core is normalized and the oligomer fluid number density at a given $\mathbf{r}^*$ contributed from a sum of fields due to $i = 1, \ldots, N$ particles is independent of position throughout the fluid phase volume. These constraints of normalization and incompressibility along with the spring energy for the oligomers lead to an oligomer-configurational entropy penalty for large spaces between the core particles. Consequently, our results will be based on a different particle interaction mechanism than previous SCFT work or the DC model and conventional scaling laws for the polymer brush conformation in an unattached solvent will no longer be appropriate in such solvent-free systems. Analytical results for the concentration field are derived from a regular perturbation scheme under a "weak-field" approximation for the oligomer concentration. In particular, when the radius of gyration of the oligomers is large compared with the core radius ($R_g/a \gg 1$), many neighboring particles contribute oligomers to any fluid volume. As a result, the effect of each particle on the local oligomer concentration field is small. Use of the resultant,

weak-field solution for the oligomer concentration field along with a density functional formulation allows a semi-analytic determination of the radial distribution function and the static structure factor of cores. While our theory does not capture the details of intra-chain excluded volume interactions, we will see that it does describe the changes in chain and core configurations caused by the requirement that all the chains from a test particle and neighboring particles must uniformly fill space.

3.3 Theory & Results

3.3.1 Point NOHMs

We first consider the case where the nanocores and oligomeric chains are modeled as point particles and bead-springs tethered to the central points, as shown in Fig. 1(c). The springs are linear, massless, and have a rest length of zero. The spring energy is defined by $F_{\text{spring}} = \frac{1}{2}\xi r^{*2}$ with ξ being the spring constant and r^* being the distance between the bead and the central point particle. The spring constant is chosen to be related to the radius of gyration R_{g} of an ideal, unattached linear chain as $\xi = k_{\text{B}}T/2R_{\text{g}}^2$. The probability distribution function of the bead, $G(\mathbf{r}^*) \sim e^{-\frac{F_{\text{spring}}}{k_{\text{B}}T}}$, satisfies the normalization condition:

$$\int_{V^*} G(\mathbf{r}^*)\mathrm{d}\mathbf{r}^* = 1. \tag{3.1}$$

The mean-square distance of the bead from the central point particle in the absence of chain–chain interactions is:

$$\langle r^{*2}\rangle = \int_{V^*} r^{*2} G(\mathbf{r}^*)\mathrm{d}\mathbf{r}^* = 6R_{\text{g}}^2. \tag{3.2}$$

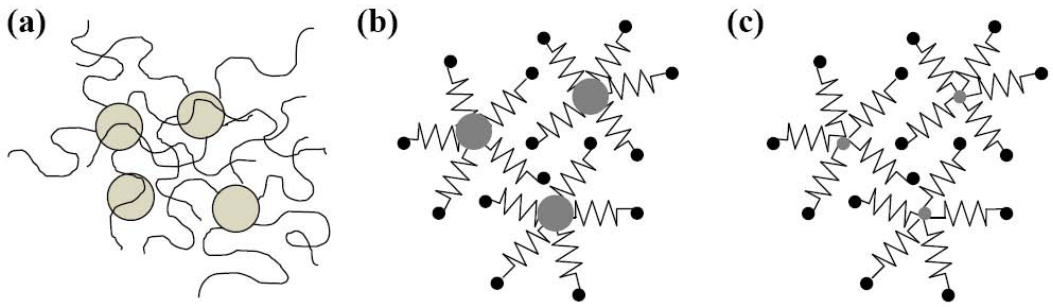

Figure 3.1: (a) A random particle array showing the oligomers can cross over several particles. (b) Schematic of the finite-core NOHMs model. The big central spheres are the hard cores and the small beads represent the monomers. The monomers are connected to the core with springs and each spring has one monomer. (c) Schematic of the point NOHMs model. The junction beads are the point cores with connected monomer beads. In our model the number of oligomers per particle is an adjustable parameter M and for clarity we only illustrate a few oligomers here.

Although the oligomers in NOHMs have only a moderate number of Kuhn steps, for simplicity we model them using an ideal chain wherein the radius of gyration is the sole parameter used for comparison with simulation and experiment. The basic form of the theory would be unaltered if a more sophisticated oligomer conformation model were adopted; this model would primarily alter the function G. All starred variables are dimensional radii, distances, volume, densities, and wave numbers. Unstarred variables are non-dimensionalized by R_g and those with an over bar "–"are non-dimensionalized by the core radius a.

The relaxation of the configuration of cores requires motion of all the oligomers attached to each core, while oligomer relaxation requires the motion of only one oligomer. Thus, the oligomers can relax quickly compared with the cores. Hence we assume that for a given particle configuration the oligomers are at equilibrium. For a system of N particles we write down the fluid phase

free energy as (after replacing ξ by $k_{\mathrm{B}}T/2R_{\mathrm{g}}^2$)

$$\frac{F_{\mathrm{f}}}{k_{\mathrm{B}}T} = \sum_{i=1}^{N} \int_V C_i(\mathbf{r}, \mathbf{r}_i) \left[\ln C_i(\mathbf{r}, \mathbf{r}_i) \Lambda_{\mathrm{b}}^3 - 1 \right] + \frac{1}{4} (\mathbf{r} - \mathbf{r}_i)^2 C_i(\mathbf{r}, \mathbf{r}_i) \mathrm{d}\mathbf{r}, \tag{3.3}$$

where the first term represents the ideal gas Helmholtz free energy of the beads, the second term accounts for the spring energy, $C_i(\mathbf{r}, \mathbf{r}_i)$ is the concentration field of the oligomers at $\mathbf{r}$ attached to particle i, $\mathbf{r}_i$ is the position of particle i, and Λ_{b} is the thermal de Broglie wavelength of the monomer beads. $C(\mathbf{r}) = \sum_{i=1}^{N} C_i(\mathbf{r}, \mathbf{r}_i)$ is the total oligomer fluid number density at $\mathbf{r}$.

To determine the equilibrium concentration field of the oligomers, we must minimize the fluid phase free energy with respect to variations in C_i subject to the constraints that the probability of finding the oligomers attached to each particle is normalized,

$$\int_V C_i(\mathbf{r}, \mathbf{r}_i) \mathrm{d}\mathbf{r} = M, \tag{3.4}$$

and the fluid number density is a constant in the suspension (incompressibility condition),

$$C(\mathbf{r}) = \sum_{i=1}^{N} C_i(\mathbf{r}, \mathbf{r}_i) = n_{\mathrm{b}} M, \tag{3.5}$$

where M is the number of oligomers per core and $n_{\mathrm{b}} \left[= n_{\mathrm{b}}^* R_{\mathrm{g}}^3 \right]$ is the bulk number density of the cores. In mathematical optimization, one can make use of Lagrange undetermined multipliers to find a maximum or minimum of a function subject to constraints. A concise introduction to this technique can be found in ref 27. The Lagrange function for minimizing the free energy of NOHMs for a given core configuration subject to the normalization and incompressibility constraints is

$$L_{\mathrm{f}} \left[C_i(\mathbf{r}, \mathbf{r}_i) \right] = \frac{F_{\mathrm{f}}}{k_{\mathrm{B}}T} - \sum_{i=1}^{N} \lambda_i \left[\int_V C_i(\mathbf{r}, \mathbf{r}_i) \mathrm{d}\mathbf{r} - M \right] - \int_V \beta(\mathbf{r}) \left[\sum_{i=1}^{N} C_i(\mathbf{r}, \mathbf{r}_i) - n_{\mathrm{b}} M \right] \mathrm{d}\mathbf{r}, \tag{3.6}$$

where the Lagrange multipliers λ_i enforcing the normalization make up a discrete set with one multiplier for each particle and the Lagrange multipliers $\beta(\mathbf{r})$ enforcing the incompressibility constraint are a continuous set or a function of position with the value of β at position $\mathbf{r}$ ensuring that the fluid number density at position $\mathbf{r}$ is equal to the average value, $n_b M$. For a given particle configuration, the minimization $\delta L_f / \delta C_i(\mathbf{r}, \mathbf{r}_i)$ yields, after some manipulations and use of Eq. 3.4,

$$C_i(\mathbf{r}, \mathbf{r}_i) = M \Lambda_i B(\mathbf{r}) G(\mathbf{r} - \mathbf{r}_i), \tag{3.7}$$

where $B(\mathbf{r}) = e^{\beta(\mathbf{r})}$ accounts for the incompressibility, $G(\mathbf{r} - \mathbf{r}_i) = \frac{1}{(4\pi)^{\frac{3}{2}}} e^{-\frac{(\mathbf{r}-\mathbf{r}_i)^2}{4}}$, and Λ_i accounts for the normalization of the oligomers attached to particle i and other uninteresting factors not included in $B(\mathbf{r})$ or $G(\mathbf{r} - \mathbf{r}_i)$. We have made use of functional differentiations to minimize $L_f\,[C_i(\mathbf{r}, \mathbf{r}_i)]$. Some physically oriented discussion of functional differentiations can be found in ref 20.

For the density functional theory, it will prove useful to define a conditional ensemble average of the oligomer concentration. We first specify the position of particle 1 as $\mathbf{r}_1$ and make it our *chosen* particle but consider all the other *non-chosen* particles labeled 2 as indistinguishable, then define the $(N-1)$-particle conditional ensemble average of a quantity A given that particle 1's center is fixed at $\mathbf{r}_1$ as $\langle A \rangle_1(\mathbf{r}|\mathbf{r}_1) = \int_V \cdots \int_V P^{(N-1)}(\mathbf{r}^{N-1}|\mathbf{r}_1) A(\mathbf{r}) \mathrm{d}\mathbf{r}_2 \cdots \mathrm{d}\mathbf{r}_N$. Applying the conditional ensemble average to the incompressibility constraint in Eq. 3.5 yields

$$\begin{aligned}
\langle C \rangle_1(\mathbf{r}|\mathbf{r}_1) &= \int_V \cdots \int_V P^{(N-1)}(\mathbf{r}^{N-1}|\mathbf{r}_1) \left[C_1(\mathbf{r}, \mathbf{r}_1) + (N-1) C_2(\mathbf{r}, \mathbf{r}_2) \right] \mathrm{d}\mathbf{r}_2 \cdots \mathrm{d}\mathbf{r}_N \\
&= \langle C_1 \rangle_1(\mathbf{r}|\mathbf{r}_1) + (N-1) \int_V P^{(1)}(\mathbf{r}_2|\mathbf{r}_1) \langle C_2 \rangle_2(\mathbf{r}|\mathbf{r}_1, \mathbf{r}_2) \mathrm{d}\mathbf{r}_2 \\
&= n_b M,
\end{aligned} \tag{3.8}$$

where $\langle C_1 \rangle_1(\mathbf{r}|\mathbf{r}_1)$ is the conditional average of the concentration field of oligomers attached to particle 1 given that particle 1 is fixed at $\mathbf{r}_1$, $\langle C_2 \rangle_2(\mathbf{r}|\mathbf{r}_1, \mathbf{r}_2)$ is

the conditional average of the concentration field of oligomers attached to particle 2 given that particles 1 and 2 are fixed at $\mathbf{r}_1$ and $\mathbf{r}_2$, $P^{(N-1)}(\mathbf{r}^{N-1}|\mathbf{r}_1)$ is the conditional probability density function of finding $N-1$ particles given that there is a particle fixed at $\mathbf{r}_1$, and $P^{(1)}(\mathbf{r}_2|\mathbf{r}_1)$ is the conditional probability density function of finding particle 2 at $\mathbf{r}_2$ given that there is a particle fixed at $\mathbf{r}_1$, which can be related to the radial distribution function by the relation $g(\mathbf{r}_2-\mathbf{r}_1)/V = P^{(1)}(\mathbf{r}_2|\mathbf{r}_1)$.

The conditional average of the incompressibility constraint with one particle fixed in Eq. 3.8 depends on the conditional average of the concentration of the oligomers of a second particle (particle 2) with two particle positions fixed. A conditional average of the incompressibility constraint with two particle positions held fixed would depend on an oligomer concentration field with three particle positions fixed and so forth. This leads to a closure problem which is common in ensemble average treatments of fields surrounding particles. One common method of achieving closure in theories for suspensions of particles in an unattached fluid solvent is to assume that the particles are dilute so that clusters of interacting particles are rare compared with isolated particles [28,29]. However, NOHMs are never dilute. In the absence of an unattached solvent, the oligomers of particle 1 must always be intertwined with the oligomers of its neighbors and one cannot achieve a small core particle concentration in which interactions are rare.

A second situation in which ensemble average field equations can be closed is one in which many particles contribute to the field in a certain region of space with no single particle having a disproportionate influence on the field. Under these circumstances, the contribution of each particle to the field is small. Furthermore, correlations of the field due to multiparticle interactions are weak

compared with one-particle conditional averages. One precedent for this situation in the theory of particle suspensions is the fluid flow and chemical tracer dispersion in a dilute fixed bed of spheres [29, 30]. In this case, the fluid velocity and tracer concentration fields produced by a particle are only truncated due to Brinkman screening at a large distance from the particle, large enough to contain many neighboring particles.

The oligomer concentration field in NOHMs is influenced by many neighboring particles when the radius of gyration R_g of the oligomers is large compared with the interparticle spacing $n_b^{*-1/3}$, i.e., $n_b^* R_g^3 = n_b \gg 1$. We will exploit this limit to close the equations governing the oligomer concentration and core pair probability distribution function in NOHMs. The B-field represents the influence of the incompressibility constraint on the concentration of the oligomers. When $n_b \gg 1$, the oligomer concentration contributed by particle i can readily be compensated by small $O(1/n_b)$ changes in the concentration of the oligomers attached to other particles and so the B-field deviates from 1 by only an $O(1/n_b)$ amount. Similarly, the surrounding particles have only a modest influence on the normalization constant required for particle i. Thus, we can write $B(\mathbf{r}) = 1 + B'(\mathbf{r})$ and $\Lambda_i = 1 + \Lambda_i'$ with $B'(\mathbf{r})$ and Λ_i' being of $O(1/n_b)$. It will be seen that these weak fields yield a weak perturbation to the free energy of the oligomers, resulting in a small change in the pair distribution function so that $g(\mathbf{r}_2 - \mathbf{r}_1) = 1 + h_f(\mathbf{r}_2 - \mathbf{r}_1)$ with $h_f(\mathbf{r}_2 - \mathbf{r}_1) = O(1/n_b)$. The weak-field approximation allows us to neglect nonlinear $O(1/n_b^2)$ terms such as $\Lambda_i' B'(\mathbf{r})$ compared with linear $O(1/n_b)$ terms such as $B'(\mathbf{r})$ or Λ_i'. Using this approximation, the conditional averages with one and two particles fixed of the solution for the oligomer concentration in Eq. 3.7 are:

$$\langle C_1 \rangle_1(\mathbf{r}|\mathbf{r}_1) \approx M \left[1 + \langle \Lambda_1' \rangle_1(\mathbf{r}_1|\mathbf{r}_1) + \langle B' \rangle_1(\mathbf{r}|\mathbf{r}_1)\right] G(\mathbf{r} - \mathbf{r}_1) \tag{3.9}$$

and

$$\langle C_2\rangle_2(\mathbf{r}|\mathbf{r}_1,\mathbf{r}_2) \approx M\left[1+\langle\Lambda_2'\rangle_2(\mathbf{r}_2|\mathbf{r}_1,\mathbf{r}_2)+\langle B'\rangle_2(\mathbf{r}|\mathbf{r}_1,\mathbf{r}_2)\right]G(\mathbf{r}-\mathbf{r}_2). \tag{3.10}$$

When many particles ($O(n_\mathrm{b})$ particles) interact with a *chosen* particle, the correlation between the disturbances created by neighboring particles is weak. To quantify this concept, it is convenient to define a perturbation B'' to the B-field as $B'(\mathbf{r}) = B''(\mathbf{r}) + \langle B'\rangle_1(\mathbf{r}|\mathbf{r}_1) + \langle B'\rangle_1(\mathbf{r}|\mathbf{r}_2)$. Thus, B'' represents the perturbations to the B-field that are not captured by the conditional average B-field perturbations with particle 1 fixed and with particle 2 fixed separately. As a result, $\langle B''\rangle_2$ represents the B-field perturbations resulting from the correlations between particles 1 and 2. Since the perturbation caused by particle 1 is $O(1/n_\mathrm{b})$ and there are many ($O(n_\mathrm{b})$) particles interacting with particle 1, we expect that each of them will have a correlation $\langle B''\rangle_2 = O(1/n_\mathrm{b}^2)$. Keeping terms up to $O(1/n_\mathrm{b})$, we can approximate the conditional average B-field with two particles fixed as a sum of one-particle fields

$$\langle B'\rangle_2(\mathbf{r}|\mathbf{r}_1,\mathbf{r}_2) \approx \langle B'\rangle_1(\mathbf{r}|\mathbf{r}_1)+\langle B'\rangle_1(\mathbf{r}|\mathbf{r}_2). \tag{3.11}$$

Similarly, the perturbation to the normalization constant of particle i can be written as $\Lambda_i' = \Lambda_i'' + \langle\Lambda_i'\rangle_1(\mathbf{r}_i|\mathbf{r}_i)$ where Λ_i'' is the deviation of particle i's normalization constant from the conditional average of this constant with particle i fixed. The conditional average of the normalization constant with two particles fixed is

$$\langle\Lambda_2'\rangle_2(\mathbf{r}_2|\mathbf{r}_1,\mathbf{r}_2) = \langle\Lambda_2'\rangle_1(\mathbf{r}_2|\mathbf{r}_2)+\langle\Lambda_2''\rangle_2(\mathbf{r}_2|\mathbf{r}_1,\mathbf{r}_2), \tag{3.12}$$

where up to $O(1/n_\mathrm{b}^2)$ we can neglect the contributions of correlations with third particles to $\langle\Lambda_2''\rangle_2$.

After substituting Eqs. 3.9–3.12 into Eq. 3.8 we can equate terms of $O(n_\mathrm{b})$ and $O(1)$ to zero and neglect terms of higher orders. Applying the normalization condition for $\langle C_1\rangle_1$ and $\langle C_2\rangle_2$ and making use of Fourier transformations allow the $O(1)$ equation to only involve $\langle \hat{B'}\rangle_1$ in Fourier space. The characteristic length scale in this problem is R_g quantifying the range over which the disturbances to the field variables are important. Therefore we scale the wave number with R_g such that $k = k^* R_\mathrm{g}$ and upon Fourier transforming we obtain

$$\langle \hat{B'}\rangle_1(\mathbf{k}) = \frac{\hat{G}(\mathbf{k})\left[1 + n_\mathrm{b}\hat{h}_\mathrm{f}(\mathbf{k})\right]}{n_\mathrm{b}\left[\hat{G}(\mathbf{k}^2) - 1\right]}, \tag{3.13}$$

$$\langle \hat{\Lambda_2''}\rangle_2(\mathbf{k}) = -\langle \hat{B'}\rangle_1(\mathbf{k})\hat{G}(\mathbf{k}), \tag{3.14}$$

and

$$\langle \Lambda_i'\rangle_1(\mathbf{r}_i|\mathbf{r}_i) = -\frac{1}{(2\pi)^3}\int_{V_k} \langle \hat{B'}\rangle_1(\mathbf{k})\hat{G}(-\mathbf{k})\mathrm{d}\mathbf{k} \tag{3.15}$$

with V_k being all space in $\mathbf{k}$, and the subscript i is 1 or 2. Note that $\hat{G}$ is of $O(1)$ and $\hat{h}_\mathrm{f}$ is of $O(1/n_\mathrm{b})$ as we have assumed, so $\langle \hat{B'}\rangle_1$ is of $O(1/n_\mathrm{b})$ as is shown explicitly in Eq. 3.13. The same is true for $\langle \hat{\Lambda_2''}\rangle_2$ and $\langle \Lambda_i'\rangle_1$. Since we have neglected terms of orders higher than $1/n_\mathrm{b}$ in this analysis and proven the consistency of the order of magnitude, the perturbations to the field variables are correct to order $1/n_\mathrm{b}$. The Fourier transform of $f(\mathbf{x})$ and the inverse transform of $\hat{f}(\mathbf{s})$ are defined by $\hat{f}(\mathbf{s}) = \int f(\mathbf{x})e^{-i\mathbf{s}\cdot\mathbf{x}}\mathrm{d}\mathbf{x}$ and $f(\mathbf{x}) = \frac{1}{(2\pi)^3}\int \hat{f}(\mathbf{s})e^{i\mathbf{s}\cdot\mathbf{x}}\mathrm{d}\mathbf{s}$.

We have solved for the conditional average concentration field of oligomers attached to a particle analytically. Our goal is to find the radial distribution function of the particles subject to the fluid phase free energy contributed from the oligomers. We can apply a density functional approach to achieve this. The essence of the density functional theory is to formulate an expression for the grand potential Ω, which is related to the Helmholtz free energy F_Helm of the entire system by $\Omega = F_\mathrm{Helm} - \mu N$, with μ being the chemical potential of the

particles. While the Helmholtz free energy is the thermodynamic potential of the canonical ensemble, the grand potential corresponds to the thermodynamic potential of the grand canonical ensemble [27]. If we follow Percus' observation [24, 25], when we fix a *chosen* particle labeled 1 at the origin, there will be a one-body density profile of other *non-chosen* particles labeled 2 around particle 1, $n(\mathbf{r}_\mathrm{p}) = n_\mathrm{b} g(\mathbf{r}_\mathrm{p})$, with $\mathbf{r}_\mathrm{p}$ being $\mathbf{r}_2 - \mathbf{r}_1$. The grand potential is therefore a functional of this one-body density profile, $\Omega = F_\mathrm{total} - \mu \int_V n(\mathbf{r}_\mathrm{p}) \mathrm{d}\mathbf{r}_\mathrm{p}$, and now F_total includes F_Helm and an additional "external" potential due to the fact that a particle has been fixed. This external potential can be determined if the fixed particle occupies a certain volume and interacts with other particles via a specific potential. In a NOHMs system with point cores interacting via a free energy due to the oligomers calculated by the equilibrium oligomer structure that we have determined, the external potential due to the fixed core is zero and the excess free energy contributed from the fixed particle's oligomers can be included within a part of the Helmholtz free energy denoted by F_ex. The grand potential is therefore written as

$$\Omega\left[n(\mathbf{r}_\mathrm{p})\right] = F_{id}\left[n(\mathbf{r}_\mathrm{p})\right] + F_\mathrm{ex}\left[n(\mathbf{r}_\mathrm{p})\right] - \mu \int_V n(\mathbf{r}_\mathrm{p}) \mathrm{d}\mathbf{r}_\mathrm{p}. \tag{3.16}$$

The ideal gas part of the free energy functional of the cores is

$$\frac{F_\mathrm{id}\left[n(\mathbf{r}_\mathrm{p})\right]}{k_\mathrm{B}T} = \int_V n(\mathbf{r}_\mathrm{p}) \left\{ \ln\left[n(\mathbf{r}_\mathrm{p})\Lambda_\mathrm{p}^3\right] - 1 \right\} \mathrm{d}\mathbf{r}_\mathrm{p} \tag{3.17}$$

with Λ_p being the thermal de Broglie wavelength of the particles. For a given core configuration the free energy of the oligomers is smeared out as a "mediated interparticle potential" (not the conventional pairwise one) between the cores. Mathematically, the excess free energy relative to the ideal gas is therefore the fluid phase free energy of the tethered oligomers conditionally averaged

over the configuration of $N-1$ particles given that particle 1 is fixed at the origin,

$$\begin{aligned}\frac{F_{\mathrm{ex}}\left[n(\mathbf{r}_{\mathrm{p}})\right]}{k_{\mathrm{B}}T} &= \left\langle \frac{F_{\mathrm{f}}}{k_{\mathrm{B}}T} \right\rangle_1 \\ &= \int_V \langle C_1 \ln C_1 \Lambda_{\mathrm{b}}^3 \rangle_1(\mathbf{r}|\mathbf{0}) + \left[\frac{\mathbf{r}^2}{4} - 1\right] \langle C_1 \rangle_1(\mathbf{r}|\mathbf{0}) \mathrm{d}\mathbf{r} + \\ &\quad \int_V n(\mathbf{r}_{\mathrm{p}}) \int_V \langle C_2 \ln C_2 \Lambda_{\mathrm{b}}^3 \rangle_2(\mathbf{r}|\mathbf{0}, \mathbf{r}_{\mathrm{p}}) + \left[\frac{(\mathbf{r}-\mathbf{r}_{\mathrm{p}})^2}{4} - 1\right] \langle C_2 \rangle_2(\mathbf{r}|\mathbf{0}, \mathbf{r}_{\mathrm{p}}) \mathrm{d}\mathbf{r}\mathrm{d}\mathbf{r}_{\mathrm{p}},\end{aligned} \tag{3.18}$$

where $\mathbf{r}_{\mathrm{p}}$ is the position of particles labeled 2 relative to the origin and $\mathbf{r}$ is the position of the beads in the suspension relative to the origin.

At equilibrium, minimization of the grand potential $\delta\Omega[n(\mathbf{r}_{\mathrm{p}})]/\delta n(\mathbf{r}_{\mathrm{p}})$ and application of $\mu = \mu_{\mathrm{bulk}} = \mu|_{\mathbf{r}_{\mathrm{p}}\to\infty}$ yield

$$n(\mathbf{r}_{\mathrm{p}}) = n_{\mathrm{b}} g(\mathbf{r}_{\mathrm{p}}) = n_{\mathrm{b}} \exp\left\{c^{(1)}(\mathbf{r}_{\mathrm{p}}) - c_{\mathrm{b}}^{(1)}\right\}, \tag{3.19}$$

where $c^{(1)}(\mathbf{r}_{\mathrm{p}}) = -\delta\left(F_{\mathrm{ex}}[n(\mathbf{r}_{\mathrm{p}})]/k_{\mathrm{B}}T\right)/\delta n(\mathbf{r}_{\mathrm{p}})$ is the so-called one-body direct correlation function evaluated at $\mathbf{r}_{\mathrm{p}}$, and $c_{\mathrm{b}}^{(1)} = -\left[\delta\left(F_{\mathrm{ex}}[n(\mathbf{r}_{\mathrm{p}})]/k_{\mathrm{B}}T\right)/\delta n(\mathbf{r}_{\mathrm{p}})\right]|_{\mathbf{r}_{\mathrm{p}}\to\infty}$. The superscript "(1)" is to remind ourselves that the direct correlation function here is obtained from taking "one" functional derivative of F_{ex} and is for one particle, distinguished from the "two-body" direct correlation function used in literature of the integral equation theory. Under a weak-field approximation for the oligomers, we assume that the change in the excess free energy due to the change in particle configuration is of $O(1/n_{\mathrm{b}})$ and the exponent can be linearized such that we obtain

$$h_{\mathrm{f}}(\mathbf{r}_{\mathrm{p}}) \approx c^{(1)}(\mathbf{r}_{\mathrm{p}}) - c_{\mathrm{b}}^{(1)}. \tag{3.20}$$

After substituting the field variables Λ_i and $B(\mathbf{r})$ into Eq. 3.18, we can neglect the correlations between the field variables caused by a second or third particle such that $\langle \Lambda_2''^2 \rangle_2 \approx \langle \Lambda_2'' \rangle_2^2$, $\langle B'^2 \rangle_1 \approx \langle B' \rangle_1^2$, and $\langle \Lambda_2'' B' \rangle_2 \approx \langle \Lambda_2'' \rangle_2 \langle B' \rangle_2$, etc. based on the ob-

servation that multi-particle correlations are weak for $n_b \gg 1$ as discussed previously. Then functional differentiation $\delta\left(F_{ex}[n(\mathbf{r}_p)]/n_b k_B T\right)/\delta h_f(\mathbf{r}_p)$ with standard chain rules finally yields to $O(1/n_b)$,

$$h_f(\mathbf{r}_p) \approx 2M \int_V \langle \Lambda_2'' \rangle_2(\mathbf{r}_p'|\mathbf{0}, \mathbf{r}_p) \frac{\delta \langle \Lambda_2'' \rangle_2(\mathbf{r}_p'|\mathbf{0}, \mathbf{r}_p)}{\delta h_f(\mathbf{r}_p)} d\mathbf{r}_p' - 2M \int_V \langle B' \rangle_1(\mathbf{r}'|\mathbf{0}) \frac{\delta \langle B' \rangle_1(\mathbf{r}'|\mathbf{0})}{\delta h_f(\mathbf{r}_p)} d\mathbf{r}'. \tag{3.21}$$

Since the changes in all the other particles' field variables due to the pair probability of a given pair of particles 1 and 2 are important only within a distance $\sim R_g$ from the fixed particle 1, we conclude that when particle 2 is deep in the bulk $\delta \langle \Lambda_2'' \rangle_2(\mathbf{r}_p'|\mathbf{0}, \mathbf{r}_p)/\delta h_f(\mathbf{r}_p)$ and $\delta \langle B' \rangle_1(\mathbf{r}'|\mathbf{0})/\delta h_f(\mathbf{r}_p)$ are essentially zero making the integrals in Eq. 3.21 convergent. Equation 3.21 contains convolution integrals which are simplified by Fourier transforming and using the convolution theorem. Making use of Eqs. 3.13 and 3.14, we thereby obtain

$$\hat{h_f}(\mathbf{k}) = -\frac{2M}{n_b} \left\{ \frac{\hat{G}(\mathbf{k})^2}{1 - \hat{G}(\mathbf{k})^2 + 2M\hat{G}(\mathbf{k})^2} \right\}. \tag{3.22}$$

The prefactor $1/n_b$ shown explicitly again justifies the weak-field approximation. With this form of the perturbation to the pair probability in Fourier space, we can obtain the static structure factor of this one-component fluid defined by $S(\mathbf{k}) = 1 + n_b \int_V [g(\mathbf{r}_p) - 1] e^{-i\mathbf{k}\cdot\mathbf{r}_p} d\mathbf{r}_p = 1 + n_b \hat{h}_f(\mathbf{k})$ [20] directly. When $\mathbf{k} \to 0$ we have $\hat{G}(\mathbf{0}) = 1$ and $S(\mathbf{0}) = 0$, which is consistent with the physical argument that each core in a solventless system must exclude one neighbor. The radial distribution function or the pair probability $g(\mathbf{r}_p)$ can be calculated by taking an inverse Fourier transform of $\hat{h}_f(\mathbf{k})$.

Figure 3.2 shows the scaled perturbation to the pair probability $\tilde{h}_f\,(= n_b h_f)$ and the static structure factor $S(k)$ for point NOHMs. The perturbation to the pair probability yields a decrease in the number of near neighbors and a slight increase in the number of neighbors at a distance of about three radii of gyration

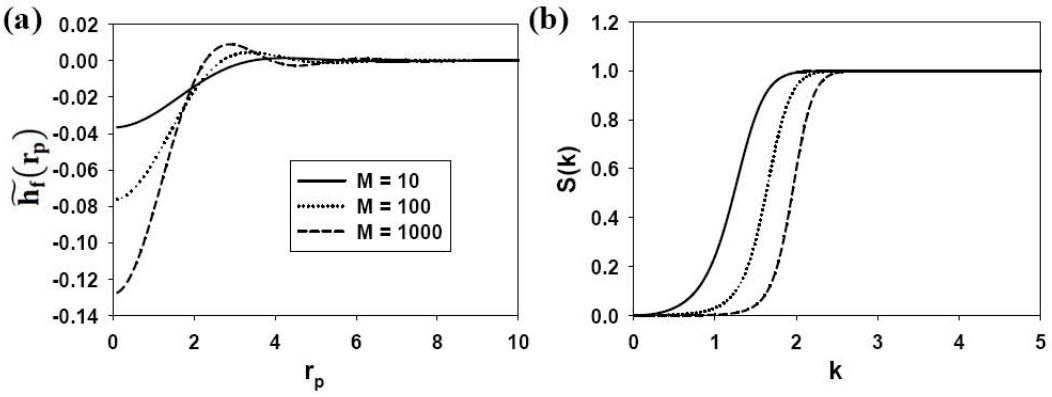

Figure 3.2: (a) The scaled perturbation to the pair probability $\tilde{h}_f$ (= $n_b h_f$) as a function of the interparticle distance r_p and (b) the static structure factor S as a function of the wave number k for the point NOHMs model. M is the number of oligomers per core.

of the oligomers. As one might expect, these features become more pronounced as the number of oligomers per particle M is increased. Although we choose R_g to be the characteristic length scale quantifying the range of field interactions without treating the chain configurations explicitly, the "stronger" field observed in $\tilde{h}_f$ for more number of chains per core could also be rationalized by the more uniformly stretched oligomer brush resulting in a more structured pair probability. The decrease in the pair distribution function is relatively modest even when scaled with $1/n_b$. However, the deficit extends to sufficiently large distances allowing its volume integral to reach minus one so that each particle excludes one neighbor and $S(k = 0) = 0$. This may be seen in Fig. 3.2(b) where the static structure factor is plotted as a function of k for various M. In a suspension of point particles without tethered molecules $S = 1$ throughout space. The onset of the deficit of neighboring particles, corresponding to a decrease in S with decreasing k occurs at larger k values for larger M due to the stronger effects from the oligomers.

3.3.2 Finite-Core NOHMs

In this section, we model the structure of a suspension of NOHMs with finite cores having radius a and core volume fraction ϕ_b with bead-spring oligomers tethered to the centers of the cores as illustrated in Fig. 3.1(b). We consider linear springs whose rest length may be either zero or the core radius a. The spring energy of the springs with a rest length of a is $F_{\text{spring}} = \frac{1}{2}\xi(r^* - a)^2$. The normalization of the configurational probability of the oligomers and the definition of the mean-square distance of the chain from the center of the core are given by Eq. 3.1 and the first equality in Eq. 3.2. We will continue to use the radius of gyration of an ideal unattached spring with rest length zero and spring constant ξ, i.e., $R_g = (k_B T/2\xi)^{1/2}$, to parameterize the stiffness of the oligomers even when discussing results for springs with rest length a.

We will consider the limit in which the radius of gyration is large compared with the core radius $R_g^3 \gg a^3$ and moderate core volume fractions $\phi_b \sim O(1)$. These conditions imply that $n_b^* R_g^3 = n_b \gg 1$ so that there are many neighboring particles within the distance R_g as there were in the point NOHMs model. The oligomers again cross many neighboring cores as illustrated in Fig. 3.1(a). In evaluating the pair distribution function, we can separate two length scales: the length scale a over which hard-core interactions influence the distribution of neighboring cores and the length scale R_g where most of a chosen particle's oligomers lie and over which those oligomers influence the probability of finding neighboring cores. Over the length scale R_g characteristic of the oligomer concentration field C_i we can neglect the hard-core correlations and assume that the cores simply fill a fraction ϕ_b of the volume.

The condition $n_b \gg 1$ allows us to use a weak-field approximation in de-

termining the oligomer concentration field, neglecting correlations smaller than $O(1/n_\mathrm{b})$ as was done in the point NOHMs model. The determination of the oligomer concentration field and the free energy due to the oligomers is then nearly identical to the treatment of the point NOHMs model in the previous section. We formulate the oligomer free energy and minimize it subject to constraints of normalization of the concentration of oligomers attached to a given core and incompressibility (or constant total oligomer concentration throughout space). This leads to a fluid phase free energy of the form of Eq. 3.3 except that the spring energy is now $\int_V \frac{1}{4}\left(|\mathbf{r}-\mathbf{r}_i| - \frac{a}{R_\mathrm{g}}\right)^2 C_i(\mathbf{r},\mathbf{r}_i)\mathrm{d}\mathbf{r}$ for the case where the rest length of the spring is a. The Lagrangian is still of the form Eq. 3.6 and the minimization of the Lagrangian $\delta L_\mathrm{f}/\delta C_i(\mathbf{r},\mathbf{r}_i) = 0$ for a given particle configuration again yields the concentration field in the form of Eq. 3.7, where $G(\mathbf{r}-\mathbf{r}_i) = K_1 e^{-\frac{1}{4}\left(|\mathbf{r}-\mathbf{r}_i|-\frac{a}{R_\mathrm{g}}\right)^2}$ with K_1 being the normalization constant for G. Because most of the oligomers attached to a test particle are at an $O(R_\mathrm{g})$ distance from the particle center we can allow G and the field variables Λ_i and B to be non-zero even within the core while making a small $O(a^3/R_\mathrm{g}^3)$ error in the free energy. Applying the conditional ensemble average to the total concentration shown in Eq. 3.5 yields the incompressibility constraint Eq. 3.8.

To obtain an analytical solution to the oligomer concentration equations, we can exploit the limits $R_\mathrm{g}^3 \gg a^3$ and $n_\mathrm{b} \gg 1$, as we did for the point NOHMs model, to assume small perturbations from uniform fields, i.e., $\Lambda_i = 1 + \Lambda_i'$ and $B(\mathbf{r}) = 1 + B'(\mathbf{r})$ with Λ_i' and $B'(\mathbf{r})$ being of $O(a^3/R_\mathrm{g}^3)$. Neglecting the higher order correlations between the field variables as before, we can write $\langle C_1\rangle_1(\mathbf{r}|\mathbf{r}_1)$ and $\langle C_2\rangle_2(\mathbf{r}|\mathbf{r}_1,\mathbf{r}_2)$ as Eqs. 3.9 and 3.10. The incompressibility condition, Eq. 3.8, involves the pair distribution function, which is now influenced by both hard-core and oligomer-mediated core–core interactions. However, we will see that

the weak oligomer fields imply that the pair probability can also be assumed to have a small $h_f = O(a^3/R_g^3)$ perturbation from a reference hard sphere distribution so that

$$g(\mathbf{r}_2 - \mathbf{r}_1) = 1 + h_{HS}(\mathbf{r}_2 - \mathbf{r}_1) + h_f(\mathbf{r}_2 - \mathbf{r}_1), \tag{3.23}$$

where h_{HS} is the total correlation function of the reference hard sphere suspension without the oligomers. Substituting Eqs. 3.9–3.12 and 3.23 into the incompressibility constraint (Eq. 3.8) results in $O(R_g^3/a^3)$ and $O(1)$ equations that relate the field variables and the core pair probability. Specifically, the $O(1)$ equation is written as

$$G(\mathbf{r} - \mathbf{r}_1) + n_b \int_V [\langle \Lambda_2' \rangle_1(\mathbf{r}_2|\mathbf{r}_2) + \langle \Lambda_2'' \rangle_2(\mathbf{r}_2|\mathbf{r}_1, \mathbf{r}_2) + \langle B' \rangle_1(\mathbf{r}|\mathbf{r}_1) + \langle B' \rangle_1(\mathbf{r}|\mathbf{r}_2) + h_{HS}(\mathbf{r}_2 - \mathbf{r}_1) + h_f(\mathbf{r}_2 - \mathbf{r}_1)] G(\mathbf{r} - \mathbf{r}_2) d\mathbf{r}_2 = 0. \tag{3.24}$$

While h_f is $O(a^3/R_g^3)$ smaller than h_{HS}, h_f extends over a volume of order R_g^3 and h_{HS} extends only over a volume of order a^3, so that both terms make contributions of the same order to the Fourier transform of the field variables and to the static structure factor. Application of the normalization conditions for $\langle C_1 \rangle_1$ and $\langle C_2 \rangle_2$ and Fourier transformation of Eq. 3.24 eventually lead to

$$\langle \hat{B}' \rangle_1(\mathbf{k}) = \frac{\hat{G}(\mathbf{k}) \left[1 + n_b \hat{h_{HS}}(\mathbf{k}) + n_b \hat{h_f}(\mathbf{k}) \right]}{n_b \left[\hat{G}(\mathbf{k})^2 - 1 \right]}. \tag{3.25}$$

$\langle \hat{\Lambda_2''} \rangle_2(\mathbf{k})$ and $\langle \Lambda_i' \rangle_1(\mathbf{r}_i|\mathbf{r}_i)$ have the same relations (Eqs. 3.14 and 3.15) to $\langle \hat{B}' \rangle_1(\mathbf{k})$ as the point NOHMs model.

We again apply a density functional approach to solve for the radial distribution function. The grand potential Ω is similar to the point NOHMs model except that the excess free energy now has two terms: one is contributed from the hard spheres $F_{ex}^{HS}[n(\mathbf{r}_p)]$ and the other caused by the tethered oligomers filling the interparticle space $F_{ex}^{fluid}[n(\mathbf{r}_p)]$. Also, the grand potential now includes an

external potential due to the hard-sphere excluded volume of the fixed *chosen* particle, $V_1(\mathbf{r}_p)$. Thus, the grand potential is

$$\Omega\left[n(\mathbf{r}_p)\right] = F_{id}\left[n(\mathbf{r}_p)\right] + F_{ex}^{HS}\left[n(\mathbf{r}_p)\right] + F_{ex}^{fluid}[n(\mathbf{r}_p)] + \int_V n(\mathbf{r}_p)\left[V_1(\mathbf{r}_p) - \mu\right]d\mathbf{r}_p \quad (3.26)$$

with F_{ex}^{fluid} being of the same form as Eq. 3.18 except that the spring energy of the oligomers attached to the fixed particle is now $\int_V \left[\frac{1}{4}\left(|\mathbf{r}| - \frac{a}{R_g}\right)^2 - 1\right]\langle C_1\rangle_1(\mathbf{r}|\mathbf{0})d\mathbf{r}$ and the spring energy of the oligomers attached to all the other particles is $\int_V n(\mathbf{r}_p)\int_V \left[\frac{1}{4}\left(|\mathbf{r} - \mathbf{r}_p| - \frac{a}{R_g}\right)^2 - 1\right]\langle C_2\rangle_2(\mathbf{r}|\mathbf{0}, \mathbf{r}_p)d\mathbf{r}d\mathbf{r}_p$ if the rest length of the spring is a. The ideal gas free energy of the cores $F_{id}[n(\mathbf{r}_p)]$ also remains the same as Eq. 3.17. The minimization $\delta\Omega[n(\mathbf{r}_p)]/\delta n(\mathbf{r}_p) = 0$ and application of equal chemical potential of the neighboring particles, $\mu = \mu_{bulk} = \mu|_{\mathbf{r}_p\to\infty}$, yield

$$n(\mathbf{r}_p) = n_b g(\mathbf{r}_p) = n_b \exp\left\{c_{HS}^{(1)}(\mathbf{r}_p) - c_{HS,b}^{(1)} - \frac{V_1(\mathbf{r}_p)}{k_B T} + c_f^{(1)}(\mathbf{r}_p) - c_{f,b}^{(1)}\right\}, \quad (3.27)$$

where $c_{HS}^{(1)}(\mathbf{r}_p) = -\frac{\delta\left(F_{ex}^{HS}[n(\mathbf{r}_p)]/k_B T\right)}{\delta n(\mathbf{r}_p)}$, $c_{HS,b}^{(1)} = -\frac{\delta\left(F_{ex}^{HS}[n(\mathbf{r}_p)]/k_B T\right)}{\delta n(\mathbf{r}_p)}|_{\mathbf{r}_p\to\infty}$, $c_f^{(1)}(\mathbf{r}_p) = -\frac{\delta\left(F_{ex}^{fluid}[n(\mathbf{r}_p)]/k_B T\right)}{\delta n(\mathbf{r}_p)}$, and $c_{f,b}^{(1)} = -\frac{\delta\left(F_{ex}^{fluid}[n(\mathbf{r}_p)]/k_B T\right)}{\delta n(\mathbf{r}_p)}|_{\mathbf{r}_p\to\infty}$. Equation 27 implies that the pair probability can be expressed in the form $g(\mathbf{r}_p) = g_{HS}(\mathbf{r}_p)g_f(\mathbf{r}_p)$, where $g_{HS}(\mathbf{r}_p) = e^{\left[c_{HS}^{(1)}(\mathbf{r}_p) - c_{HS,b}^{(1)} - \frac{V_1(\mathbf{r}_p)}{k_B T}\right]} = 1 + h_{HS}(\mathbf{r}_p)$ is the radial distribution function of the reference hard sphere suspension with $h_{HS}(\mathbf{r}_p)$ being the corresponding total correlation function, and $g_f(\mathbf{r}_p) = e^{\left[c_f^{(1)}(\mathbf{r}_p) - c_{f,b}^{(1)}\right]} = 1 + h_f(\mathbf{r}_p)$ can be viewed as an additional factor accounting for the change in the apparent core radial distribution function relative to the bare hard spheres due to the tethered oligomer fluid with $h_f(\mathbf{r}_p)$ being the total correlation function contributed from the oligomers. If we expand the product and write $g(\mathbf{r}_p) = 1 + h_{HS}(\mathbf{r}_p) + h_{HS}(\mathbf{r}_p)h_f(\mathbf{r}_p) + h_f(\mathbf{r}_p)$, we can see that $h_{HS}(\mathbf{r}_p)h_f(\mathbf{r}_p)$ is smaller than $h_{HS}(\mathbf{r}_p)$ in the inner region and negligible in the outer region where $h_f(\mathbf{r}_p)$ dominates. Therefore we can neglect the cross term and obtain an expression for $g(\mathbf{r}_p)$ that is consistent with the form Eq. 3.23 assumed based on the regular perturbation expansion. Meanwhile, the separation

of length scales implies that the change in $F_{\text{ex}}^{\text{HS}}[n(\mathbf{r}_\text{p})]$ due to variations in $h_\text{f}(\mathbf{r}_\text{p})$ is only an $O(a^3/R_\text{g}^3)$ perturbation to the change in $F_{\text{ex}}^{\text{HS}}[n(\mathbf{r}_\text{p})]$ due to variations in $h_{\text{HS}}(\mathbf{r}_\text{p})$ at separations of $O(a)$; while the change in $F_{\text{ex}}^{\text{fluid}}[n(\mathbf{r}_\text{p})]$ due to variations of $h_{\text{HS}}(\mathbf{r}_\text{p})$ is essentially zero on the length scale of R_g because $h_{\text{HS}}(\mathbf{r}_\text{p} \to \infty) \to 0$. By keeping the dominant contributions from these variations of the free energy we conclude that $c_\text{f}^{(1)}(\mathbf{r}_\text{p}) \approx -\frac{\delta\left(F_{\text{ex}}^{\text{fluid}}[n(\mathbf{r}_\text{p})]/k_\text{B}T\right)}{n_\text{b}\delta h_\text{f}(\mathbf{r}_\text{p})}$ and $c_{\text{HS}}^{(1)}(\mathbf{r}_\text{p}) \approx -\frac{\delta\left(F_{\text{ex}}^{\text{HS}}[n(\mathbf{r}_\text{p})]/k_\text{B}T\right)}{n_\text{b}\delta h_{\text{HS}}(\mathbf{r}_\text{p})}$. This is equivalent to neglecting the coupling between g_{HS} and g_f. Thus, we can use standard approaches in the literature to solve for g_{HS} without considering the effects due to the oligomer configuration. Conventional density functional approaches such as the weighted-density approximations (WDA) have been used to solve for g_{HS} [26]. However, instead of using a density functional approach for g_{HS} in this article, we directly evaluate it by solving the Ornstein–Zernike equation with the Percus–Yevick approximation [20, 27]. Using the weak-field approximation, we can linearize the expression for g_f and obtain:

$$h_\text{f}(\mathbf{r}_\text{p}) \approx c_\text{f}^{(1)}(\mathbf{r}_\text{p}) - c_{\text{f,b}}^{(1)}. \tag{3.28}$$

Substitution of the field variables Λ_i and $B(\mathbf{r})$ into $F_{\text{ex}}^{\text{fluid}}[n(\mathbf{r}_\text{p})]/k_\text{B}T$ shown in Eq. 3.18, truncation of the higher order correlations between the particles, and functional differentiation $\frac{\delta\left(F_{\text{ex}}^{\text{fluid}}[n(\mathbf{r}_\text{p})]/k_\text{B}T\right)}{n_\text{b}\delta h_\text{f}(\mathbf{r}_\text{p})}$ finally yield h_f in the same form as Eq. 3.21. After making use of the convolution theorem and the expressions for $\langle\hat{B}'\rangle_1(\mathbf{k})$ and $\langle\hat{\Lambda_2''}\rangle_2(\mathbf{k})$, in Fourier space we obtain

$$\hat{h_\text{f}}(\mathbf{k}) = -\frac{2M}{n_\text{b}}\left\{\frac{\hat{G}(\mathbf{k})^2\left[1 + n_\text{b}\hat{h_{\text{HS}}}(\mathbf{k})\right]}{1 - \hat{G}(\mathbf{k})^2 + 2M\hat{G}(\mathbf{k})^2}\right\}. \tag{3.29}$$

The static structure factor is now defined by $S(\mathbf{k}) = 1 + n_\text{b}\hat{h_{\text{HS}}}(\mathbf{k}) + n_\text{b}\hat{h_\text{f}}(\mathbf{k})$ and $S(\mathbf{0}) = 0$.

Results for the radial distribution function and static structure factor for finite-core NOHMs with the model of zero-rest-length springs are shown in

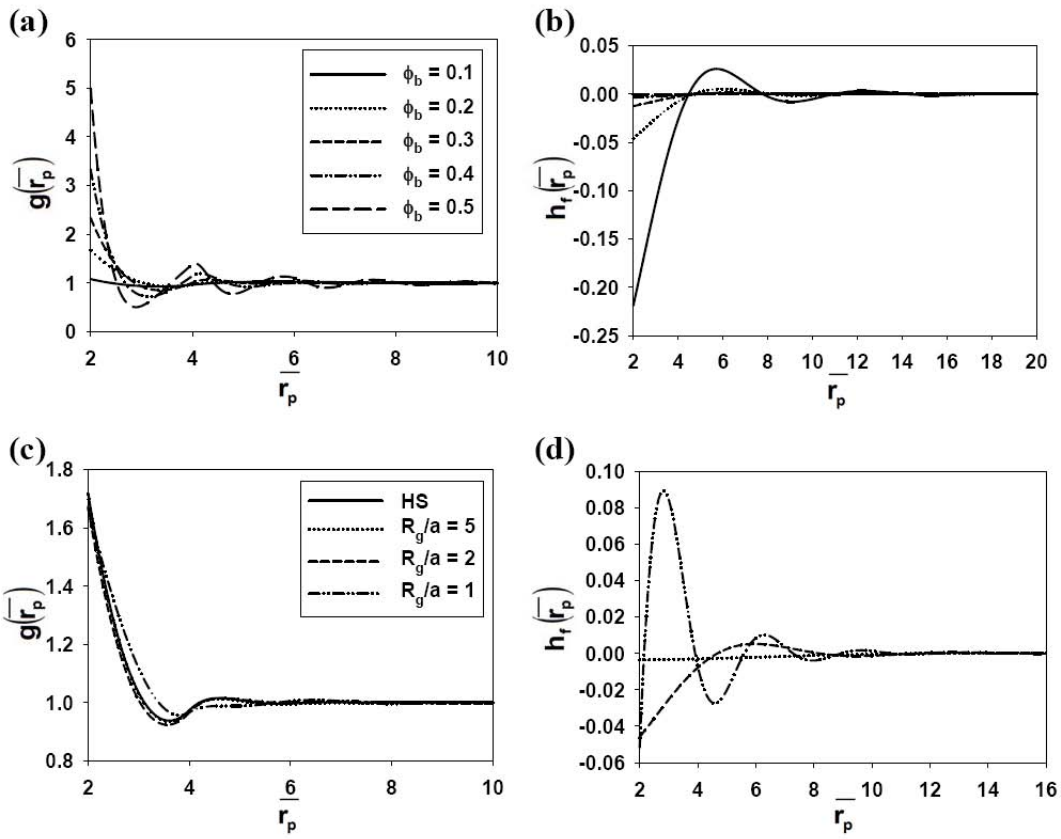

Figure 3.3: Results are for the finite-core NOHMs model with zero-rest-length springs: (a) The radial distribution function g as a function of the interparticle distance non-dimensionalized by the core radius, $\bar{r}_p$, for different core volume fractions with $R_g/a = 2$ and (b) the corresponding perturbation to the pair probability due to the oligomers, h_f, with the same parameters and curve descriptions as given in (a). (c) The comparison of g for different R_g/a and for a reference hard sphere suspension. The core volume fraction is 0.2. (d) The corresponding comparison of h_f.

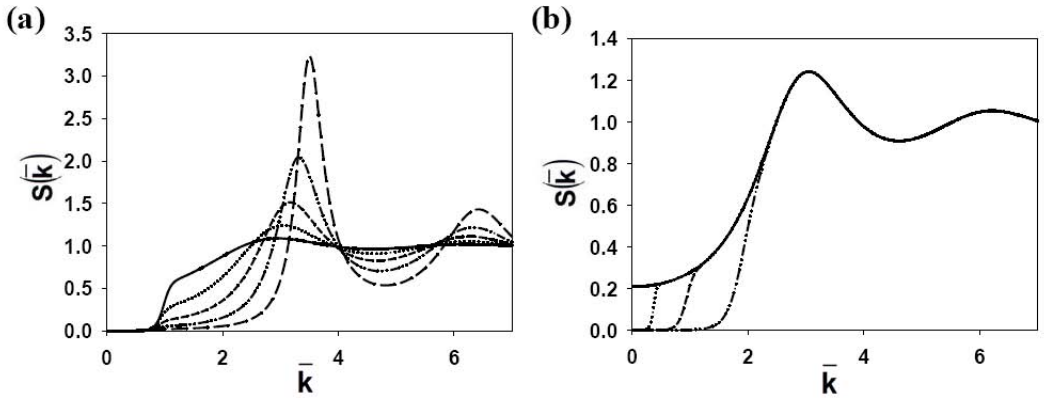

Figure 3.4: (a) The static structure factor S for the finite-core NOHMs with zero-rest-length oligomers as a function of the wave number non-dimensionalized by the inverse core radius, $\bar{k}$, for different core volume fractions with $R_g/a = 2$. The lines are defined as in Fig. 3.3(a). (b) The comparison of S for finite-core NOHMs with different R_g/a ratios and the reference hard sphere suspension for a core volume fraction of 0.2. The lines are defined as in Fig. 3.3(c).

Figs. 3.3 and 3.4. To observe the hard-core contributions in a familiar way, the results are plotted as a function of the distance or wave number scaled by a. The core radial distribution functions in Fig. 3.3(a) exhibit peaks similar to the hard sphere distribution. From the perturbation to the core pair probability h_f plotted in Fig. 3.3(b) we can see that the oligomer effects increase as the core volume fraction decreases. Experimentally [4], for a fixed molecular weight of the tethered chains, the grafting density of the chains per particle changes when the weight percentage of the cores varies so that the oligomer fluid fills the space and yields a nearly constant fluid number density. Therefore, in the following calculations for the finite-core NOHMs model, we choose the number of oligomers per core as 600 when $\phi_b = 0.15$ to be consistent with the experiment and fix the fluid number density based on this chosen value; when we change the core volume fraction the number of oligomers per core changes accordingly.

When the core volume fraction is lower we have more oligomer beads per particle so the field produced by the space-filling oligomers is more substantial and we obtain a stronger exclusion from the fixed particle. The effects of the oligomers on the static structure factor are more striking than their effects on the pair distribution function. In Fig. 3.4(a) we find two distinct length scales in the static structure factor. For large $\bar{k}$ values, the hard-core correlations dominate corresponding to the length scale of a; for small $\bar{k}$ values, a continuous deficit of the particles around the fixed particle due to the space-filling oligomers takes place on the length scale of R_g and enforces a zero $S(0)$. To probe the change in the structure due to the oligomer stiffness, we compare results with different oligomer radii of gyration and the purely hard spheres for a given ϕ_b in Fig. 3.3(c). The first peaks in $g(\bar{r}_p)$ for NOHMs are slightly damped implying that the oligomers produce a *softened* potential. This *softening* becomes more important when R_g/a is smaller because the effects of stiffer oligomers are stronger. This can be confirmed by observing the perturbation to the core pair probability h_f presented in Fig. 3.3(d). As R_g/a decreases h_f becomes more and more important and the positions of the peaks change with R_g. This can be rationalized by noting that, when R_g is shorter, the exclusion due to the fixed particle becomes more significant but on the other hand the entropic penalty of the oligomers makes a positive contribution to the probability of finding neighboring particles at close separation from the fixed particle. The corresponding $S(\bar{k})$ results for different radii of gyration in Fig. 3.4(b) show two distinct length scales as in Fig. 3.4(a), characterizing different contributions from hard-core correlations and space-filling oligomers. Once more, we see $S(0) = 0$ for finite-core NOHMs. It is noteworthy that $S(0)$ for the reference hard sphere suspension with the same ϕ_b does not go to zero. One can make it closer to zero by increasing the

core volume fraction but in general $S(0)$ is never zero for hard spheres immersed in a solvent. The continuous deficit of neighboring particles occurs at a higher $\bar{k}$ when R_g/a is smaller showing a stronger penetration of the oligomer effects into the region where hard-core correlations occur if the oligomers are stiffer. Of course, the perturbation analysis will become less accurate as R_g/a decreases but the model still provides physically reasonable results and we plan to test its accuracy by comparison with molecular dynamics simulations in a future study.

One might imagine that experimentally a slight deviation of $S(0)$ from zero could occur due to the intrinsic polydispersity in the core size and variations in the surface grafting density of the chains. We expect that a deficit in $S(k)$ would still occur in a polydisperse system at a similar length scale to that for a monodisperse system even if $S(0)$ deviates from zero, because this length scale is controlled by the oligomer chain length. In a future study, we will consider a NOHMs system with a bidispersity in the core size as well as the chain grafting density and compare with experimental measurements.

The constraint that the cores and oligomers must fill the volume of the suspension implies that the grafting density M in an experimental system must be changed while changing the particle volume fraction ϕ_b at fixed R_g/a. We took account of this effect in our calculations. The change in the volume filled by polymers with different R_g implies that M in an experimental system must also decrease with increasing R_g by an amount that depends on such details as the size of the monomer, the number of monomers per Kuhn step, and the number of Kuhn steps per oligomer. For simplicity, we have neglected this change in grafting density M with R_g in our calculations. From the results in Fig. 3.2 for the point NOHMs system, one can see that the effect of M on the structure is

weaker than the effect of R_g, so that the results in Figs. 3.3(c), 3.3(d), and the following Figs. 3.5 and 3.6 would not be substantially altered by accounting for the changes in grafting density.

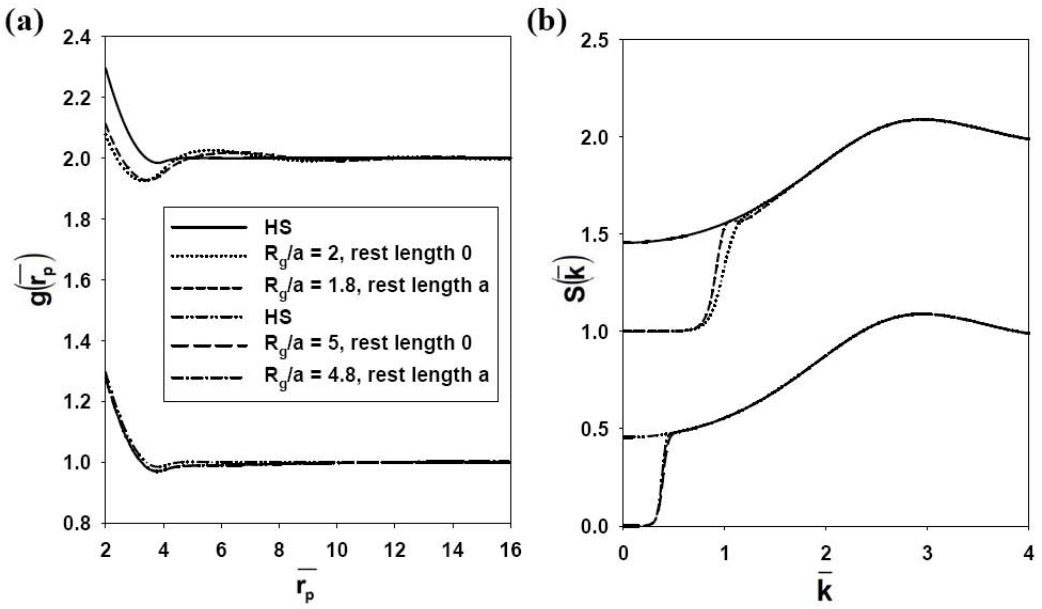

Figure 3.5: (a) The comparison of the radial distribution function g as a function of the interparticle distance $\bar{r}_p$ for models with different spring rest lengths for two R_g/a ratios and the reference hard sphere suspension when $\phi_b = 0.1$. The value of R_g/a for the model with non-zero rest length is adjusted so that the two models yield the same mean-square distance of the beads from the core center. (b) The corresponding comparison of the static structure factor S as a function of the wave number $\bar{k}$ with the same parameters and line definitions as in (a). The curves for different R_g are shifted vertically by 1 for clarity.

The qualitative behavior we have discussed remains the same for the model with the rest length of the springs being the core radius a. To make a reasonable comparison, the radii of gyration for the two models are chosen such that the calculated mean-square distances of the chain from the core center as defined by the first equality in Eq. 3.2 are the same. After calibrating the radius of gyra-

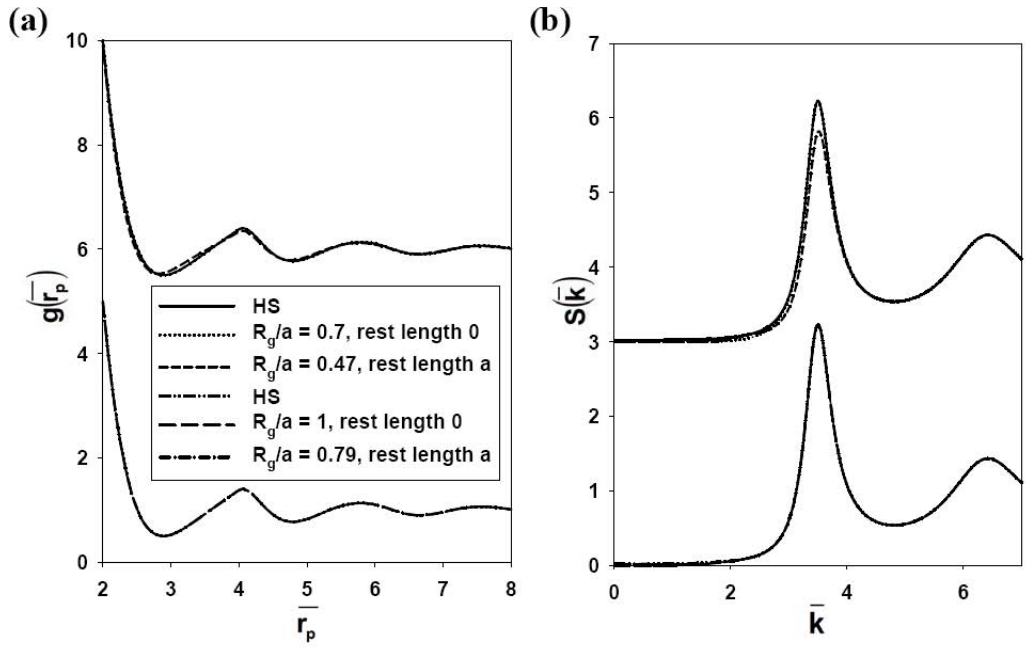

Figure 3.6: (a) The comparison of the radial distribution function g as a function of the interparticle distance $\bar{r}_{\mathrm{p}}$ for models with different spring rest lengths for two R_{g}/a ratios and for the reference hard sphere suspension when $\phi_{\mathrm{b}} = 0.5$. (b) The corresponding comparison of the static structure factor S as a function of the wave number $\bar{k}$ for the same parameters and line definitions as in (a). The curves for different R_{g} are shifted vertically by 5 for (a) and by 3 for (b).

tion, we can see that the two models give very similar results. The difference in the quantitative results for the two models becomes more and more negligible when we have longer oligomers or higher core volume fractions. Specifically, we compare the two models for two different oligomer radii of gyration and the reference hard sphere system for $\phi_{\mathrm{b}} = 0.1$ in Fig. 3.5. When the mean-square distance is chosen such that $R_{\mathrm{g}}/a = 5$ for the model with zero rest length springs, the two models exhibit basically the same g and S; when $R_{\mathrm{g}}/a = 2$ for the zero-rest-length-spring model, the $S(k)$ plot exhibits an offset in the wave number at which the deficit of particles occurs and a slight phase shift and change in peak

heights in g. If we push our calculations further to even smaller R_g/a values, as can be seen from Fig. 3.6, when $\phi_b = 0.5$ the two models predict very similar structure of finite-core NOHMs. While differences in g and S are observable for the case of $R_g/a = 0.7$ for the zero-rest-length-spring model, the results for the two models basically coincide when $R_g/a = 1$. In this figure, the static structure factor for the reference hard spheres show small but non-zero $S(0)$ because the core volume fraction is relatively high.

3.4 Conclusions

We have formulated a density functional approach to address the structure of a suspension of solvent-free nanoparticle–organic hybrid materials. Distinct from conventional theoretical treatments of equilibrium properties for complex materials in which a pairwise-additive potential is assumed, we propose a direct description of the fluid phase free energy functional as a mediated interparticle potential. With the widely used coarse-grained models such as point particles or finite hard cores with bead-spring oligomers attached, the radial distribution function and the static structure factor are solved in a quasi-analytical fashion exploiting a limit where the radius of gyration of the oligomers is large compared with the interparticle spacing. A simple estimate based on a typical oligomer's isothermal compressibility indicates that the mediate oligomer fluid is incompressible with a constant fluid number density. The effects due to these space-filling oligomers on the nanostructure become more substantial when the ratio between the oligomer radius of gyration and the core radius is smaller and/or the volume fraction of the core is lower. Under all conditions of core volume fraction and oligomer radius of gyration, the static structure

factor goes to zero for zero wave number. This reflects the fact that a particle carries its share of the fluid with it so that the particle and its oligomers fill a volume of space that excludes exactly one neighboring particle. While this situation is surprising from the perspective of colloidal science where particle cores typically exhibit non-zero $S(0)$ it is not surprising to the thermodynamicist who realizes that the nanoparticle–organic hybrid suspension constitutes an *incompressible single-component fluid*. Given a radial distribution function, one can also get insight into the non-pairwise-additive interparticle potential in such solventless systems by direct calculation of the potential of mean force defined by $\frac{V_{\mathrm{mf}}(\bar{r}_{\mathrm{p}})}{k_{\mathrm{B}}T} = -\ln g(\bar{r}_{\mathrm{p}})$ [20, 27]. V_{mf} therefore depends on the geometric parameters such as the core volume fraction, surface grafting density of the chains as well as the size ratio between the chains and the cores.

BIBLIOGRAPHY

[1] A. B. Bourlinos, R. Herrera, N. Chalkias, D. D. Jiang, Q. Zhang, L. A. Archer, and E. P. Giannelis, Adv. Mater. **17**, 234 (2005).

[2] A. B. Bourlinos, S. R. Chowdhury, R. Herrera, D. D. Jiang, Q. Zhang, L. A. Archer, and E. P. Giannelis, Adv. Funct. Mater. **15**, 1285 (2005).

[3] A. B. Bourlinos, E. P. Giannelis, Q. Zhang, L. A. Archer, G. Floudas, and G. Fytas, Eur. Phys. J. E **20**, 109 (2006).

[4] R. Rodriguez, R. Herrera, L. A. Archer, and E. P. Giannelis, Adv. Mater. **20**, 4353 (2008).

[5] P. Agarwal, H. Qi, and L. A. Archer, Nano Lett. **10**, 111 (2010).

[6] W. B. Russel, D. A. Saville, and W. R. Schowalter, *Colloidal Dispersions*, Cambridge University Press, New York, 1989.

[7] M. Z. Yates, P. S. Shah, K. P. Johnston, K. T. Lim, and S. Webber, J. Colloid Interface Sci. **227**, 176 (2000).

[8] C. J. Drummond and D. Y. C. Chan, Langmuir **13**, 3890 (1997).

[9] C. M. Wijmans and E. B. Zhulina, Macromolecules **26**, 7214 (1993).

[10] E. K. Lin and A. P. Gast, Macromolecules **29**, 390 (1996).

[11] C. Singh, G. T. Pickett, E. B. Zhulina, and A. C. Balazs, J. Phys. Chem. B **101**, 10614 (1997).

[12] M. Surve, V. Pryamitsyn, and V. Ganesan, Langmuir **22**, 969 (2006).

[13] T. A. Witten and P. A. Pincus, Macromolecules **19**, 2509 (1986).

[14] P. A. Pincus, Macromolecules **24**, 2912 (1991).

[15] M. Badia, M. Benhamou, A. Derouiche, and J. L. Bretonnet, Colloid Polym. Sci. **279**, 763 (2001).

[16] C. M. Marques, D. Izzo, T. Charitat, and E. Mendes, Eur. Phys. J. B **3**, 353 (1998).

[17] E. B. Zhulina, T. M. Birshtein, and O. V. Borisov, Eur. Phys. J. E **20**, 243 (2006).

[18] A. Jayaraman and K. S. Schweizer, J. Chem. Phys. **128**, 164904 (2008).

[19] A. Jayaraman and K. S. Schweizer, Langmuir **24**, 11119 (2008).

[20] J.-P. Hansen and I. R. McDonald, *Theory of Simple Liquids*, Academic Press, London, 3 edition, 2006.

[21] M. R. Wilson, A. B. Thomas, M. Dennison, and A. J. Masters, Soft Matter **5**, 363 (2009).

[22] B. Bozorgui, M. Sen, W. L. Miller, J. C. Pàmies, and A. Cacciuto, J. Chem. Phys. **132**, 014901 (2010).

[23] I. C. Sanchez and J. Cho, Polymer **36**, 2929 (1995).

[24] J. K. Percus, Phys. Rev. Lett. **8**, 462 (1962).

[25] J. L. Lebowitz and J. K. Percus, J. Math. Phys. **4**, 248 (1963).

[26] D. Henderson, editor, *Fundamentals of Inhomogeneous Fluids*, Marcel Dekker, New York, 1992.

[27] D. A. McQuarrie, *Statistical Mechanics*, University Science Books, Sausalito, 2000.

[28] D. J. Jeffrey, Proc. R. Soc. London, Ser. A **335**, 355 (1973).

[29] E. J. Hinch, J. Fluid Mech. **83**, 695 (1977).

[30] D. L. Koch and J. F. Brady, J. Fluid Mech. **154**, 399 (1985).

CHAPTER 4

STRUCTURE FACTOR OF SOLVENT-FREE BINARY NANOPARTICLE–ORGANIC HYBRID MATERIALS

4.1 Abstract

We derive the apparent static structure factor for the core particles in model bidisperse nanoparticle–organic hybrid materials using a density-functional theory. The system consists of nanoparticles and tethered incompressible oligomers in the absence of an intervening solvent. While for a monodisperse system the materials can be viewed as an incompressible single component fluid showing zero structure factor at zero wave number, variations of the core size or the oligomer grafting density on the particle surface yield variations in the tethered fluid volume per particle and distort the bulk structure at large length scales. The theory exploits the limit where the oligomer radius of gyration is much greater than the average core radius such that semi-analytic expressions for the oligomer concentration and the core distribution functions are accessible. The resulting structure factor exhibits non-zero value at zero wave number and bidispersity in the oligomer grafting density has stronger effects than bidispersity in the core radius.

4.2 Introduction

Nanoparticle–organic hybrid materials (NOHMs) contain inorganic nanocores surface functionalized by oligomeric chains in the absence of unattached sol-

vent molecules [1–5]. While these systems can be viewed as incompressible single-component fluids with the structural properties been well-described by a theoretical model of monodisperse hard cores, each of which is surrounded by its tethered fluid [6], the intrinsic polydispersity in the core size and variations in the oligomer surface grafting density lead to further structural complexity observed experimentally. In this work, we aim to formulate a density-functional theory for a bidisperse system of solventless NOHMs to demonstrate how the observed static structure factor can be affected by polydispersity.

In our recent paper [6], we developed a density-functional theory for monodisperse, pure NOHMs, in which we considered a coarse-grained model of hard spheres and bead-spring oligomers tethered to the centers of cores with one bead per chain and the stiffness of the linear spring being described by the oligomer radius of gyration. When the oligomer radius of gyration is much greater than the core radius, many particles contribute oligomers to any fluid volume such that the effect of each particle on the local oligomer concentration is weak. With the aid of a regular perturbation analysis under this weak-field approximation, the equilibrium configuration of the tethered oligomers and the core distribution function were obtained analytically by free energy minimization subject to the constraints of normalization and incompressibility of oligomers. Since each particle carries its own share of fluid with it, the particle and its oligomers form an entity that fills a volume of space excluding exactly one neighboring particle. Therefore the resulting static structure factor $S(k)$, defined by $S(\mathbf{k}) = 1 + n_\mathrm{b} \int \left[g(\mathbf{r}_\mathrm{p}) - 1 \right] e^{-i\mathbf{k}\cdot\mathbf{r}_\mathrm{p}} \mathrm{d}\mathbf{r}_\mathrm{p}$ with n_b being the bulk number density of particles, $g(\mathbf{r}_\mathrm{p})$ being the radial distribution function, and r_p being the interparticle distance, approached zero at zero wave number k. However, experimentally there could be polydispersity in silica core radius (typically 10–20%)

as well as oligomer molecular weight ($\lesssim 10\%$) [4], and variations of oligomer grafting density. As a result, the system contains entities occupying an amount of space that is not proportional to their scattering volume. This leads to a deviation of $S(0)$ from zero for an apparent $S(k)$ defined on the basis of assuming a monodisperse system.

To address the deviation of $S(0)$ from zero due to polydispersity effects, for simplicity, we generalize the finite-core NOHMs model of our previous monodisperse theory to the one that considers a system of bidisperse, solvent-free NOHMs. As justified in the previous work, the oligomer radius of gyration affects the length scale at which we observe a drop in $S(k)$ denoting the deficit of neighboring particles but does not change $S(0)$, therefore we will only account for bidispersities in the core radius and the oligomer surface grafting density given an average radius of gyration. Of course, the molecular weight of oligomers also affects the oligomer volume. The effect on $S(0)$ due to variations of oligomer molecular weight is expected to be similar to the effect due to variations of oligomer grafting density in the sense of different fluid volumes. In section 4.3, we present a density-functional theory for a binary mixture of nanoparticles with different core radii and oligomer grafting densities. Similar to Ref. [6], we treat the oligomers as incompressible and first derive the oligomer concentration field around each type of particles by minimizing the total oligomer free energy for a given particle configuration subject to the normalization and incompressibility constraints. Application of the weak-oligomeric-field approximation allows us to relate the oligomer concentrations to the correlation functions of 1–1, 1–2, and 2–2 pairs and determine the apparent static structure factor that would be obtained in scattering experiments on NOHMs with bidispersity. In section 4.4, we present the calculated $S(k)$ and compare the effects for differ-

ent extents of bidispersity. Finally, we conclude our work in section 4.5.

4.3 Theory

We consider a system composed of hard cores of radii a_1 and a_2 with M_1 and M_2 identical bead-spring oligomers attached to the centers of cores, as depicted in Fig. 4.1(b). The oligomer grafting densities on the core surface are $\sigma_{s1} = M_1/(4\pi a_1^2)$ and $\sigma_{s2} = M_2/(4\pi a_2^2)$. We choose the component 2 to have the larger radius such that the ratio between the two radii is $\gamma = a_1/a_2$ with $0 \leq \gamma \leq 1$. Since the two components are of the same chemical species, it is reasonable to assume that the volumes of the two components are additive without any volume change of mixing. Given that the core volume fraction of component j is $\phi_j = (4\pi/3)a_j^3 n_j$ with n_j being the core number density of component j and $j = 1$ or 2, we obtain the volume-weighted average core radius, $a = \left[(a_1^3 n_1 + a_2^3 n_2)/n_b\right]^{1/3}$, and the average number of oligomers per core, $M = (n_1 M_1 + n_2 M_2)/n_b$, with $n_b = n_1 + n_2$ being the bulk number density of cores. Each oligomer has one monomer at the free end of the spring and the springs are linear, massless, and have a rest length of zero. The spring energy is $\frac{1}{4}\frac{k_B T}{R_g^2} r^2$ with r being the distance between the oligomer bead and the core center, k_B being the Boltzmann constant, T being the temperature, and the stiffness of the spring being characterized by the radius of gyration R_g of an ideal, unattached, linear chain. The probability distribution function of the bead, $G(\mathbf{r}) \sim e^{-\frac{r^2}{4R_g^2}}$, is normalized such that

$$\int_V G(\mathbf{r}) d\mathbf{r} = 1, \tag{4.1}$$

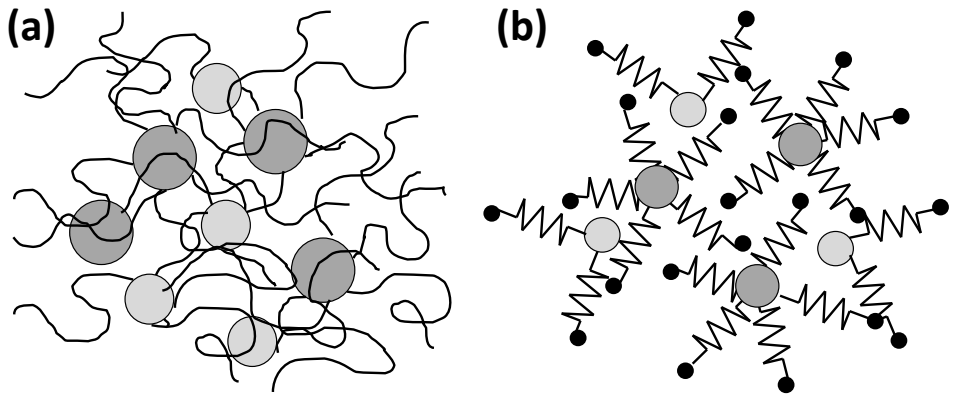

Figure 4.1: (a) A random array of particles of two different sizes with oligomers long enough to span cross over several particles. (b) Schematic of the coarse-grained model. The big central spheres with two different radii (a_1 and a_2) are the hard cores and the small beads represent the monomers. The monomers are connected to the core with springs and each spring has one monomer. The numbers of oligomers per particle for species 1 and 2 are adjustable variables M_1 and M_2.

and the mean-square distance of the bead from the core center in the absence of chain–chain interactions is

$$\langle r^2 \rangle = \int_V r^2 G(\mathbf{r}) \mathrm{d}\mathbf{r} = 6R_\mathrm{g}^2 \tag{4.2}$$

with V being the suspension volume.

When $R_\mathrm{g} \gg a$, the oligomers can cross several neighboring particles as shown in Fig. 4.1(a) such that many particles contribute their oligomers to fill any given fluid space. The theory exploits this weak-oligomeric-field limit in which we can separate the two length scales of R_g and a and make different approximations. For particle separations of order a hard-core correlations dominate since oligomers only contribute to a small perturbation while at separa-

tions of order R_g the interactions of oligomers dominate. In the latter region, we can neglect the detailed core–core correlations and assume that the particles simply fill a fraction $\phi_b = \phi_1 + \phi_2$ of the space. As shown in Ref. [6], the condition $n_b R_g^3 \gg 1$ also allows us to close the equations governing the oligomer concentrations and the core distribution functions by neglecting correlations smaller than $O(1/n_b R_g^3)$ or $O(a^3/R_g^3)$.

We assume that the tethered oligomers have a faster relaxation time than the cores such that for a given particle configuration the oligomers can reach an equilibrium. For a system of N_1 type 1 particles and N_2 type 2 particles with $N_1 + N_2 = N$, the fluid phase free energy from the oligomers is written as

$$\frac{F_f}{k_B T} = \sum_{j=1}^{2} \sum_{i=1}^{N_j} \int_V C_{j,i}(\mathbf{r}, \mathbf{r}_{j,i}) \left[\ln C_{j,i}(\mathbf{r}, \mathbf{r}_{j,i}) \Lambda_b^3 - 1 \right] + \frac{1}{4R_g^2} \left(\mathbf{r} - \mathbf{r}_{j,i} \right)^2 C_{j,i}(\mathbf{r}, \mathbf{r}_{j,i}) d\mathbf{r}, \quad (4.3)$$

where the first term represents the ideal gas Helmholtz free energy of the beads, the second term accounts for the spring energy, $C_{j,i}(\mathbf{r}, \mathbf{r}_{j,i})$ is the concentration field of the oligomers at $\mathbf{r}$ attached to particle i of type j, $\mathbf{r}_{j,i}$ is the position of particle i of type j, and Λ_b is the thermal de Broglie wavelength of the monomer beads.

At equilibrium, the concentration field of the oligomers is determined by minimizing the fluid phase free energy with respect to variations in $C_{j,i}$ subject to the constraints that the probability of finding the oligomers attached to each particle of type j is normalized,

$$\int_V C_{j,i}(\mathbf{r}, \mathbf{r}_{j,i}) d\mathbf{r} = M_j, \quad (4.4)$$

and the total monomer number density is a constant throughout the suspension (incompressibility condition),

$$C(\mathbf{r}) = \sum_{j=1}^{2} \sum_{i=1}^{N_j} C_{j,i}(\mathbf{r}, \mathbf{r}_{j,i}) = n_b M. \quad (4.5)$$

Making use of Lagrange undetermined multipliers for finding a minimum of a function subject to constraints leads to the following Lagrange function:

$$L_{\mathrm{f}}\left[C_{j,i}(\mathbf{r},\mathbf{r}_{j,i})\right] = \frac{F_{\mathrm{f}}}{k_B T} - \sum_{j=1}^{2}\sum_{i=1}^{N_j}\lambda_{j,i}\left[\int_V C_{j,i}(\mathbf{r},\mathbf{r}_{j,i})\mathrm{d}\mathbf{r} - M_j\right] - \int_V \beta(\mathbf{r})\left[\sum_{j=1}^{2}\sum_{i=1}^{N_j} C_{j,i}(\mathbf{r},\mathbf{r}_{j,i}) - n_{\mathrm{b}}M\right]\mathrm{d}\mathbf{r}, \tag{4.6}$$

where the Lagrange multipliers $\lambda_{j,i}$ enforcing the normalization make up a discrete set with one multiplier for each particle and the functional Lagrange multiplier $\beta(\mathbf{r})$ enforcing the incompressibility constraint ensures that the fluid number density at position $\mathbf{r}$ is equal to the average value, $n_{\mathrm{b}}M$. For a given particle configuration, the minimization $\delta L_f/\delta C_{j,i}(\mathbf{r},\mathbf{r}_{j,i})$ with the normalization condition yields

$$C_{j,i}(\mathbf{r},\mathbf{r}_{j,i}) = M_j\Lambda_{j,i}B(\mathbf{r})G(\mathbf{r}-\mathbf{r}_{j,i}), \tag{4.7}$$

where $B(\mathbf{r}) = e^{\beta(\mathbf{r})} = 1 + B(\mathbf{r})'$ accounts for the incompressibility, $G(\mathbf{r}-\mathbf{r}_{j,i}) = \left(4\pi R_{\mathrm{g}}^2\right)^{-\frac{3}{2}} e^{-\frac{\left(\mathbf{r}-\mathbf{r}_{j,i}\right)^2}{4R_{\mathrm{g}}^2}}$, and $\Lambda_{j,i} = 1 + \Lambda'_{j,i}$ accounts for the normalization of the oligomers attached to particle i of type j. The perturbations $B'(\mathbf{r})$ and $\Lambda'_{j,i}$ are $O(a^3/R_{\mathrm{g}}^3)$ when $R_{\mathrm{g}}^3 \gg a^3$.

Following Ref. [6], we specify the position of particle 1 of any given type as $\mathbf{r}_1$ and make it our *chosen* particle but consider all the other *non-chosen* particles labeled 2 as indistinguishable. The probability that the chosen particle is of type j is n_j/n_{b}; given the chosen particle of type 1, there will be distribution functions of non-chosen particles of types 1 and 2 relative to the chosen particle, and vice versa. We consider the case where the chosen particle is of type 1 and derive the expressions for the resulting field variables $B'(\mathbf{r})$ and $\Lambda'_{j,i}$. The symmetric case for a fixed type 2 particle would be similar. Applying the conditional ensemble average to Eq. 4.5 leads to an equation for the conditional average concentration

$\langle C\rangle_{1,1}(\mathbf{r}|\mathbf{r}_1)$ with one core particle of species 1 fixed at $\mathbf{r}_1$ that reads:

$$\begin{aligned}\langle C\rangle_{1,1}(\mathbf{r}|\mathbf{r}_1) &= \langle C_1\rangle_{1,1}(\mathbf{r}|\mathbf{r}_1) + n_1\int_V g_{11}(\mathbf{r}_2-\mathbf{r}_1)\langle C_2\rangle_{2,11}(\mathbf{r}|\mathbf{r}_1,\mathbf{r}_2)\mathrm{d}\mathbf{r}_2 \\ &\quad + n_2\int_V g_{12}(\mathbf{r}_2-\mathbf{r}_1)\langle C_2\rangle_{2,12}(\mathbf{r}|\mathbf{r}_1,\mathbf{r}_2)\mathrm{d}\mathbf{r}_2 \\ &= n_\mathrm{b}M, \end{aligned} \tag{4.8}$$

where $\langle C_1\rangle_{1,1}(\mathbf{r}|\mathbf{r}_1)$ is the conditional average of the concentration field of oligomers attached to particle 1 of type 1 given that particle 1 is fixed at $\mathbf{r}_1$, $\langle C_2\rangle_{2,11}(\mathbf{r}|\mathbf{r}_1,\mathbf{r}_2)$ is the conditional average of the concentration field of oligomers attached to particle 2 of type 1 given that particles 1 and 2 are fixed at $\mathbf{r}_1$ and $\mathbf{r}_2$, $\langle C_2\rangle_{2,12}(\mathbf{r}|\mathbf{r}_1,\mathbf{r}_2)$ is the conditional average of the concentration field of oligomers attached to particle 2 of type 2 given that particles 1 and 2 are fixed at $\mathbf{r}_1$ and $\mathbf{r}_2$, and $g_{11}(\mathbf{r}_2-\mathbf{r}_1)$ and $g_{12}(\mathbf{r}_2-\mathbf{r}_1)$ are the radial distribution functions of 1–1 and 1–2 component pairs. In our notation of $\langle A_b\rangle_{c,d}$ with $b = 1$ or 2, $c = 1$ or 2 and $d = 1$, 11, or 12, the subscript b determines whether the quantity A is associated with the particle labeled 1 or 2, the subscript c denotes the number of fixed particles and the subscript d means the types of the particles that are fixed. Application of the weak-field approximation retaining correlations up to $O(a^3/R_\mathrm{g}^3)$ allows us to write

$$\langle C_1\rangle_{1,1}(\mathbf{r}|\mathbf{r}_1) \approx M_1\left[1+\langle\Lambda_1'\rangle_{1,1}(\mathbf{r}_1|\mathbf{r}_1)+\langle B'\rangle_{1,1}(\mathbf{r}|\mathbf{r}_1)\right]G(\mathbf{r}-\mathbf{r}_1), \tag{4.9}$$

$$\begin{aligned}\langle C_2\rangle_{2,11}(\mathbf{r}|\mathbf{r}_1,\mathbf{r}_2) \approx M_1[1 &+ \langle\Lambda_2'\rangle_{1,1}(\mathbf{r}_2|\mathbf{r}_2)+\langle\Lambda_2''\rangle_{2,11}(\mathbf{r}_2|\mathbf{r}_1,\mathbf{r}_2) \\ &+ \langle B'\rangle_{1,1}(\mathbf{r}|\mathbf{r}_1)+\langle B'\rangle_{1,1}(\mathbf{r}|\mathbf{r}_2)]G(\mathbf{r}-\mathbf{r}_2),\end{aligned} \tag{4.10}$$

$$\begin{aligned}\langle C_2\rangle_{2,12}(\mathbf{r}|\mathbf{r}_1,\mathbf{r}_2) \approx M_2[1 &+ \langle\Lambda_2'\rangle_{1,2}(\mathbf{r}_2|\mathbf{r}_2)+\langle\Lambda_2''\rangle_{2,12}(\mathbf{r}_2|\mathbf{r}_1,\mathbf{r}_2) \\ &+ \langle B'\rangle_{1,1}(\mathbf{r}|\mathbf{r}_1)+\langle B'\rangle_{1,2}(\mathbf{r}|\mathbf{r}_2)]G(\mathbf{r}-\mathbf{r}_2),\end{aligned} \tag{4.11}$$

$$g_{11}(\mathbf{r}_2-\mathbf{r}_1) = 1 + h_{\mathrm{HS}11}(\mathbf{r}_2-\mathbf{r}_1) + h_{\mathrm{f}11}(\mathbf{r}_2-\mathbf{r}_1), \tag{4.12}$$

and

$$g_{12}(\mathbf{r}_2 - \mathbf{r}_1) = 1 + h_{\mathrm{HS}12}(\mathbf{r}_2 - \mathbf{r}_1) + h_{\mathrm{f}12}(\mathbf{r}_2 - \mathbf{r}_1), \tag{4.13}$$

where $h_{\mathrm{HS}11}$ and $h_{\mathrm{HS}12}$ are the total correlation functions of the reference hard-sphere mixture for 1–1 and 1–2 interactions, and $h_{\mathrm{f}11}$ and $h_{\mathrm{f}12}$ are the corresponding perturbations to the hard-sphere radial distribution functions due to oligomers. $h_{\mathrm{f}11}$, $h_{\mathrm{f}12}$, and the conditional average field variables are $O(a^3/R_{\mathrm{g}}^3)$. Substituting Eqs. 4.9–4.13 into Eq. 4.8 yields an equation of incompressibility for $O(1)$ contributions:

$$\begin{aligned} M_1 G(\mathbf{r} - \mathbf{r}_1) + n_1 M_1 \int_V [&\langle \Lambda_2' \rangle_{1,1}(\mathbf{r}_2|\mathbf{r}_2) + \langle \Lambda_2'' \rangle_{2,11}(\mathbf{r}_2|\mathbf{r}_1, \mathbf{r}_2) + \langle B' \rangle_{1,1}(\mathbf{r}|\mathbf{r}_1) + \langle B' \rangle_{1,1}(\mathbf{r}|\mathbf{r}_2) \\ &+ h_{\mathrm{HS}11}(\mathbf{r}_2 - \mathbf{r}_1) + h_{\mathrm{f}11}(\mathbf{r}_2 - \mathbf{r}_1)] G(\mathbf{r} - \mathbf{r}_2) \mathrm{d}\mathbf{r}_2 \\ + n_2 M_2 \int_V [&\langle \Lambda_2' \rangle_{1,2}(\mathbf{r}_2|\mathbf{r}_2) + \langle \Lambda_2'' \rangle_{2,12}(\mathbf{r}_2|\mathbf{r}_1, \mathbf{r}_2) + \langle B' \rangle_{1,1}(\mathbf{r}|\mathbf{r}_1) + \langle B' \rangle_{1,2}(\mathbf{r}|\mathbf{r}_2) \\ &+ h_{\mathrm{HS}12}(\mathbf{r}_2 - \mathbf{r}_1) + h_{\mathrm{f}12}(\mathbf{r}_2 - \mathbf{r}_1)] G(\mathbf{r} - \mathbf{r}_2) \mathrm{d}\mathbf{r}_2 = 0, \end{aligned} \tag{4.14}$$

where the first term denotes the unperturbed oligomer concentration of the chosen particle, the second integral term comes from the perturbations to oligomer concentrations of non-chosen particles of type 1, and the third integral term is the corresponding perturbations from non-chosen particles of type 2. We can see that the equilibrium core configuration also affects the cooperation of oligomers in filling the space via the correlation functions h. After applying the normalization conditions for $\langle C_1 \rangle_{1,1}$, $\langle C_2 \rangle_{2,11}$ and $\langle C_2 \rangle_{2,12}$, and noting that $h_{\mathrm{HS}12} = h_{\mathrm{HS}21}$ and $h_{\mathrm{f}12} = h_{\mathrm{f}21}$ from symmetry, Fourier transformation of Eq. 4.14 eventually leads to

$$\hat{\langle B' \rangle}_{1,1}(\mathbf{k}) = \frac{\hat{G}(\mathbf{k}) \left\{ M_1 + n_1 M_1 \left[\hat{h}_{\mathrm{HS}11}(\mathbf{k}) + \hat{h}_{\mathrm{f}11}(\mathbf{k}) \right] + n_2 M_2 \left[\hat{h}_{\mathrm{HS}12}(\mathbf{k}) + \hat{h}_{\mathrm{f}12}(\mathbf{k}) \right] \right\}}{n_{\mathrm{b}} M \left[\hat{G}(\mathbf{k})^2 - 1 \right]}, \tag{4.15}$$

$$\hat{\langle \Lambda_2'' \rangle}_{2,11}(\mathbf{k}) = \hat{\langle \Lambda_2'' \rangle}_{2,12}(\mathbf{k}) = -\hat{\langle B' \rangle}_{1,1}(\mathbf{k}) \hat{G}(\mathbf{k}), \tag{4.16}$$

and

$$\langle \Lambda_i' \rangle_{1,1}(\mathbf{r}_i|\mathbf{r}_i) = -\frac{1}{(2\pi)^3} \int_{V_k} \langle \hat{B}' \rangle_{1,1}(\mathbf{k}) \hat{G}(-\mathbf{k}) \mathrm{d}\mathbf{k} \tag{4.17}$$

with V_k being an unbounded wave number space and the subscript i is 1 or 2. It follows directly that the field variables associated with the case where the fixed chosen particle is of type 2 are

$$\langle \hat{B}' \rangle_{1,2}(\mathbf{k}) = \frac{\hat{G}(\mathbf{k}) \left\{ M_2 + n_1 M_1 \left[\hat{h}_{\mathrm{HS}12}(\mathbf{k}) + \hat{h}_{\mathrm{f}12}(\mathbf{k}) \right] + n_2 M_2 \left[\hat{h}_{\mathrm{HS}22}(\mathbf{k}) + \hat{h}_{\mathrm{f}22}(\mathbf{k}) \right] \right\}}{n_\mathrm{b} M \left[\hat{G}(\mathbf{k})^2 - 1 \right]}, \tag{4.18}$$

$$\langle \hat{\Lambda_2''} \rangle_{2,22}(\mathbf{k}) = \langle \hat{\Lambda_2''} \rangle_{2,21}(\mathbf{k}) = -\langle \hat{B}' \rangle_{1,2}(\mathbf{k}) \hat{G}(\mathbf{k}), \tag{4.19}$$

and

$$\langle \Lambda_i' \rangle_{1,2}(\mathbf{r}_i|\mathbf{r}_i) = -\frac{1}{(2\pi)^3} \int_{V_k} \langle \hat{B}' \rangle_{1,2}(\mathbf{k}) \hat{G}(-\mathbf{k}) \mathrm{d}\mathbf{k}. \tag{4.20}$$

As $\mathbf{k} \to 0$, $\hat{G}(\mathbf{0}) = 1$. The Fourier transform of $F(\mathbf{x})$ and the inverse transform of $\hat{F}(\mathbf{k})$ are defined by $\hat{F}(\mathbf{k}) = \int F(\mathbf{x}) e^{-i\mathbf{k}\cdot\mathbf{x}} \mathrm{d}\mathbf{x}$ and $F(\mathbf{x}) = \frac{1}{(2\pi)^3} \int \hat{F}(\mathbf{k}) e^{i\mathbf{k}\cdot\mathbf{x}} \mathrm{d}\mathbf{k}$.

To solve for the distribution functions for 1–1, 1–2, and 2–2 pairs, we apply a density-functional approach similar to Ref. [6]. We define the grand potential Ω of the entire system given that a chosen particle 1 of type i is fixed at the origin as a functional of the one-body density profiles of other non-chosen particles 2 of type j around particle 1, $n_{ij}(\mathbf{r}_\mathrm{p})$, with $\mathbf{r}_\mathrm{p} = \mathbf{r}_2 - \mathbf{r}_1$ and i and j being 1 or 2:

$$\begin{aligned} \Omega \left[n_{ij}(\mathbf{r}_\mathrm{p}) \right] = {} & F_\mathrm{id} \left[n_{ij}(\mathbf{r}_\mathrm{p}) \right] + F_\mathrm{ex}^\mathrm{HS} \left[n_{ij}(\mathbf{r}_\mathrm{p}) \right] + F_\mathrm{ex}^\mathrm{fluid} [n_{ij}(\mathbf{r}_\mathrm{p})] \\ & + \sum_{i=1}^{2} \sum_{j=1}^{2} \frac{n_i}{n_\mathrm{b}} \int_V n_{ij}(\mathbf{r}_\mathrm{p}) \left[V_{1,i}(\mathbf{r}_\mathrm{p}) - \mu_{ij} \right] \mathrm{d}\mathbf{r}_\mathrm{p}, \end{aligned} \tag{4.21}$$

where the ideal gas free energy of the cores is

$$\frac{F_\mathrm{id} \left[n_{ij}(\mathbf{r}_\mathrm{p}) \right]}{k_\mathrm{B} T} = \sum_{i=1}^{2} \sum_{j=1}^{2} \frac{n_i}{n_\mathrm{b}} \int_V n_{ij}(\mathbf{r}_\mathrm{p}) \left\{ \ln \left[n_{ij}(\mathbf{r}_\mathrm{p}) \Lambda_{\mathrm{p}j}^3 \right] - 1 \right\} \mathrm{d}\mathbf{r}_\mathrm{p} \tag{4.22}$$

with $\Lambda_{\mathrm{p}j}$ being the thermal de Broglie wavelength of type j particles, μ_{ij} is the chemical potential of type j particles given that a type i particle is fixed at the

origin, $V_{1,i}(\mathbf{r}_\mathrm{p})$ is the external potential due to the hard-sphere excluded volume of the fixed type i particle 1, $F_\mathrm{ex}^\mathrm{HS}$ is the excess free energy contributed from the binary hard-sphere mixture, and $F_\mathrm{ex}^\mathrm{fluid}$ is the excess free energy contributed from the fluid phase oligomers. For a given particle configuration, we may smear out the free energy of oligomers as a "mediated interparticle potential" as the oligomers can always possess an equilibrium state according to the distribution of cores. Therefore we obtain $F_\mathrm{ex}^\mathrm{fluid}$ by conditionally averaging the fluid phase free energy shown in Eq. 4.3 over the configuration of $N-1$ particles given that particle 1 of type 1 or 2 is fixed at the origin:

$$\begin{aligned}
\frac{F_\mathrm{ex}^\mathrm{fluid}\left[n_{ij}(\mathbf{r}_\mathrm{p})\right]}{k_\mathrm{B}T} &= \left\langle \frac{F_\mathrm{f}}{k_\mathrm{B}T} \right\rangle_1 \\
&= \sum_{i=1}^{2} \frac{n_i}{n_\mathrm{b}} \left\{ \int_V \langle C_1 \ln C_1 \Lambda_\mathrm{b}^3 \rangle_{1,i}(\mathbf{r}|\mathbf{0}) + \left[\frac{\mathbf{r}^2}{4R_\mathrm{g}^2} - 1 \right] \langle C_1 \rangle_{1,i}(\mathbf{r}|\mathbf{0}) \mathrm{d}\mathbf{r} \right. \\
&\quad \left. + \sum_{j=1}^{2} \int_V n_{ij}(\mathbf{r}_\mathrm{p}) \int_V \langle C_2 \ln C_2 \Lambda_\mathrm{b}^3 \rangle_{2,ij}(\mathbf{r}|\mathbf{0},\mathbf{r}_\mathrm{p}) + \left[\frac{(\mathbf{r}-\mathbf{r}_\mathrm{p})^2}{4R_\mathrm{g}^2} - 1 \right] \langle C_2 \rangle_{2,ij}(\mathbf{r}|\mathbf{0},\mathbf{r}_\mathrm{p}) \mathrm{d}\mathbf{r}\mathrm{d}\mathbf{r}_\mathrm{p} \right\},
\end{aligned} \tag{4.23}$$

where $\mathbf{r}_\mathrm{p}$ is the position of neighboring core particles labeled 2 and $\mathbf{r}$ is the position of oligomer beads. The first term accounts for the contribution from the oligomers of the chosen particle and the second term arises from the oligomers of all the other non-chosen particles.

At equilibrium, the minimization $\delta\Omega[n_{ij}(\mathbf{r}_\mathrm{p})]/\delta n_{ij}(\mathbf{r}_\mathrm{p}) = 0$ and application of equal-chemical-potential condition for the particles of type j given a fixed particle of type i, $\mu_{ij} = \mu_{ij,\mathrm{bulk}} = \mu_{ij}|_{\mathbf{r}_\mathrm{p}\to\infty}$, yield

$$\begin{aligned}
n_{ij}(\mathbf{r}_\mathrm{p}) &= n_j g_{ij}(\mathbf{r}_\mathrm{p}) \\
&= n_j \exp\left\{ \frac{n_\mathrm{b}}{n_i} \left[c_{\mathrm{HS}ij}^{(1)}(\mathbf{r}_\mathrm{p}) - c_{\mathrm{HS}ij,\mathrm{b}}^{(1)} \right] - \frac{V_{1,i}(\mathbf{r}_\mathrm{p})}{k_\mathrm{B}T} + \frac{n_\mathrm{b}}{n_i} \left[c_{\mathrm{f}ij}^{(1)}(\mathbf{r}_\mathrm{p}) - c_{\mathrm{f}ij,\mathrm{b}}^{(1)} \right] \right\},
\end{aligned} \tag{4.24}$$

where the one-body direct correlation functions for each i–j pair are defined by

$c^{(1)}_{\mathrm{HS}ij}(\mathbf{r}_\mathrm{p}) = -\frac{\delta\left(F^{\mathrm{HS}}_{\mathrm{ex}}[n_{ij}(\mathbf{r}_\mathrm{p})]/k_\mathrm{B}T\right)}{\delta n_{ij}(\mathbf{r}_\mathrm{p})}$, $c^{(1)}_{\mathrm{HS}ij,\mathrm{b}} = -\frac{\delta\left(F^{\mathrm{HS}}_{\mathrm{ex}}[n_{ij}(\mathbf{r}_\mathrm{p})]/k_\mathrm{B}T\right)}{\delta n_{ij}(\mathbf{r}_\mathrm{p})}|_{\mathbf{r}_\mathrm{p}\to\infty}$, $c^{(1)}_{\mathrm{f}ij}(\mathbf{r}_\mathrm{p}) = -\frac{\delta\left(F^{\mathrm{fluid}}_{\mathrm{ex}}[n_{ij}(\mathbf{r}_\mathrm{p})]/k_\mathrm{B}T\right)}{\delta n_{ij}(\mathbf{r}_\mathrm{p})}$, and $c^{(1)}_{\mathrm{f}ij,\mathrm{b}} = -\frac{\delta\left(F^{\mathrm{fluid}}_{\mathrm{ex}}[n_{ij}(\mathbf{r}_\mathrm{p})]/k_\mathrm{B}T\right)}{\delta n_{ij}(\mathbf{r}_\mathrm{p})}|_{\mathbf{r}_\mathrm{p}\to\infty}$. As justified in Ref. [6], under the weak-field approximation for oligomers and the separation of length scales as $R_\mathrm{g}/a \gg 1$, we can obtain the core distribution functions expressed in Eqs. 4.12 and 4.13 with $1 + h_{\mathrm{HS}ij}(\mathbf{r}_\mathrm{p}) = \exp\left\{(n_\mathrm{b}/n_i)\left[c^{(1)}_{\mathrm{HS}ij}(\mathbf{r}_\mathrm{p}) - c^{(1)}_{\mathrm{HS}ij,\mathrm{b}}\right] - V_{1,i}(\mathbf{r}_\mathrm{p})/k_\mathrm{B}T\right\}$ and $h_{\mathrm{f}ij}(\mathbf{r}_\mathrm{p}) \approx (n_\mathrm{b}/n_i)\left[c^{(1)}_{\mathrm{f}ij}(\mathbf{r}_\mathrm{p}) - c^{(1)}_{\mathrm{f}ij,\mathrm{b}}\right]$. Keeping dominant contributions from these variations of the free energy allows us to neglect the coupling between $h_{\mathrm{HS}ij}$ and $h_{\mathrm{f}ij}$ and we obtain $c^{(1)}_{\mathrm{HS}ij}(\mathbf{r}_\mathrm{p}) \approx -\frac{\delta\left(F^{\mathrm{HS}}_{\mathrm{ex}}[n_{ij}(\mathbf{r}_\mathrm{p})]/k_\mathrm{B}T\right)}{n_j\delta h_{\mathrm{HS}ij}(\mathbf{r}_\mathrm{p})}$ and $c^{(1)}_{\mathrm{f}ij}(\mathbf{r}_\mathrm{p}) \approx -\frac{\delta\left(F^{\mathrm{fluid}}_{\mathrm{ex}}[n_{ij}(\mathbf{r}_\mathrm{p})]/k_\mathrm{B}T\right)}{n_j\delta h_{\mathrm{f}ij}(\mathbf{r}_\mathrm{p})}$. Therefore we may directly adopt the literature results of $h_{\mathrm{HS}11}$, $h_{\mathrm{HS}22}$, and $h_{\mathrm{HS}12}$ obtained from solving the Ornstein–Zernike equation with the Percus–Yevick approximation for a mixture of hard spheres [7, 8]. Substitution of the oligomer concentration field variables Λ_i and $B(\mathbf{r})$ into $F^{\mathrm{fluid}}_{\mathrm{ex}}[n_{ij}(\mathbf{r}_\mathrm{p})]/k_\mathrm{B}T$ shown in Eq. 4.23, truncation of the higher order correlations between the particles, and functional differentiation $\frac{\delta\left(F^{\mathrm{fluid}}_{\mathrm{ex}}[n_{ij}(\mathbf{r}_\mathrm{p})]/k_\mathrm{B}T\right)}{n_j\delta h_{\mathrm{f}ij}(\mathbf{r}_\mathrm{p})}$ finally yield to $O(a^3/R_\mathrm{g}^3)$:

$$h_{\mathrm{f}11}(\mathbf{r}_\mathrm{p}) \approx \sum_{i=1}^{2}\left\{\frac{2n_iM_i}{n_1}\int_V \langle\Lambda_2''\rangle_{2,1i}(\mathbf{r}_\mathrm{p}'|\mathbf{0},\mathbf{r}_\mathrm{p})\frac{\delta\langle\Lambda_2''\rangle_{2,1i}(\mathbf{r}_\mathrm{p}'|\mathbf{0},\mathbf{r}_\mathrm{p})}{\delta h_{\mathrm{f}11}(\mathbf{r}_\mathrm{p})}\mathrm{d}\mathbf{r}_\mathrm{p}' - \frac{2n_iM_i}{n_1}\int_V \langle B'\rangle_{1,1}(\mathbf{r}'|\mathbf{0})\frac{\delta\langle B'\rangle_{1,1}(\mathbf{r}'|\mathbf{0})}{\delta h_{\mathrm{f}11}(\mathbf{r}_\mathrm{p})}\mathrm{d}\mathbf{r}'\right\}, \tag{4.25}$$

$$\begin{aligned} h_{\mathrm{f}12}(\mathbf{r}_\mathrm{p}) \approx \sum_{i=1}^{2}\Bigg\{&\frac{2n_iM_i}{n_2}\int_V \langle\Lambda_2''\rangle_{2,1i}(\mathbf{r}_\mathrm{p}'|\mathbf{0},\mathbf{r}_\mathrm{p})\frac{\delta\langle\Lambda_2''\rangle_{2,1i}(\mathbf{r}_\mathrm{p}'|\mathbf{0},\mathbf{r}_\mathrm{p})}{\delta h_{\mathrm{f}12}(\mathbf{r}_\mathrm{p})}\mathrm{d}\mathbf{r}_\mathrm{p}' \\ &- \frac{2n_iM_i}{n_2}\int_V \langle B'\rangle_{1,1}(\mathbf{r}'|\mathbf{0})\frac{\delta\langle B'\rangle_{1,1}(\mathbf{r}'|\mathbf{0})}{\delta h_{\mathrm{f}12}(\mathbf{r}_\mathrm{p})}\mathrm{d}\mathbf{r}' \\ &+ \frac{2n_iM_i}{n_1}\int_V \langle\Lambda_2''\rangle_{2,2i}(\mathbf{r}_\mathrm{p}'|\mathbf{0},\mathbf{r}_\mathrm{p})\frac{\delta\langle\Lambda_2''\rangle_{2,2i}(\mathbf{r}_\mathrm{p}'|\mathbf{0},\mathbf{r}_\mathrm{p})}{\delta h_{\mathrm{f}12}(\mathbf{r}_\mathrm{p})}\mathrm{d}\mathbf{r}_\mathrm{p}' \\ &- \frac{2n_iM_i}{n_1}\int_V \langle B'\rangle_{1,2}(\mathbf{r}'|\mathbf{0})\frac{\delta\langle B'\rangle_{1,2}(\mathbf{r}'|\mathbf{0})}{\delta h_{\mathrm{f}12}(\mathbf{r}_\mathrm{p})}\mathrm{d}\mathbf{r}'\Bigg\}, \end{aligned} \tag{4.26}$$

and $h_{\mathrm{f}22}(\mathbf{r}_\mathrm{p})$ can be obtained from Eq. 4.25 by changing n_1 to n_2, $h_{\mathrm{f}11}(\mathbf{r}_\mathrm{p})$ to $h_{\mathrm{f}22}(\mathbf{r}_\mathrm{p})$, $\langle\Lambda_2''\rangle_{2,1i}$ to $\langle\Lambda_2''\rangle_{2,2i}$, and $\langle B'\rangle_{1,1}$ to $\langle B'\rangle_{1,2}$. These integrals are convergent since the changes in the field variables due to the core distributions are important only

within a distance of $O(R_g)$ from the fixed particle 1. When particle 2 is deep in the bulk $\delta\langle\Lambda_2''\rangle_{2,ij}(\mathbf{r}_p'|\mathbf{0},\mathbf{r}_p)/\delta h_{fij}(\mathbf{r}_p)$ and $\delta\langle B'\rangle_{1,i}(\mathbf{r}'|\mathbf{0})/\delta h_{fij}(\mathbf{r}_p)$ are essentially zero. After making use of the convolution theorem and the expressions for $\langle\hat{B}'\rangle_{1,i}(\mathbf{k})$ and $\langle\hat{\Lambda}_2''\rangle_{2,ij}(\mathbf{k})$, in Fourier space we obtain

$$\hat{h}_{f11}(\mathbf{k}) = \frac{2M_1\hat{G}(\mathbf{k})^2\left[M_1 + n_1M_1\hat{h}_{HS11}(\mathbf{k}) + n_2M_2\hat{h}_{HS12}(\mathbf{k}) + n_2M_2\hat{h}_{f12}(\mathbf{k})\right]}{n_bM\left[\hat{G}(\mathbf{k})^2 - 1\right] - 2n_1M_1^2\hat{G}(\mathbf{k})^2}, \tag{4.27}$$

$$\hat{h}_{f22}(\mathbf{k}) = \frac{2M_2\hat{G}(\mathbf{k})^2\left[M_2 + n_1M_1\hat{h}_{HS12}(\mathbf{k}) + n_2M_2\hat{h}_{HS22}(\mathbf{k}) + n_1M_1\hat{h}_{f12}(\mathbf{k})\right]}{n_bM\left[\hat{G}(\mathbf{k})^2 - 1\right] - 2n_2M_2^2\hat{G}(\mathbf{k})^2}, \tag{4.28}$$

and

$$\begin{aligned}\hat{h}_{f12}(\mathbf{k}) = {} & \frac{2M_2\hat{G}(\mathbf{k})^2\left\{n_bM\left[\hat{G}(\mathbf{k})^2 - 1\right] - 2n_2M_2^2\hat{G}(\mathbf{k})^2\right\}}{\left\{n_bM\left[\hat{G}(\mathbf{k})^2 - 1\right] - 2(n_1M_1^2 + n_2M_2^2)\hat{G}(\mathbf{k})^2\right\}^2 - 4n_1n_2M_1^2M_2^2\hat{G}(\mathbf{k})^4} \\ & \times\left[M_1 + n_1M_1\hat{h}_{HS11}(\mathbf{k}) + n_2M_2\hat{h}_{HS12}(\mathbf{k})\right] \\ & + \frac{2M_1\hat{G}(\mathbf{k})^2\left\{n_bM\left[\hat{G}(\mathbf{k})^2 - 1\right] - 2n_1M_1^2\hat{G}(\mathbf{k})^2\right\}}{\left\{n_bM\left[\hat{G}(\mathbf{k})^2 - 1\right] - 2(n_1M_1^2 + n_2M_2^2)\hat{G}(\mathbf{k})^2\right\}^2 - 4n_1n_2M_1^2M_2^2\hat{G}(\mathbf{k})^4} \\ & \times\left[M_2 + n_1M_1\hat{h}_{HS12}(\mathbf{k}) + n_2M_2\hat{h}_{HS22}(\mathbf{k})\right].\end{aligned} \tag{4.29}$$

When $n_1 = n_b$, $n_2 = 0$, and $M_1 = M$ such that $h_{f11} = h_f$ and $h_{HS11} = h_{HS}$, or when $M_1 = M_2$, $a_1 = a_2$, and $n_1 = n_2 = \frac{n_b}{2}$ such that $h_{HS11} = h_{HS12} = h_{HS}$ and $h_{f11} = h_{f12} = h_f$, Eq. 4.27 automatically reduces to Eq. 29 of Ref. [6] for monodisperse NOHMs.

We define the structure factor S_{ij} for any i–j pair as $S_{ii}(k) = 1 + n_i\left[\hat{h}_{HSii}(k) + \hat{h}_{fii}(k)\right]$ for i being 1 or 2 and $S_{12}(k) = S_{21}(k) = \sqrt{n_1n_2}\left[\hat{h}_{HS12}(k) + \hat{h}_{f12}(k)\right]$. If we assume that the cores have a constant scattering density up to a radial distance a_i, the "effective" structure factor defined based on interpreting a scattering experiment as if it were performed on a monodisperse system is written as a "weighted-average" result accounting for the differences in the scatterer size

and the number density [9–11]:

$$S(k) = \frac{\gamma^6 n_1 P_1(k) S_{11}(k) + 2\gamma^3 \sqrt{n_1 n_2 P_1(k) P_2(k)} S_{12}(k) + n_2 P_2(k) S_{22}(k)}{\gamma^6 n_1 P_1(k) + n_2 P_2(k)}, \tag{4.30}$$

where $P_i(k) = \frac{9}{(ka_i)^6} [\sin(ka_i) - ka_i \cos(ka_i)]^2$ is the normalized form factor for species i. As $k \to 0$, $P_i(0) \to 1$ and $S(0)$ is non-zero, in general. The isothermal compressibility χ_T is defined by [12]

$$\chi_T k_B T = \frac{S_{11}(0) S_{22}(0) - S_{12}^2(0)}{n_1 S_{22}(0) + n_2 S_{11}(0) - 2\sqrt{n_1 n_2} S_{12}(0)}. \tag{4.31}$$

It is straightforward to show that our expressions for h_{fij} automatically lead to $S_{11}(0)S_{22}(0) = S_{12}^2(0)$ such that $\chi_T k_B T = 0$, the system is incompressible although $S(0) \neq 0$. Again, when $n_1 = n_b$ and $n_2 = 0$ or when $\gamma = 1$ and $n_1 = n_2$, we obtain the structure factor for a monodisperse NOHMs system with $S(0) = 0$ for incompressible single-component fluids.

4.4 Results & Discussion

As in Ref. [6], in the calculations we fix the oligomer number density to be the value that corresponds to an average number of oligomers per core of 600 when $\phi_b = 0.15$. As ϕ_b varies, M changes accordingly. For simplicity, we choose $n_1 = n_2$ and introduce either bidispersity in the core radius or in the oligomer grafting density. We focus on the structure factor of systems with different extents of bidispersity at the same total core volume fraction, ϕ_b, and the same ratio of the oligomer radius of gyration to the average core radius, R_g/a, to emphasize the effects purely due to bidispersity. The effects of variations of these geometrical parameters on the structure factor would be the same as those demonstrated in Ref. [6]. If the system has x% bidispersity in the core radius but the oligomer

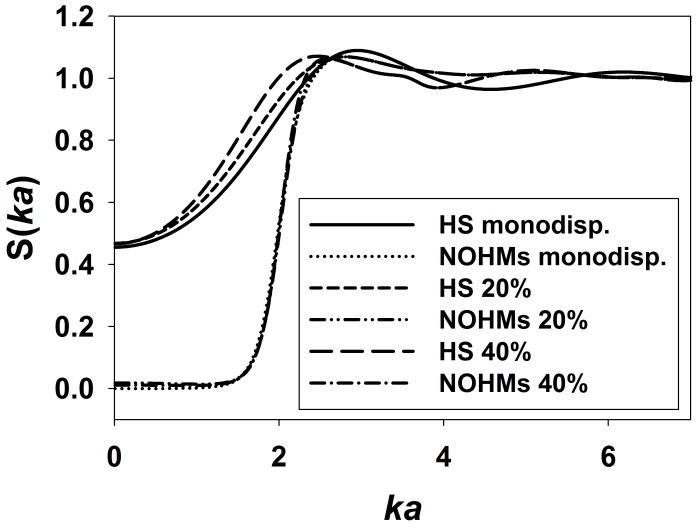

Figure 4.2: The apparent static structure factor S as a function of the wave number non-dimensionalized by the inverse average core radius, ka, for different bidispersities in the core radius a_i but fixed oligomer grafting density σ_s with $\phi_b = 0.1$ and $R_g/a = 1$. Results for the reference hard-sphere suspension with different bidispersities and the monodisperse NOHMs suspension obtained from Ref. [6] are shown for comparison.

grafting density is fixed ($\sigma_s = \sigma_{s1} = \sigma_{s2}$), we define $\gamma = (1 - x\%)/(1 + x\%)$, $M_1 = \gamma^2 M_2$, and $M_2 = 2M/(1 + \gamma^2)$; for systems with $x\%$ bidispersity in the oligomer grafting density but with a fixed core radius ($a = a_1 = a_2$), we obtain $M_1 = (1 - x\%)M$ and $M_2 = (1 + x\%)M$.

In Fig. 4.2, we first compare the apparent structure factor for NOHMs with different bidispersities in the core radius at $\phi_b = 0.1$ and $R_g/a = 1$. For solventless NOHMs, we can observe two distinct length scales: at larger k we observe the hard-core correlations that vary on the length scale of a; at smaller k the density fluctuations are suppressed and we observe a continuous drop in $S(k)$ roughly on the length scale of R_g, independent of bidispersity. In the specific

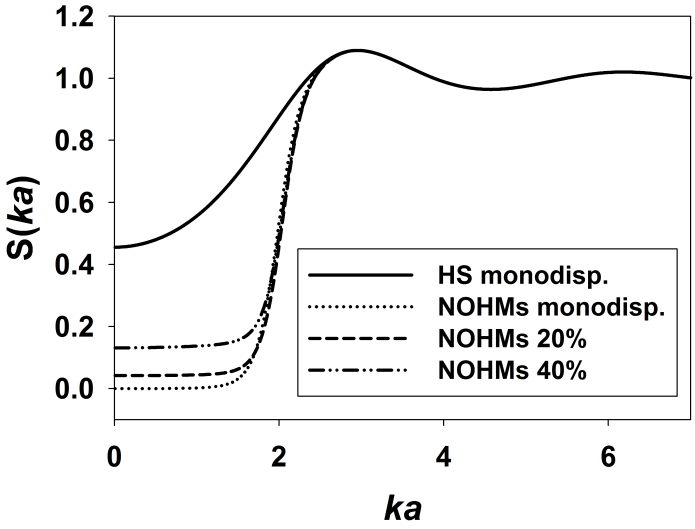

Figure 4.3: The apparent static structure factor S as a function of the wave number non-dimensionalized by the core radius, ka, for different bidispersities in the oligomer grafting density σ_{si} but fixed core radius a with $\phi_b = 0.1$ and $R_g/a = 1$. Results for the monodisperse hard spheres and NOHMs obtained from Ref. [6] are shown for comparison.

case of $R_g/a = 1$ shown here, the deficit of particles occurs right below the k value of the first peak in $S(k)$. The complicated side peaks shown in the hard–core correlations for bidisperse NOHMs and the reference hard spheres are due to different separation distances for i–j pairs. While for monodisperse NOHMs the deficit of neighboring particles at small k eventually yields zero $S(0)$, bidisperse NOHMs show slight deviations from zero because different particles carry different amounts of fluid space not proportional to their core volumes so they are permitted to take on configurations that lead to fluctuations in scattering density. For hard spheres, $S(0)$ for a bidisperse system also exhibits a positive deviation from the value for a monodisperse system because smaller particles can fill in the interstices around larger particles.

On the other hand, if the system has a fixed core size but bidispersity in the oligomer grafting density, in Fig. 4.3 we find that while $S(k)$ also exhibits two length scales characterizing different particle correlations, the deviations of $S(0)$ from zero are more substantial than those shown in Fig. 4.2 given the same extent of bidispersity. This can be rationalized by the fact that when we vary σ_{si} or M_i we directly vary the fluid volume that each particle carries; however, when we fix σ_s but change the core radius the share of the fluid volume each particle carries is proportional to a_i^2, not much different from the variation of core volume which is proportional to a_i^3. Therefore, the weaker effect on the variation in the tethered oligomer fluid volume caused by the variation of the core radius at a fixed oligomer grafting density leads to less deviation of $S(0)$ from zero. It is noteworthy that even with a moderate extent of bidispersity, $S(0)$ for NOHMs is still substantially smaller than $S(0)$ for the reference hard spheres. This indicates that in the absence of unattached solvents, the space-filling tethered oligomers tend to enforce a uniform particle distribution and reduce the apparent long range density fluctuations defined by an effective monodisperse system.

We tabulate the value of $S(0)$ shown in Figs. 4.2 and 4.3 for different bidispersities in table 4.1 to directly see the stronger effects due to bidispersity in the oligomer grafting density than bidispersity in the core radius. It is expected that if we consider both bidispersities at the same time, the tabulated theoretical $S(0)$ at different conditions would allow us to characterize the polydispersity in the experimental system.

Based on the physical argument that a non-zero $S(0)$ is caused by variations of the volume excluded from each particle and its tethered fluid, it is expected

Table 4.1: Predicted Apparent Static Structure Factor at Zero Wave Number for Different Bidisperse NOHMs at $\phi_b = 0.1$ and $R_g/a = 1$

	$S(0)$ varying	
Bidispersity (%)	Core radius (a_i)	Grafting density (σ_{si})
10	0.009	0.011
20	0.018	0.042
40	0.011	0.131

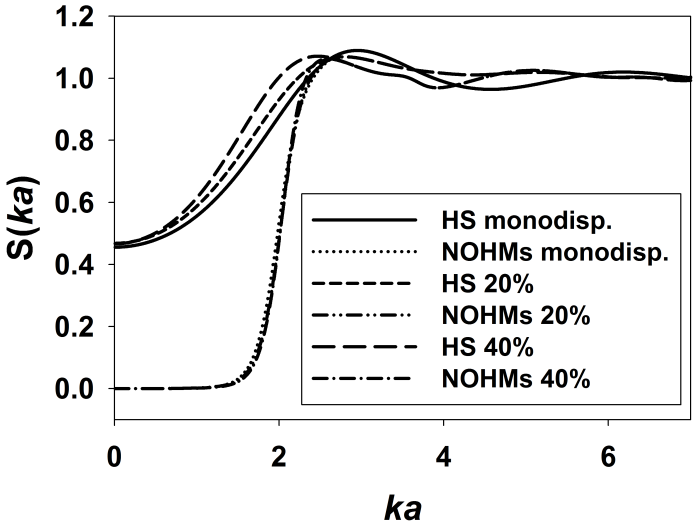

Figure 4.4: The apparent static structure factor S as a function of the wave number non-dimensionalized by the inverse average core radius, ka, for different bidispersities in the core radius a_i but fixed share of fluid space to core volume ratio, σ_{si}/a_i, with $\phi_b = 0.1$ and $R_g/a = 1$. Results for the reference hard-sphere suspension with different bidispersities and the monodisperse NOHMs suspension obtained from Ref. [6] are shown for comparison.

that when the ratio of the share of fluid volume to the core volume ($v_{\mathrm{f}i}/v_{\mathrm{p}i}$) for each particle is held fixed we obtain $S(0) = 0$. Since the volume of each oligomer is assumed constant, the condition of fixing $v_{\mathrm{f}i}/v_{\mathrm{p}i}$ is equivalent to fixing $\sigma_{\mathrm{s}i}/a_i$ given a variation in the core radius. In this condition, each particle excludes a number of particles proportional to its own volume from the neighborhood, as in a monodisperse system where each particle excludes exactly one particle from its neighborhood. As presented in Fig. 4.4, the apparent static structure factor shows zero value at $k = 0$, independent of bidispersity.

4.5 Conclusions

We have generalized the density-functional theory presented in Ref. [6] for monodisperse NOHMs to a binary mixture of NOHMs. The coarse-grained model considered here contains hard cores and linear bead-chains tethered to the core center and allows us to directly formulate the oligomer free energy as a mediated interparticle potential given a core distribution. As $R_{\mathrm{g}} \gg a$, many cores' oligomers cooperate to fill any given fluid space such that the weak-oligomeric field approximation is valid. When treating the detailed core–core packing configuration on a length scale of a, the perturbation due to the oligomers is minor; when dealing with the effect on the structure due to the space-filling oligomers over a larger length scale of R_{g}, the cores merely occupy a portion of space. As a result, the oligomer contributions are viewed as perturbations to the equilibrium hard-sphere configuration and we derive the effective structure factor for bidisperse NOHMs. Based on the assumption of volume additivity for the two components, the theory predicts a non-zero $S(0)$ when variations of the fluid volume each core carries are not proportional to variations

of the core volume. Therefore, if we treat bidispersities in the core radius and in the oligomer grafting density as two independent variables, we observe that while bidispersity in the core size mostly distorts the hard-core correlations in $S(k)$ without deviating $S(0)$ too much from zero, bidispersity in the oligomer grafting density, on the other hand, yields more disturbances to the uniform structure at larger length scales such that we observe stronger deviation of $S(0)$ from zero.

Although it is anticipated that the observed structure factor would exhibit more complicated behavior for a polydisperse system with variations in the core size, oligomer grafting density, and oligomer radius of gyration, the main feature of solvent-free NOHMs would be a smaller value of $S(0)$ than the reference hard-sphere suspension with the same core volume fraction as the tethered incompressible oligomers tend to fill the space uniformly. Meanwhile, $S(0)$ would be close to zero if the ratio of the tethered oligomer volume to the core volume is close to a constant, irrespective of polydispersity.

We conjecture that variation of oligomer molecular weight will have similar effects to variation of oligomer grafting density as both influence the fluid volume per particle. Consequently, it is important to have good monodispersity of these quantities. An experimentalist trying to show $S(0) \approx 0$ in NOHMs would need to be especially careful to have ideal oligomers but could be more lax in the monodispersity of the particles.

BIBLIOGRAPHY

[1] A. B. Bourlinos, R. Herrera, N. Chalkias, D. D. Jiang, Q. Zhang, L. A. Archer, and E. P. Giannelis, Adv. Mater. **17**, 234 (2005).

[2] A. B. Bourlinos, E. P. Giannelis, Q. Zhang, L. A. Archer, G. Floudas, and G. Fytas, Eur. Phys. J. E **20**, 109 (2006).

[3] R. Rodriguez, R. Herrera, L. A. Archer, and E. P. Giannelis, Adv. Mater. **20**, 4353 (2008).

[4] P. Agarwal, H. Qi, and L. A. Archer, Nano Lett. **10**, 111 (2010).

[5] J. L. Nugent, S. S. Moganty, and L. A. Archer, Adv. Mater. **22**, 3677 (2010).

[6] H.-Y. Yu and D. L. Koch, Langmuir **26**, 16801 (2010).

[7] J. L. Lebowitz, Phys. Rev. **133**, A895 (1964).

[8] N. W. Ashcroft and D. C. Langreth, Phys. Rev. **156**, 685 (1967).

[9] P. N. Pusey, H. M. Fijnaut, and A. Vrij, J. Chem. Phys. **77**, 4270 (1982).

[10] J. Moonen, C. de Kruif, and A. Vrij, Colloid Polym. Sci. **266**, 1068 (1988).

[11] B. Weyerich, J. Brunner-Popela, and O. Glatter, J. Appl. Cryst. **32**, 197 (1999).

[12] J. G. Kirkwood and F. P. Buff, J. Chem. Phys. **19**, 774 (1951).

CHAPTER 5

DENSITY-FUNCTIONAL THEORY FOR THE SOLVENT CAPACITY OF NANOPARTICLE–ORGANIC HYBRID MATERIALS

5.1 Abstract

We predict the solvent capacity of nanoparticle–organic hybrid materials (NOHMs) using a density-functional theory for a binary mixture of NOHMs and an added solute. The tethered oligomers and captured solute molecules cooperate to form an incompressible fluid with the oligomer–solute interaction being modeled using a Flory–Huggins parameter and their configurations are assumed to be at equilibrium for a given core distribution. To determine the solvent capacity of the system, we first derive semi-analytic solutions for the static structure factor and distribution functions of the cores, tethered oligomers, and captured solute based on a regular perturbation analysis valid for large oligomer radius of gyration compared with the core radius. These equilibrium configurations then allow us to calculate the system free energy and obtain the sorption isotherm of gases in the suspension. As the solute dilutes the hybrid, the potential of mean force among the cores is weakened and the system exhibits more density fluctuations. Meanwhile, the relaxation of the entropic frustrations of the attached oligomeric chains upon uptake of the solute provides an entropic driving force that is unique to NOHMs. The solvent capacity of NOHMs is therefore a combined effects of the change in the oligomer-configurational entropy and the enthalpic affinity to the solute. The general theory is applied to consider poly(ethylene glycol)-tethered NOHMs and ionid-liquid-tethered NOHMs. With Henry's constants of gases in unattached oligomer melts as in-

put for the interaction parameter, comparison for Henry's constants of gases in NOHMs shows that NOHMs could have reasonably good CO_2 selectivity over N_2 and CH_4 and less poisoned by high affinity molecules such as SO_2 relative to the melts.

5.2 Introduction

Nanoparticle–organic hybrid materials (NOHMs) consist of inorganic cores self-fluidized by the organic oligomers tethered to their surfaces. In pure, solventless condition, these materials exhibit fluid behavior experimentally [1–5] and a recent density-functional theory shows that the equilibrium structure is governed by the configurational-entropic penalty associated with the need for the oligomer hairs to fill the interstitial space [6]. Therefore, NOHMs are disordered, uniform liquid and yet the conformational space for the attached oligomers is limited. It is envisioned that the addition of a second fluid species into NOHMs may release the entropic frustrations of oligomers and decrease the system free energy. This relaxation of the entropic penalty may provide a thermodynamic driving force for solute uptake. In this work, we propose a density-functional theory for a binary mixture in which we treat the NOHMs fluid as a solvent absorbing a dissolved gas solute. Our objective is to predict the solvent capacity of pure NOHMs and utilize the materials to capture CO_2.

In terms of removing CO_2 from high temperature combustion effluent, the vaporization and the thermal stability of solvents are issues faced in the development of efficient carbon capture processes. Hence, NOHMs liquid can be a good candidate for CO_2 capture as the materials have negligible vapor pres-

sure and the anchoring of the oligomers to the particles improves the thermal stability of the oligomer melt [7]. Besides the practical advantages, the geometrical parameters such as the volume fraction of the cores, relative ratio between the oligomer radius of gyration and the core radius, and the grafting density of oligomers, can be adjusted experimentally [3, 4] to introduce different "intrinsic" configurational-entropic penalty for the tethered oligomers. Meanwhile, the chemistry of oligomers can also be carefully chosen to have different affinities between the NOHMs system and the absorbed solute [8, 9]. As a result, the solvent capacity of NOHMs is determined by the change in the configurational entropy of the oligomers in conjunction with the enthalpic tendency upon uptake of the solute. While alkanolamine solutions [10, 11], amine-based solid sorbents [12, 13], and room temperature ionic liquids (RTILs) [14–16] have been developed to capture CO_2 via direct chemical or physical interactions, NOHMs provide a new platform that allows us to engineer different carbon capture mechanisms by utilizing the unique entropic driving force. The theory aims to provide a framework to understand the effect of the aformentioned physical (geometrical) parameters and of chemical parameters such as the Flory–Huggins interaction parameter on the solute uptake to guide the material design for NOHMs solvents.

To quantify the solvent capacity of pure NOHMs, it is essential to first determine the equilibrium structure of the system as it provides us with the information of the system free energy. In a pure, incompressible single-component fluid, the static structure factor at zero wave number k^* is zero, $S(k^* = 0) = 0$ [17]. This means that each fluid molecule excludes exactly one other molecule from its neighborhood and the molecular distribution is uniform. Similarly, in pure NOHMs each entity contains the core and its share of incompressible fluid space

and $S(0) = 0$ implies that the attached oligomeric hairs feel an entropic penalty that governs both the oligomer configuration and the core distribution to prevent large void spaces among particles [6]. When there is a second fluid species present, the bulk structure of the system is altered. On one hand, the second fluid can cooperate with the oligomers in filling the space such that the oligomer concentration field is regulated and the deficit of neighbors around any given NOHMs particle becomes less than one; $S(0) \neq 0$. On the other, non-zero $S(0)$ means that the system is slightly compressible with more observable density fluctuations at larger length scales. Therefore the particle distribution is more random than the pure NOHMs system and the additional fluid space weakens the potential of mean force among the cores.

In this study, we propose a classical density-functional approach for a binary system of oligomer-tethered nanoparticles as solvent and untethered molecules as solute. Starting with the same NOHMs model as shown in the finite-core NOHMs section of Ref. [6], we treat the core particles and the tethered oligomers as hard spheres and bead-springs, respectively, and consider the solute molecules as free, untethered beads in the fluid space. The soft spring connecting the bead to the core models the chain configuration with the spring energy contributing to the oligomer-configurational entropy. We first formulate the fluid phase free energy of the oligomers and solute for a given core particle configuration. After neglecting the interactions between the solute and the cores, the enthalpic affinity between the NOHMs suspension and solute is characterized solely by the Flory–Huggins interaction parameter of oligomer–solute pairs. The fluid phase free energy is a sum of each species' entropic contribution, spring energy for the tethering, and the enthalpic interaction. The expression for the equilibrium concentration field of the oligomers attached to a core is first ob-

tained by minimizing the fluid phase free energy subject to the constraint of the normalization of oligomer field. Since the dissolved gas molecules would have strong close attractive and repulsive interactions with the oligomers just like the interactions of the base oligomer liquid, the total fluid is incompressible and the solute concentration field at a given position is determined by the oligomer field subject to the requirement that the fluid phase volume is uniformly filled. In the limit of large oligomer radius of gyration compared with the core radius ($R_g/a \gg 1$) we may apply a "weak-field" approximation for the oligomers to obtain analytical expressions for the fluid species concentration fields using a regular perturbation analysis. Under the density-functional formulation, the weak-field solutions for these concentration fields allow a semi-analytic determination of the radial distribution function and the static structure factor of cores in the two-species system.

The core radial distribution function along with the fluid species concentration fields can be utilized to calculate the total free energy of the entire system as well as the solute chemical potential under a given solute concentration. For gas capture, application of the equal-fugacity (equivalent to equal-chemical-potential) criterion of a two-phase equilibrium allows us to determine the sorption isotherm and the Henry's constant of the gas in NOHMs. In this work, we utilize the proposed theory to consider the captured gas as CO_2 and show how the geometrical parameters such as the core volume fraction and the oligomer radius of gyration can affect the carbon capture ability of the NOHMs system. Depending on the chemistry of the oligomers, the interaction parameter is presumed based on literature values for specific interactions between the active group along the chain and CO_2. Our results for NOHMs with a given amount of the tethered oligomers are compared with the same amount of the

identical untethered oligomer melt to characterize the physical driving force or resistance produced by the attachment of the chains in addition to the enthalpic or chemical interactions between the oligomer hairs and CO_2 molecules. While the theory is general and can be applied to any given oligomer and solute pair, we will specifically consider poly(ethylene glycol)-tethered NOHMs and ionic-liquid-tethered NOHMs as examples. Since the separation of CO_2 from air or post-combustion flue gas and the removal of CO_2 from natural gas have gained much attention, we discuss the ideal solubility selectivity of CO_2 in NOHMs over different gases such as CH_4, C_2H_6, N_2, and SO_2 based on a comparison of the predicted Henry's constants for these species in NOHMs.

The theory and results are shown simultaneously. In section 5.3, we introduce the coarse-grained model and formulate the density-functional theory followed by the results for equilibrium structure of the two-species system. In section 5.4, we construct a vapor-liquid equilibrium. The sorption isotherms of CO_2 solute physically absorbed in poly(ethylene glycol)-tethered NOHMs systems are presented in section 5.4.1 and the isotherms of chemically absorbed CO_2 in amine-based NOHMs are shown in section 5.4.2. The estimated ideal selectivities of different gases in poly(ethylene glycol)-tethered NOHMs and ionic-liquid-tethered NOHMs are presented in section 5.4.3. Finally, we conclude our work in section 5.5.

5.3 Structure of NOHMs–Solute Mixtures

In this section, we first consider a NOHMs system containing a specified content of solute. We aim to find the concentrations of oligomers and solute as well as

the distribution function of particles around a given fixed particle, which may provide the information of system free energy that is essential in determining the solute solubility in NOHMs. From the particle distribution function, we may also obtain the static structure factor of particles in the mixture.

In the pure NOHMs system considered in Ref. [6], the entity of the single-component fluid contained the core particle and the share of fluid attached to it. We applied an incompressibility condition of the oligomers such that the tethered bead-spring oligomers filled the interstitial fluid space where the monomer number density was held fixed. Here, we consider a two-species suspension in which the NOHMs fluid acts as the solvent soaking up a given amount of the solute molecules. As depicted in Fig. 5.1, the solvent NOHMs are modeled as hard cores having radius a and core volume fraction ϕ_{b} with bead-spring oligomers tethered to the centers of the cores. The springs are linear, massless, and have a rest length of zero. The stiffness of the chains is parameterized with the radius of gyration R_{g} of an ideal, unattached, linear chain such that the spring contribution to the free energy is defined by $F_{\mathrm{spring}} = \frac{1}{4}\frac{k_{\mathrm{B}}T}{R_{\mathrm{g}}^2}r^{*2}$ with r^* being the distance between the oligomer bead and the core center, k_{B} being the Boltzmann constant, and T being the temperature. The probability distribution function of the oligomer bead, $G(\mathbf{r}^*) \sim e^{-\frac{F_{\mathrm{spring}}}{k_{\mathrm{B}}T}}$, is normalized via

$$\int_{V^*} G(\mathbf{r}^*)\mathrm{d}\mathbf{r}^* = 1 \tag{5.1}$$

with V^* being the total suspension volume; the mean-square distance of the oligomer bead from the core center in the absence of chain–chain interactions is

$$\langle r^{*2}\rangle = \int_{V^*} r^{*2}G(\mathbf{r}^*)\mathrm{d}\mathbf{r}^* = 6R_{\mathrm{g}}^2. \tag{5.2}$$

The solute molecules are modeled as untethered beads in the fluid phase and contribute to a portion of the fluid space. We assume that in general one so-

lute molecule occupies a different volume from one oligomer and the volume ratio between one solute and one oligomer is γ_s. This ratio could incorporate the detailed excluded volume between monomers and solute but for simplicity we just use γ_s as an adjustable parameter. All starred variables are dimensional radii, distances, volume, densities, and wave numbers. In the following analysis, unstarred variables are length scales non-dimensionalized by a.

The theory exploits a weak oligomeric-field approximation valid when $R_g \gg a$, so that many cores' oligomers collaborate with solute molecules to fill any region of the fluid space. In this limit, we can use different approximations over two different length scales. For separations of order a hard-core interactions dominate, while the fluid-species (oligomers and solute) interactions dominate at separations of order R_g. In the latter region, we can neglect the detailed packing configuration of the particles and assume that the particles simply fill a fraction ϕ_b of the volume. The condition $n_b^* R_g^3$ with n_b^* being the bulk number density of the cores also allows us to close the equations governing the oligomer concentration, solute concentration, and the core radial distribution function by neglecting correlations smaller than $O(1/n_b^* R_g^3)$ or $O(a^3/R_g^3)$ as justified in Ref. [6].

We assume that the oligomers and the solute can relax quickly compared with the cores. Therefore we can first formulate the equilibrium fluid phase free energy for a given particle configuration. For a system of M_s solute molecules and N NOHMs particles each of which has M tethered oligomers, the ideal gas, translational free energy of the fluid phase species is

$$\frac{F_f^{tr}}{k_B T} = NM \ln\left(\frac{NM\Lambda_o^3}{V}\right) - NM + M_s \ln\left(\frac{M_s \Lambda_s^3}{V}\right) - M_s, \tag{5.3}$$

where Λ_o and Λ_s are the thermal de Broglie wavelengths of oligomers and solute, respectively. Since we are interested in the equilibrium configuration of

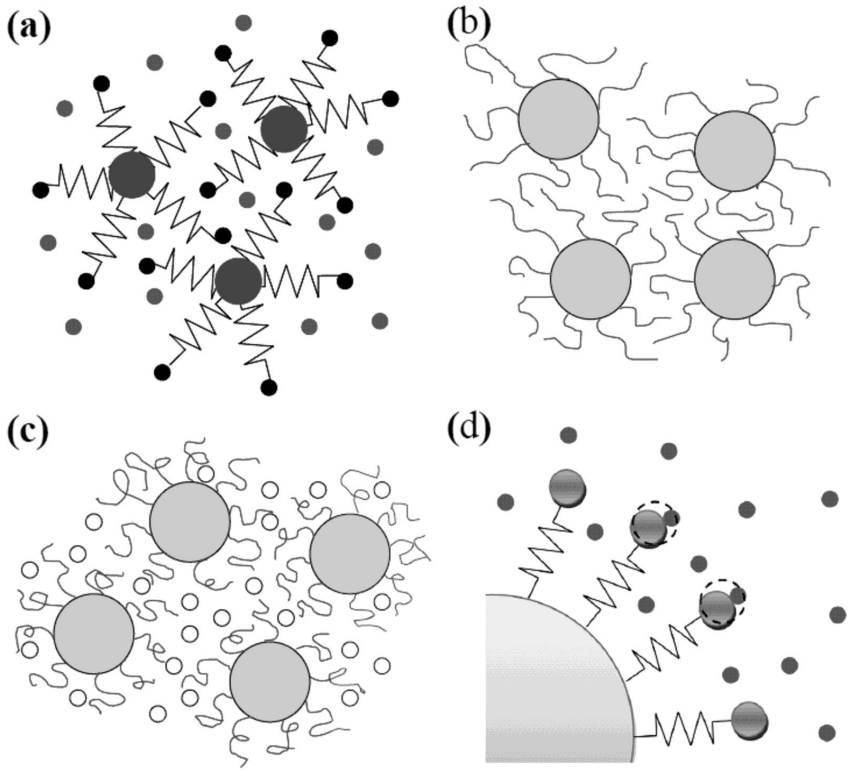

Figure 5.1: (a) Schematic of the coarse-grained model considered in this work. The big central spheres are the hard cores and the small beads connected to the cores with springs represent oligomers. Each spring has one monomer. The unconnected beads are solute molecules. (b) A random particle array showing that the oligomer configuration is restricted in the absence of other fluid molecules filling the space. (c) A random particle array showing that the physically added solute molecules help the oligomers release the entropic frustration. (d) Schematic of tethered oligomers with both physically (small beads free in space) and chemically (small beads bonded to the oligomer bead) absorbed solute molecules. The dashed circles represent the new oligomer bead when the solute is chemically bonded. In our model the number of oligomers per particle is an adjustable parameter M and for clarity we only illustrate a few oligomers here.

oligomers tethered to the core and the solute distribution, we may introduce spatial variations in the oligomer and solute distributions in Eq. 5.3 and write $\frac{M}{V}$ as $C_i(\mathbf{r}, \mathbf{r}_i)$, the concentration field (number density) of the oligomers at $\mathbf{r}$ attached to particle i with a position $\mathbf{r}_i$, N as $\sum_{i=1}^{N}$, and $\frac{M_s}{V}$ as $C_s(\mathbf{r})$, the concentration field of the solute at $\mathbf{r}$. As a result, the fluid phase free energy for a given particle configuration takes the following form:

$$\frac{F_f}{k_B T} = \sum_{i=1}^{N} \left\{ \int_V C_i(\mathbf{r}, \mathbf{r}_i) \left[\ln \frac{C_i(\mathbf{r}, \mathbf{r}_i)}{1 - \phi_b} \Lambda_o^3 - 1 \right] + \frac{a^2}{4R_g^2} (\mathbf{r} - \mathbf{r}_i)^2 \, C_i(\mathbf{r}, \mathbf{r}_i) d\mathbf{r} \right\}$$
$$+ \int_V C_s(\mathbf{r}) \left[\ln \frac{C_s(\mathbf{r})}{1 - \phi_b} \Lambda_s^3 - 1 \right] d\mathbf{r} + \frac{\chi}{1 - \phi_b} \sum_{i=1}^{N} \left\{ \int_V \phi_i(\mathbf{r}, \mathbf{r}_i) C_s(\mathbf{r}) d\mathbf{r} \right\} + NM \ln(N), \tag{5.4}$$

where χ is the Flory–Huggins interaction parameter for oligomer–solute enthalpic interactions. The first integral contains the oligomer-configurational entropy and the spring energy, the second integral represents the solute-translational entropy, and the third integral accounts for the additional monomer–solute enthalpic interactions relative to the monomer–monomer and solute–solute interactions. The last constant term does not affect the equilibrium configurations $C_i(\mathbf{r}, \mathbf{r}_i)$ and $C_s(\mathbf{r})$ and is kept for consistency. $\phi_i(\mathbf{r}, \mathbf{r}_i) = v_o C_i(\mathbf{r}, \mathbf{r}_i)$ with v_o being the volume of one oligomer. We include a factor of $1/(1 - \phi_b)$ in the configurational/translational-entropic and the enthalpic terms because in the mean-field fashion the concentrations in the volume not occupied by the cores would be larger than the one in the total volume by this factor.

The dissolved gas solute and the oligomers form an incompressible fluid. Therefore we may choose the pure, incompressible NOHMs system without the solute as our reference state and define the fluid species' total concentration. If we neglect the volume change on mixing the two species, the concentrations of

oligomers and solute satisfy the "incompressibility relation":

$$\sum_{i=1}^{N} C_i(\mathbf{r}, \mathbf{r}_i) + \gamma_s C_s(\mathbf{r}) = n_b^0 M \frac{1-\phi_b}{1-\phi_b^0}, \tag{5.5}$$

where n_b^0 and ϕ_b^0 are the particle number density and volume fraction for the reference pure NOHMs system before the solute is absorbed. The factor $\frac{1-\phi_b}{1-\phi_b^0}$ on the right hand side takes into account the increase in the fluid phase volume as the solute is added. $n_b = n_b^0 / \left[1 + m_s\gamma_s\left(1-\phi_b^0\right)\right]$ and $\phi_b = \phi_b^0 / \left[1 + m_s\gamma_s\left(1-\phi_b^0\right)\right]$ with $m_s = \frac{M_s}{MN}$ being the ratio of the total number of solute molecules to the total number of oligomers, or the molar ratio of solute to oligomer liquid in the system.

The equilibrium concentration field of the oligomers can be determined by minimizing the fluid phase free energy with respect to variations in C_i subject to the constraint that the probability of finding the oligomers attached to a given particle is normalized,

$$\int_V C_i(\mathbf{r}, \mathbf{r}_i) \mathrm{d}\mathbf{r} = M. \tag{5.6}$$

Therefore we define the Lagrange function

$$L_f\left[C_i(\mathbf{r}, \mathbf{r}_i)\right] = \frac{F_f}{k_B T} - \sum_{i=1}^{N} \lambda_i \left[\int_V C_i(\mathbf{r}, \mathbf{r}_i)\mathrm{d}\mathbf{r} - M\right], \tag{5.7}$$

where the Lagrange multipliers λ_i enforcing the normalization make up a discrete set with one multiplier for each particle. For a given particle configuration, the minimization $\delta L_f / \delta C_i(\mathbf{r}, \mathbf{r}_i)$ and making use of Eqs. 5.5 and 5.6 yield

$$C_i(\mathbf{r}, \mathbf{r}_i) = \frac{M\left[C_s(\mathbf{r})^{1/\gamma_s}\right] \exp\left\{-2\chi v_o \frac{C_s(\mathbf{r})}{1-\phi_b} - \frac{a^2}{4R_g^2}(\mathbf{r}-\mathbf{r}_i)^2\right\}}{\int_V \left[C_s(\mathbf{r}')^{1/\gamma_s}\right] \exp\left\{-2\chi v_o \frac{C_s(\mathbf{r}')}{1-\phi_b} - \frac{a^2}{4R_g^2}(\mathbf{r}'-\mathbf{r}_i)^2\right\} \mathrm{d}\mathbf{r}'}. \tag{5.8}$$

When $R_g^3 \gg a^3$, many particles' oligomers contribute to the local fluid density at $\mathbf{r}$ and each particle's oligomers only cause a small $O(a^3/R_g^3)$ disturbance to the

fluid density. Since this disturbance is compensated by the solute molecules to satisfy the incompressibility condition, we may write $C_{\rm s}(\mathbf{r}) = C_{\rm s,b}\left[1 + C'_{\rm s}(\mathbf{r})\right]$ with $C_{\rm s,b} = m_{\rm s} n_{\rm b} M$ being the bulk solute concentration and $C'_{\rm s}(\mathbf{r})$ being of $O(a^3/R_{\rm g}^3)$. After substituting this expression into Eq. 5.8 and some manipulations we obtain

$$C_i(\mathbf{r}, \mathbf{r}_i) = M\Lambda_i \left[1 + \frac{C'_{\rm s}(\mathbf{r})}{\gamma_{\rm s}}\right]\left[1 - 2\chi v_{\rm o}\frac{C_{\rm s,b}}{1-\phi_{\rm b}}C'_{\rm s}(\mathbf{r})\right] G\left(\mathbf{r} - \mathbf{r}_i\right), \tag{5.9}$$

where $G(\mathbf{r} - \mathbf{r}_i) = \left(\frac{4\pi R_{\rm g}^2}{a^2}\right)^{-\frac{3}{2}} e^{-\frac{a^2(\mathbf{r}-\mathbf{r}_i)^2}{4R_{\rm g}^2}}$ is the probability of finding a monomer bead in the absence of particle interactions and $\Lambda_i = 1 + \Lambda'_i$ is a normalization constant with Λ'_i being of $O(a^3/R_{\rm g}^3)$.

Following the procedure used in Ref. [6], Eq. 5.5 yields the conditional average total fluid species' concentration $\langle C\rangle_1(\mathbf{r}|\mathbf{r}_1)$ with one core particle fixed at $\mathbf{r}_1$,

$$\begin{aligned}\langle C\rangle_1(\mathbf{r}|\mathbf{r}_1) &= \langle C_1\rangle_1(\mathbf{r}|\mathbf{r}_1) + n_{\rm b}\int_V g(\mathbf{r}_2 - \mathbf{r}_1)\langle C_2\rangle_2(\mathbf{r}|\mathbf{r}_1, \mathbf{r}_2)\mathrm{d}\mathbf{r}_2 + \gamma_{\rm s} C_{\rm s,b}\left[1 + \langle C'_{\rm s}\rangle_1(\mathbf{r}|\mathbf{r}_1)\right] \\ &= n_{\rm b}^0 M\frac{1-\phi_{\rm b}}{1-\phi_{\rm b}^0},\end{aligned} \tag{5.10}$$

where $\langle C_1\rangle_1(\mathbf{r}|\mathbf{r}_1)$ is the conditional average of the concentration field of oligomers attached to particle 1 given that particle 1 is fixed at $\mathbf{r}_1$, $\langle C_2\rangle_2(\mathbf{r}|\mathbf{r}_1, \mathbf{r}_2)$ is the conditional average of the concentration field of oligomers attached to particle 2 given that particles 1 and 2 are fixed at $\mathbf{r}_1$ and $\mathbf{r}_2$, and $g(\mathbf{r}_2 - \mathbf{r}_1)$ is the core radial distribution function. Under the weak-field approximation retaining up to $O(a^3/R_{\rm g}^3)$ correlations,

$$\langle C_1\rangle_1(\mathbf{r}|\mathbf{r}_1) \approx M\left[1 + \langle\Lambda'_1\rangle_1(\mathbf{r}_1|\mathbf{r}_1) + \left(\frac{1}{\gamma_{\rm s}} - 2\chi v_{\rm o}\frac{C_{\rm s,b}}{1-\phi_{\rm b}}\right)\langle C'_{\rm s}\rangle_1(\mathbf{r}|\mathbf{r}_1)\right] G(\mathbf{r} - \mathbf{r}_1), \tag{5.11}$$

$$\begin{aligned}\langle C_2\rangle_2(\mathbf{r}|\mathbf{r}_1, \mathbf{r}_2) \approx M\{&1 + \langle\Lambda'_2\rangle_1(\mathbf{r}_2|\mathbf{r}_2) + \langle\Lambda''_2\rangle_2(\mathbf{r}_2|\mathbf{r}_1, \mathbf{r}_2) \\ &+ \left(\frac{1}{\gamma_{\rm s}} - 2\chi v_{\rm o}\frac{C_{\rm s,b}}{1-\phi_{\rm b}}\right)[\langle C'_{\rm s}\rangle_1(\mathbf{r}|\mathbf{r}_1) + \langle C'_{\rm s}\rangle_1(\mathbf{r}|\mathbf{r}_2)]\}G(\mathbf{r} - \mathbf{r}_2),\end{aligned} \tag{5.12}$$

and

$$g(\mathbf{r}_2 - \mathbf{r}_1) = 1 + h_{\mathrm{HS}}(\mathbf{r}_2 - \mathbf{r}_1) + h_{\mathrm{f}}(\mathbf{r}_2 - \mathbf{r}_1), \tag{5.13}$$

where h_{HS} is the total correlation function of the reference hard sphere suspension without the oligomers and h_{f} is the perturbation to the hard sphere pair distribution function due to the oligomers. The conditional average field variables and h_{f} are of $O(a^3/R_{\mathrm{g}}^3)$. Substituting Eqs. 5.11–5.13 into Eq. 5.10 yields the $O(1)$ equation:

$$\begin{aligned} G(\mathbf{r} - \mathbf{r}_1) + \gamma_{\mathrm{s}} m_{\mathrm{s}} n_{\mathrm{b}} \langle C_{\mathrm{s}}' \rangle_1(\mathbf{r}|\mathbf{r}_1) + n_{\mathrm{b}} \int_V \{ \langle \Lambda_2' \rangle_1(\mathbf{r}_2|\mathbf{r}_2) + \langle \Lambda_2'' \rangle_2(\mathbf{r}_2|\mathbf{r}_1, \mathbf{r}_2) \\ + \left(\frac{1}{\gamma_{\mathrm{s}}} - 2\chi v_{\mathrm{o}} \frac{C_{\mathrm{s,b}}}{1 - \phi_{\mathrm{b}}} \right) [\langle C_{\mathrm{s}}' \rangle_1(\mathbf{r}|\mathbf{r}_1) + \langle C_{\mathrm{s}}' \rangle_1(\mathbf{r}|\mathbf{r}_2)] \\ + h_{\mathrm{HS}}(\mathbf{r}_2 - \mathbf{r}_1) + h_{\mathrm{f}}(\mathbf{r}_2 - \mathbf{r}_1) \} G(\mathbf{r} - \mathbf{r}_2) \mathrm{d}\mathbf{r}_2 = 0. \end{aligned} \tag{5.14}$$

Application of the normalization conditions for $\langle C_1 \rangle_1$ and $\langle C_2 \rangle_2$ and Fourier transformation of Eq. 5.14 yield the field variables required to obtain the oligomer and solute concentration fields to $O(a^3/R_{\mathrm{g}}^3)$:

$$\langle \hat{C}_{\mathrm{s}}' \rangle_1(\mathbf{k}) = \frac{\hat{G}(\mathbf{k}) \left[1 + n_{\mathrm{b}} \hat{h_{\mathrm{HS}}}(\mathbf{k}) + n_{\mathrm{b}} \hat{h_{\mathrm{f}}}(\mathbf{k}) \right]}{n_{\mathrm{b}} \left\{ \left(\frac{1}{\gamma_{\mathrm{s}}} - 2\chi v_{\mathrm{o}} \frac{C_{\mathrm{s,b}}}{1 - \phi_{\mathrm{b}}} \right) \left[\hat{G}(\mathbf{k})^2 - 1 \right] - \gamma_{\mathrm{s}} m_{\mathrm{s}} \right\}}, \tag{5.15}$$

$$\langle \hat{\Lambda_2''} \rangle_2(\mathbf{k}) = -\left(\frac{1}{\gamma_{\mathrm{s}}} - 2\chi v_{\mathrm{o}} \frac{C_{\mathrm{s,b}}}{1 - \phi_{\mathrm{b}}} \right) \langle \hat{C}_{\mathrm{s}}' \rangle_1(\mathbf{k}) \hat{G}(\mathbf{k}), \tag{5.16}$$

and

$$\langle \Lambda_i' \rangle_1(\mathbf{r}_i|\mathbf{r}_i) = -\left(\frac{1}{\gamma_{\mathrm{s}}} - 2\chi v_{\mathrm{o}} \frac{C_{\mathrm{s,b}}}{1 - \phi_{\mathrm{b}}} \right) \frac{1}{(2\pi)^3} \int_{V_k} \langle \hat{C}_{\mathrm{s}}' \rangle_1(\mathbf{k}) \hat{G}(-\mathbf{k}) \mathrm{d}\mathbf{k} \tag{5.17}$$

with V_k being all space in $\mathbf{k}$, and the subscript i is 1 or 2. The Fourier transform of $F(\mathbf{x})$ and the inverse transform of $\hat{F}(\mathbf{k})$ are defined by $\hat{F}(\mathbf{k}) = \int F(\mathbf{x}) e^{-i\mathbf{k}\cdot\mathbf{x}} \mathrm{d}\mathbf{x}$ and $F(\mathbf{x}) = \frac{1}{(2\pi)^3} \int \hat{F}(\mathbf{k}) e^{i\mathbf{k}\cdot\mathbf{x}} \mathrm{d}\mathbf{k}$.

With the expressions for the field variables on hand, we now apply a conventional density-functional approach to solve for the core radial distribution

function. The grand potential Ω of the entire system given that a *chosen* particle labeled 1 is at the origin can be expressed as a functional of the one-body density profile of other *non-chosen* particles labeled 2 around particle 1, $n(\mathbf{r}_\mathrm{p}) = n_\mathrm{b} g(\mathbf{r}_\mathrm{p})$, with $\mathbf{r}_\mathrm{p}$ being $\mathbf{r}_2 - \mathbf{r}_1$:

$$\Omega\left[n(\mathbf{r}_\mathrm{p})\right] = F_\mathrm{id}\left[n(\mathbf{r}_\mathrm{p})\right] + F_\mathrm{ex}^\mathrm{HS}\left[n(\mathbf{r}_\mathrm{p})\right] + F_\mathrm{ex}^\mathrm{fluid}[n(\mathbf{r}_\mathrm{p})] + \int_V n(\mathbf{r}_\mathrm{p})\left[V_1(\mathbf{r}_\mathrm{p}) - \mu\right]\mathrm{d}\mathbf{r}_\mathrm{p}, \quad (5.18)$$

where the ideal gas part of the free energy functional of the cores is

$$\frac{F_\mathrm{id}\left[n(\mathbf{r}_\mathrm{p})\right]}{k_\mathrm{B}T} = \int_V n(\mathbf{r}_\mathrm{p})\left\{\ln\left[n(\mathbf{r}_\mathrm{p})\Lambda_\mathrm{p}^3\right] - 1\right\}\mathrm{d}\mathbf{r}_\mathrm{p} \quad (5.19)$$

with Λ_p being the thermal de Broglie wavelength of the particles, μ is the chemical potential of the particles, V_1 is the external potential due to the hard-sphere excluded volume of the fixed particle 1, $F_\mathrm{ex}^\mathrm{HS}$ is the excess free energy contributed from the hard spheres, and $F_\mathrm{ex}^\mathrm{fluid}$ is the excess free energy contributed from the fluid phase oligomers and solute. For a given core configuration, the free energy of the fluid species is smeared out as a "mediated interparticle potential" between the cores. Therefore we obtain $F_\mathrm{ex}^\mathrm{fluid}$ by conditionally averaging the fluid phase free energy shown in Eq. 5.4 over the configuration of $N-1$ particles given that particle 1 is fixed at the origin:

$$\begin{aligned}
\frac{F_\mathrm{ex}^\mathrm{fluid}\left[n(\mathbf{r}_\mathrm{p})\right]}{k_\mathrm{B}T} &= \left\langle \frac{F_\mathrm{f}}{k_\mathrm{B}T} \right\rangle_1 \\
&= \int_V \left\{ \left\langle C_1 \ln \frac{C_1}{1-\phi_\mathrm{b}} \Lambda_\mathrm{o}^3 \right\rangle_1 (\mathbf{r}|\mathbf{0}) + \left[\frac{a^2\mathbf{r}^2}{4R_\mathrm{g}^2} - 1\right] \langle C_1 \rangle_1 (\mathbf{r}|\mathbf{0}) \right\} \mathrm{d}\mathbf{r} \\
&+ \int_V n(\mathbf{r}_\mathrm{p}) \int_V \left\{ \left\langle C_2 \ln \frac{C_2}{1-\phi_\mathrm{b}} \Lambda_\mathrm{o}^3 \right\rangle_2 (\mathbf{r}|\mathbf{0}, \mathbf{r}_\mathrm{p}) + \left[\frac{a^2(\mathbf{r}-\mathbf{r}_\mathrm{p})^2}{4R_\mathrm{g}^2} - 1\right] \langle C_2 \rangle_2 (\mathbf{r}|\mathbf{0}, \mathbf{r}_\mathrm{p}) \right\} \mathrm{d}\mathbf{r}\mathrm{d}\mathbf{r}_\mathrm{p} \\
&+ \int_V \left\{ \left\langle C_\mathrm{s} \ln \frac{C_\mathrm{s}}{1-\phi_\mathrm{b}} \Lambda_\mathrm{s}^3 \right\rangle_1 (\mathbf{r}|\mathbf{0}) - \langle C_\mathrm{s} \rangle_1 (\mathbf{r}|\mathbf{0}) \right\} \mathrm{d}\mathbf{r} \\
&+ \frac{\chi}{1-\phi_\mathrm{b}} \int_V \langle \phi_1 C_\mathrm{s} \rangle_1 (\mathbf{r}|\mathbf{0}) \mathrm{d}\mathbf{r} + \frac{\chi}{1-\phi_\mathrm{b}} \int_V n(\mathbf{r}_\mathrm{p}) \int_V \langle \phi_2 C_\mathrm{s} \rangle_2 (\mathbf{r}|\mathbf{0}, \mathbf{r}_\mathrm{p}) \mathrm{d}\mathbf{r}\mathrm{d}\mathbf{r}_\mathrm{p} + NM\ln(N),
\end{aligned} \quad (5.20)$$

where $\mathbf{r}_\mathrm{p}$ is the position of neighboring core particles labeled 2 and $\mathbf{r}$ is the position of beads.

At equilibrium, the distribution function is determined by minimizing the grand potential, $\delta\Omega[n(\mathbf{r}_\mathrm{p})]/\delta n(\mathbf{r}_\mathrm{p}) = 0$, and applying equal chemical potential of the neighboring particles, $\mu = \mu_\mathrm{bulk} = \mu|_{\mathbf{r}_\mathrm{p}\to\infty}$:

$$n(\mathbf{r}_\mathrm{p}) = n_\mathrm{b} g(\mathbf{r}_\mathrm{p}) = n_\mathrm{b} \exp\left\{c^{(1)}_\mathrm{HS}(\mathbf{r}_\mathrm{p}) - c^{(1)}_\mathrm{HS,b} - \frac{V_1(\mathbf{r}_\mathrm{p})}{k_\mathrm{B}T} + c^{(1)}_\mathrm{f}(\mathbf{r}_\mathrm{p}) - c^{(1)}_\mathrm{f,b}\right\}, \tag{5.21}$$

where the one-body direct correlation functions are defined by $c^{(1)}_\mathrm{HS}(\mathbf{r}_\mathrm{p}) = -\frac{\delta\left(F^\mathrm{HS}_\mathrm{ex}[n(\mathbf{r}_\mathrm{p})]/k_\mathrm{B}T\right)}{\delta n(\mathbf{r}_\mathrm{p})}$, $c^{(1)}_\mathrm{HS,b} = -\frac{\delta\left(F^\mathrm{HS}_\mathrm{ex}[n(\mathbf{r}_\mathrm{p})]/k_\mathrm{B}T\right)}{\delta n(\mathbf{r}_\mathrm{p})}|_{\mathbf{r}_\mathrm{p}\to\infty}$, $c^{(1)}_\mathrm{f}(\mathbf{r}_\mathrm{p}) = -\frac{\delta\left(F^\mathrm{fluid}_\mathrm{ex}[n(\mathbf{r}_\mathrm{p})]/k_\mathrm{B}T\right)}{\delta n(\mathbf{r}_\mathrm{p})}$, and $c^{(1)}_\mathrm{f,b} = -\frac{\delta\left(F^\mathrm{fluid}_\mathrm{ex}[n(\mathbf{r}_\mathrm{p})]/k_\mathrm{B}T\right)}{\delta n(\mathbf{r}_\mathrm{p})}|_{\mathbf{r}\to\infty}$. As justified in Ref. [6], under the weak-field approximation and the separation of two length scales we can obtain the core pair probability expressed in Eq. 5.13 with $1 + h_\mathrm{HS}(\mathbf{r}_\mathrm{p}) = e^{\left[c^{(1)}_\mathrm{HS}(\mathbf{r}_\mathrm{p}) - c^{(1)}_\mathrm{HS,b} - V_1(\mathbf{r}_\mathrm{p})/k_\mathrm{B}T\right]}$ and $h_\mathrm{f}(\mathbf{r}_\mathrm{p}) \approx \left[c^{(1)}_\mathrm{f}(\mathbf{r}_\mathrm{p}) - c^{(1)}_\mathrm{f,b}\right]$. We can neglect the coupling between h_HS and h_f by keeping dominant contributions from these variations of the free energy at the two length scales of a and R_g. As a result, $c^{(1)}_\mathrm{f}(\mathbf{r}_\mathrm{p}) \approx -\frac{\delta\left(F^\mathrm{fluid}_\mathrm{ex}[n(\mathbf{r}_\mathrm{p})]/k_\mathrm{B}T\right)}{n_\mathrm{b}\delta h_\mathrm{f}(\mathbf{r}_\mathrm{p})}$ and $c^{(1)}_\mathrm{HS}(\mathbf{r}_\mathrm{p}) \approx -\frac{\delta\left(F^\mathrm{HS}_\mathrm{ex}[n(\mathbf{r}_\mathrm{p})]/k_\mathrm{B}T\right)}{n_\mathrm{p}\delta h_\mathrm{HS}(\mathbf{r}_\mathrm{p})}$. Therefore we can directly evaluate h_HS by solving the Ornstein–Zernike equation with the Percus–Yevick approximation [17,18]. Substitution of the field variables Λ'_i and $C'_\mathrm{s}(\mathbf{r})$ into $F^\mathrm{fluid}_\mathrm{ex}[n(\mathbf{r}_\mathrm{p})]/k_\mathrm{B}T$ shown in Eq. 5.20, truncation of the higher order correlations between the particles, and functional differentiation $\frac{\delta\left(F^\mathrm{fluid}_\mathrm{ex}[n(\mathbf{r}_\mathrm{p})]/k_\mathrm{B}T\right)}{n_\mathrm{b}\delta h_\mathrm{f}(\mathbf{r}_\mathrm{p})}$ finally yield to $O(a^3/R_\mathrm{g}^3)$:

$$\begin{aligned} h_\mathrm{f}(\mathbf{r}_\mathrm{p}) \approx\ & 2M\left(\frac{\frac{1}{\gamma_s} - \chi\nu_\mathrm{o}\frac{C_\mathrm{s,b}}{1-\phi_\mathrm{b}}}{\frac{1}{\gamma_\mathrm{s}} - 2\chi\nu_\mathrm{o}\frac{C_\mathrm{s,b}}{1-\phi_\mathrm{b}}}\right)\int_V \langle\Lambda''_2\rangle_2(\mathbf{r}'_\mathrm{p}|\mathbf{0},\mathbf{r}_\mathrm{p})\frac{\delta\langle\Lambda''_2\rangle_2(\mathbf{r}'_\mathrm{p}|\mathbf{0},\mathbf{r}_\mathrm{p})}{\delta h_\mathrm{f}(\mathbf{r}_\mathrm{p})}\mathrm{d}\mathbf{r}'_\mathrm{p} \\ & - 2M\left[\left(\frac{1}{\gamma_s} - 2\chi\nu_\mathrm{o}\frac{C_\mathrm{s,b}}{1-\phi_\mathrm{b}}\right)\left(\frac{1}{\gamma_\mathrm{s}} - \chi\nu_\mathrm{o}\frac{C_\mathrm{s,b}}{1-\phi_\mathrm{b}}\right) + m_\mathrm{s}\right]\int_V \langle C'_\mathrm{s}\rangle_1(\mathbf{r}'|\mathbf{0})\frac{\delta\langle C'_\mathrm{s}\rangle_1(\mathbf{r}'|\mathbf{0})}{\delta h_\mathrm{f}(\mathbf{r}_\mathrm{p})}\mathrm{d}\mathbf{r}'. \end{aligned} \tag{5.22}$$

The convergence of these integrals is guaranteed since the changes in the field variables due to the pair probability is important only within a dis-

tance $\sim R_g$ from the fixed particle 1. When particle 2 is deep in the bulk, $\delta\langle\Lambda_2''\rangle_2(\mathbf{r}_p'|\mathbf{0},\mathbf{r}_p)/\delta h_f(\mathbf{r}_p) \to 0$ and $\delta\langle C_s'\rangle_1(\mathbf{r}'|\mathbf{0})/\delta h_f(\mathbf{r}_p) \to 0$. This equation indicates that the pair probability depends on the cross-correlations of the the field variables and their variations, which are in fact dependent on the pair probability. Therefore, h_f is solved in a self-consistent manner. After making use of the convolution theorem and the expressions for $\langle\hat{C}_s'\rangle_1(\mathbf{k})$ and $\langle\hat{\Lambda}_2''\rangle_2(\mathbf{k})$, in Fourier space we obtain

$$\hat{h_f}(\mathbf{k}) = -\left(\frac{2M}{n_b}\right) \times \frac{\hat{G}(\mathbf{k})^2\left\{(1-\Delta)(1-2\Delta)\left[1-\hat{G}(\mathbf{k})^2\right]+\gamma_s^2 m_s\right\}\left[1+n_b\hat{h_{HS}}(\mathbf{k})\right]}{\left\{(1-2\Delta)\left[\hat{G}(\mathbf{k})^2-1\right]-\gamma_s^2 m_s\right\}^2+2M\hat{G}(\mathbf{k})^2\left\{(1-\Delta)(1-2\Delta)\left[1-\hat{G}(\mathbf{k})^2\right]+\gamma_s^2 m_s\right\}}, \tag{5.23}$$

where the prefactor $\Delta = \chi v_o \gamma_s C_{s,b}/(1-\phi_b)$ can be viewed as the total strength of the enthalpic interaction that depends not only on the interaction parameter weighted by the size of the solute, $\chi v_o \gamma_s$, but also on the total solute concentration, $C_{s,b} = m_s n_b M$. The static structure factor of the cores is defined by $S(\mathbf{k}) = 1 + n_b\hat{h_{HS}}(\mathbf{k}) + n_b\hat{h_f}(\mathbf{k})$. As $\mathbf{k} \to 0$, $\hat{G}(\mathbf{0}) = 1$ and $S(\mathbf{0}) \neq 0$ since the added solute molecules occupy a certain amount of fluid space not belonging to the share of tethered oligomeric fluid of each core. In the absence of solute, $m_s = 0$, Eq. 5.23 is reduced to Eq. 29 in Ref. [6] for incompressible single-component NOHMs systems and we obtain $S(\mathbf{0}) = 0$. The core pair probability $g(\mathbf{r}_p)$ can be obtained by taking the inverse Fourier transform of $\hat{h_f}$ in Eq. 5.23 and adding the hard sphere pair probability. The conditional average configuration of oligomers attached to a given particle can be obtained using Eg. 5.11 and the conditional average solute concentration is $\langle C_s\rangle_1(\mathbf{r}) = C_{s,b}\left[1+\langle C_s'\rangle_1(\mathbf{r})\right]$.

We focus on the structural change due to the added solute at given geometrical parameters of NOHMs since the effects of changing geometrical parameters

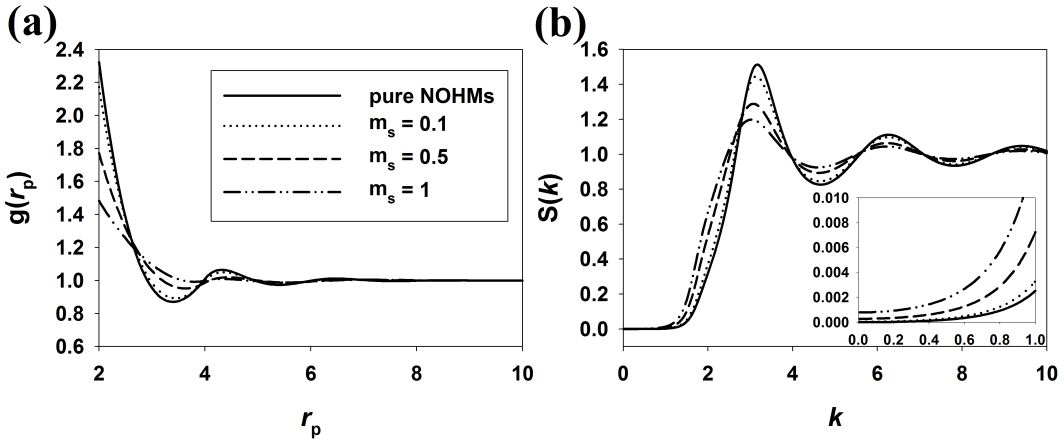

Figure 5.2: (a) The radial distribution function g as a function of the interparticle distance non-dimensionalized by the core radius, r_p, for the system with $R_g/a = 1$, $\phi_b^0 = 0.3$, $\chi = 0$, and $\gamma_s = 1$ at different moles solute/moles oligomer and (b) the corresponding static structure factor S as a function of the wave number non-dimensionalized by the core radius, k, with the same parameters and curve descriptions as given in (a). The inset shows S at small k.

have been presented elsewhere [6, 19]. We fix the fluid species number density based on the experimental value [4] such that the number of oligomers per core is 500 when $\phi_b^0 = 0.12$; in the pure system, as the core volume fraction varies the grafting density of oligomers changes accordingly.

Figure 5.2 presents the equilibrium core pair probability and static structure factor for the NOHMs system at different amounts of added solute with $\chi = 0$ and $\gamma_s = 1$. In this specific solute condition, the system can be viewed as NOHMs with some unattached oligomer melt. We find that as the amount of unattached fluid species increases, the core volume fraction decreases resulting in a less structured core pair probability and more disordered particle distribution. Since $g(r_p) = e^{-V_{mf}(r_p)/k_B T}$ with V_{mf} being the potential of mean force among the particles, damped oscillations in the core pair probability indicates

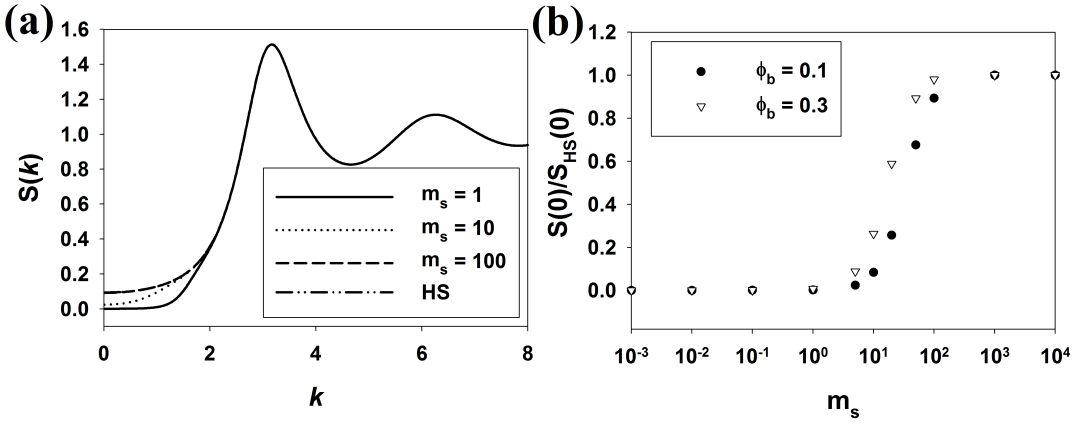

Figure 5.3: (a) The static structure factor S as a function of the wave number non-dimensionalized by the core radius, k, for the system with $R_g/a = 1$, $\chi = 0$, and $\gamma_s = 1$ at different moles unattached oligomer/moles attached oligomer with ϕ_b being fixed as 0.3. (b) The ratio of the static structure factors at zero wave number between NOHMs and hard spheres, $S(0)/S_{HS}(0)$, as a function of moles unattached oligomer/moles attached oligomer for $R_g/a = 1$, $\chi = 0$, and $\gamma_s = 1$ at two different ϕ_b.

that the interparticle potential is weakened. The static structure factor shows two distinct length scales: at larger k, the hard-core correlations are observed on the length scale of a and become weaker as there are more unattached fluid; at smaller k, the deficit of particles occurs roughly on the length scale of R_g. While for pure NOHMs system without unattached fluid $S(0) = 0$, $S(0) \neq 0$ when the unattached fluid is present. This means that we obtain more long-range density fluctuations in the system, consistent with the observation in Ref. [19] where the implicit added phantom solvent increased $S(0)$. The deviation of $S(0)$ from zero remains quite small even with moderate amount of unattached fluid. This is because that there are many degrees of freedom in the tethered and untethered species that encourage them to mix and this effect is stronger than the entropy associated with the core particle degrees of freedom.

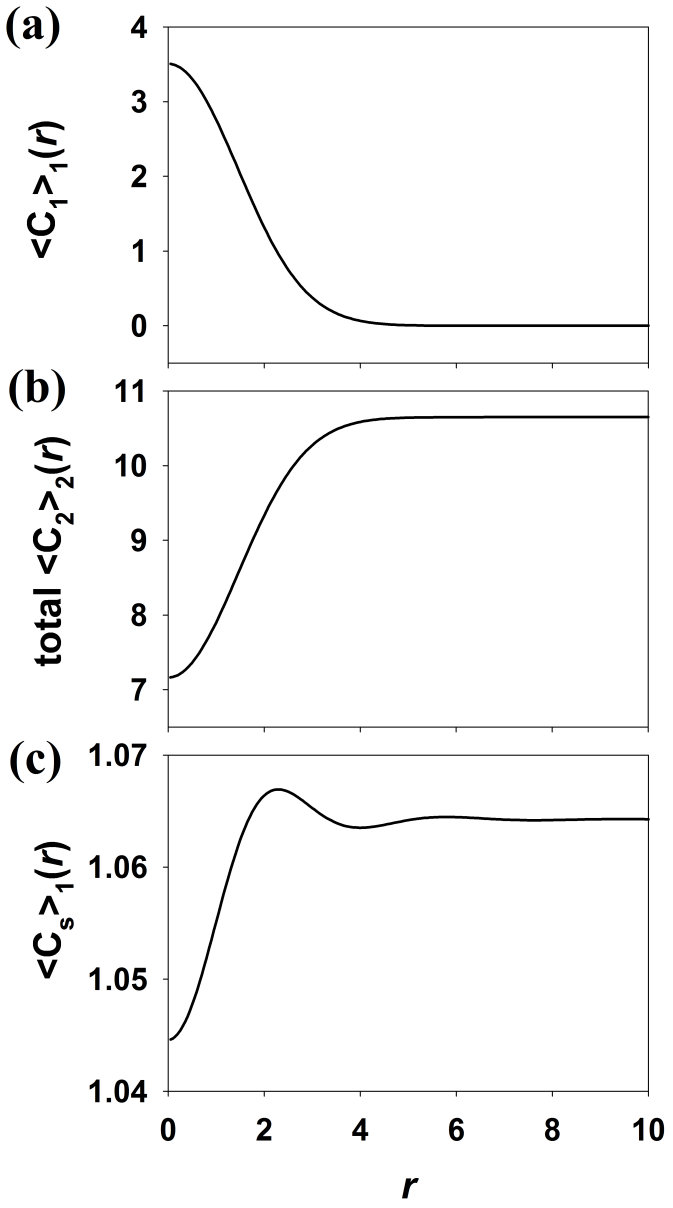

Figure 5.4: (a) The conditional average concentration of oligomers tethered to a given particle 1 $\langle C_1 \rangle_1$ as a function of the distance from the core center non-dimensionalized by the core radius, r, for the system with $R_g/a = 1$, $\phi_b^0 = 0.3$, $\chi = 0$, and $\gamma_s = 1$ at $m_s = 0.1$, (b) the conditional average total concentration of oligomers tethered to other cores, $\langle C \rangle_1 - \langle C_1 \rangle_1 - \gamma_s \langle C_s \rangle_1$, as a function of the distance from the center of particle 1 non-dimensionalized by the core radius, r, and (c) the conditional average concentration of solute around a given particle 1 $\langle C_s \rangle_1$ as a function of the distance from the center of particle 1 non-dimensionalized by the core radius, r , with the same parameters as given in (a).

While the structural variation we observe in Fig. 5.2 is also due to the change of the core volume fraction as unattached fluid "dilutes" the pure system, more subtle changes in $S(k)$ at small k can be brought out by fixing ϕ_b as ϕ_b^0 but varying the number of tethered oligomers such that m_s is the ratio of the number of untethered oligomers to the number of tethered oligomers. As can be seen from Fig. 5.3(a), if we increase m_s by decreasing the oligomer grafting density, the hard-core correlations at larger k remain unchanged but $S(k)$ at small-k region gradually approaches to that for the reference hard spheres. If we compare the ratio of $S(0)/S_{HS}(0)$ for different amounts of unattached fluid in Fig. 5.3(b), we find that $S(0)$ for NOHMs with unattached species remains fairly small until $m_s \approx 10$ and $S(0)/S_{HS}(0)$ approaches to 1 when $m_s > 100$. In the limit of large m_s, we obtain hard cores suspended in an unattached oligomer melt. This little change of $S(0)$ for NOHMs caused by increase in m_s suggests that NOHMs remain a well-dispersed system and do not immediately separate from the unattached fluid or form clusters. Therefore, NOHMs can be useful as solvents capturing a targeting gas such as CO_2 or as electrolytes where the added solute is ionic and the material retains high modulus and good diffusion of ions [5].

The incompressibility condition enforces a constant fluid phase concentration contributed from the tethered oligomers and unattached species. As depicted in Fig. 5.4, from the distributions of oligomers and solute for the same NOHMs system as Fig. 5.2 and $m_s = 0.1$, the tethered oligomers cooperate with the solute to fill the space. The deficit of other particles oligomers near particle 1 is compensated by the solute. The variations in the fields occur at a length scale of R_g, consistent with the length scale at which the deficit of a particle is observed in $S(k)$. Aside from the effect on the fields due to the incompressibil-

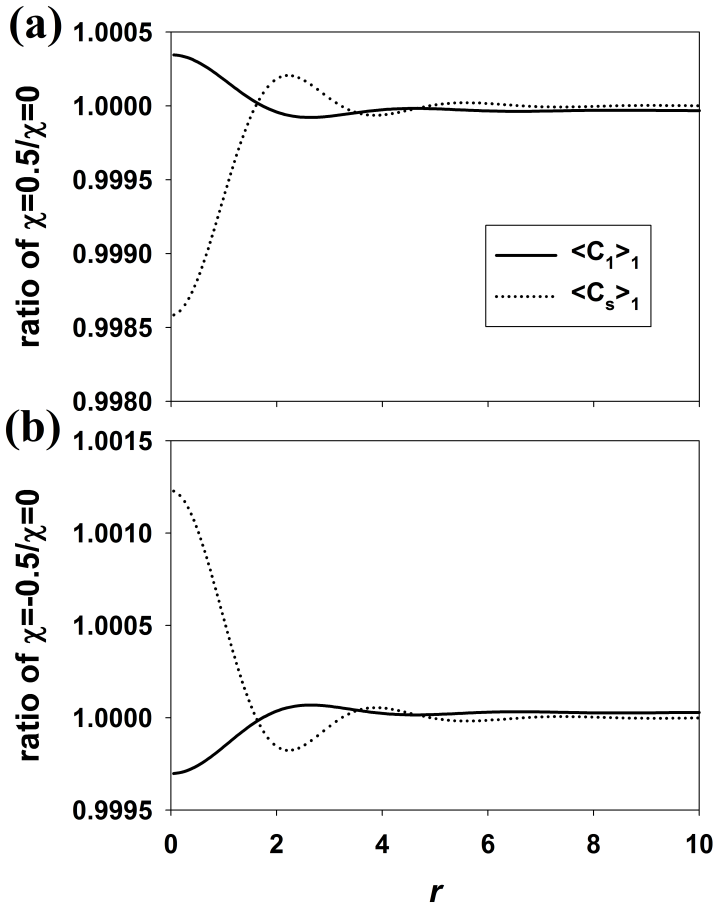

Figure 5.5: (a) The ratio between the conditional average fluid species distributions $\langle C_1 \rangle_1$ and $\langle C_s \rangle_1$ for $\chi = 0.5$ and $\chi = 0$ as a function of the distance from the core center non-dimensionalized by the core radius, r, for the system with $R_g/a = 1$, $\phi_b^0 = 0.3$, and $\gamma_s = 1$ at $m_s = 0.1$ and (b) the ratio between the conditional average fluid species distributions $\langle C_1 \rangle_1$ and $\langle C_s \rangle_1$ for $\chi = -0.5$ and $\chi = 0$ as a function of the distance from the core center non-dimensionalized by the core radius, r, with the same parameters and curve description as given in (a).

ity constraint alone, it is of interest to investigate how the enthalpic interaction between the oligomers and added solute affects the fluid species distributions. In Fig. 5.5 we introduce a non-zero χ to the system, calculate the new concentrations, and compare the new concentrations with the original concentrations for $\chi = 0$. As we can see here, compared to the case of $\chi = 0$, at $\chi = 0.5$ energetically oligomers and solute molecules like their own kinds better such that the tethered oligomers tend to stay closer to the particle where the solute concentration is lower. On the contrary, at $\chi = -0.5$ we find that the tethered oligomers tend to stretch more and mix with the solute and the solute concentration increases near the particle.

5.4 Solvent Capacity of NOHMs

5.4.1 Physisorption

In this section, we first consider the case where the gas solute is physically absorbed into the NOHMs solvent. This means that the gas is captured by the liquid phase via physical driving forces such as the changes in the system entropy and enthalpy due to mixing. As depicted in Figs. 5.1(b) and 5.1(c), while in the absence of an unattached fluid the conformations of oligomers are subject to the constraint that the tethered chains must fill the interstitial space, as solute is added to the system it facilitates the oligomeric hairs in filling the space and increases the oligomer-configurational entropy. Therefore it is anticipated that the tethered incompressible oligomers in NOHMs may provide an additional driving force for gas capture that is different from randomly mixing the

particles and the fluids.

The amount of solute captured is determined by the two-phase equilibrium. At a given temperature and pressure, the fugacity of the solute will be equal in both the liquid and vapor phases at phase equilibrium such that there is no net flux at the liquid–vapor boundary [20],

$$f_{\mathrm{s}}^{\mathrm{L}} = f_{\mathrm{s}}^{0}(T,P)e^{\frac{\mu_{\mathrm{s}}^{\mathrm{L}}(m_{\mathrm{s}})-\mu_{\mathrm{s}}^{0}}{k_{\mathrm{B}}T}} = f_{\mathrm{s}}^{\mathrm{V}} = P_{\mathrm{s}}\hat{\phi}_{\mathrm{s}}^{\mathrm{V}}(T,P), \tag{5.24}$$

where $f_{\mathrm{s}}^{\mathrm{L}}$ is the solute fugacity in the liquid-NOHMs phase, $f_{\mathrm{s}}^{\mathrm{V}}$ is the solute fugacity in the vapor phase, $f_{\mathrm{s}}^{0}(T,P)$ is the fugacity of pure solute liquid at temperature T and pressure P, $\mu_{\mathrm{s}}^{\mathrm{L}}(m_{\mathrm{s}})$ is the chemical potential of solute in the liquid-NOHMs phase and depends on the amount of solute absorbed, μ_{s}^{0} is the chemical potential of pure solute liquid, P_{s} is the partial pressure of the solute vapor, and $\hat{\phi}_{\mathrm{s}}^{\mathrm{V}}(T,P)$ is the fugacity coefficient of the pure solute vapor at T and P and can be evaluated using an equation of state. For a binary mixture of NOHMs and solute, given that NOHMs have negligible vapor pressure, $P_{\mathrm{s}} = P$. $f_{\mathrm{s}}^{0} = P^{\mathrm{sat}}\hat{\phi}_{\mathrm{s}}^{\mathrm{V}}(T,P^{\mathrm{sat}})$ with P^{sat} being the saturation pressure of pure solute liquid. f_{s}^{0} and $f_{\mathrm{s}}^{\mathrm{V}}$ are physical properties of the pure solute and determine whether the pure solute on its own has a higher tendency to be a liquid or vapor at a given T and P. The factor $e^{\frac{\mu_{\mathrm{s}}^{\mathrm{L}}(m_{\mathrm{s}})-\mu_{\mathrm{s}}^{0}}{k_{\mathrm{B}}T}}$ is a measure of the effect of mixing the pure solute liquid and the NOHMs solvent and is the only unknown in Eq. 5.24. Once this is determined we obtain the solubility of the solute in the NOHMs liquid.

$\mu_{\mathrm{s}}^{\mathrm{L}}(m_{\mathrm{s}}) - \mu_{\mathrm{s}}^{0}$ is calculated from the free energy of mixing ΔF_{mix} via

$$\mu_{\mathrm{s}}^{\mathrm{L}}(m_{\mathrm{s}}) - \mu_{\mathrm{s}}^{0} = \left(\frac{\partial \Delta F_{\mathrm{mix}}}{\partial M_{\mathrm{s}}}\right)_{T,N,M}, \tag{5.25}$$

where $M_{\mathrm{s}} = m_{\mathrm{s}}NM$ is the total number of solute molecules absorbed and

$$\frac{\Delta F_{\mathrm{mix}}}{k_{\mathrm{B}}T} = \frac{F^{\mathrm{mix}}}{k_{\mathrm{B}}T} - \frac{F^{\mathrm{L}}}{k_{\mathrm{B}}T} - \frac{F^{\mathrm{s}}}{k_{\mathrm{B}}T} \tag{5.26}$$

with F^{mix} being the total free energy of the binary mixture, F^{L} being the total free energy of the pure NOHMs liquid, and F^{s} being the total free energy of the pure solute liquid. Since the enthalpy of the mixture relative to the two pure liquids is taken into account by the interaction parameter χ, we may simply write $\frac{F^{\text{s}}}{k_{\text{B}}T} = M_{\text{s}}\left[\ln\left(C^{0}_{\text{s,b}}\Lambda^{3}_{\text{s}}\right) - 1\right]$ with $C^{0}_{\text{s,b}} = \frac{1}{\gamma_{\text{s}} v_{\text{o}}}$ being the number density of the pure solute liquid. Both F^{mix} and F^{L} contain ideal gas energy of the cores, excess energy of the cores, and excess energy of the fluid. The ideal gas energies of the cores are $\frac{F^{\text{mix}}_{\text{id}}}{k_{\text{B}}T} = N\left[\ln\left(n_{\text{b}}\Lambda^{3}_{\text{p}}\right) - 1\right]$ for the mixture and $\frac{F^{\text{L}}_{\text{id}}}{k_{\text{B}}T} = N\left[\ln\left(n^{0}_{\text{b}}\Lambda^{3}_{\text{p}}\right) - 1\right]$ for the pure NOHMs liquid. We adopt the Carnahan–Starling equation of state [21] to calculate the excess free energies from the cores in F^{mix} and F^{L} such that $\frac{F^{\text{mix}}_{\text{core}}}{k_{\text{B}}T} = N\frac{4\phi_{\text{b}} - 3\phi^{2}_{\text{b}}}{(1-\phi_{\text{b}})^{2}}$ and $\frac{F^{\text{L}}_{\text{core}}}{k_{\text{B}}T} = N\frac{4\phi^{0}_{\text{b}} - 3\phi^{02}_{\text{b}}}{(1-\phi^{0}_{\text{b}})^{2}}$. The excess free energy from the fluid phase species in these two free energies can be obtained by ensemble averaging the fluid phase free energy over all possible configurations of N particles. For a given quantity $A(\mathbf{r}) = \sum_{i}^{N}\left[\langle A_i\rangle_1(\mathbf{r}|\mathbf{r}_i) + A'_i(\mathbf{r})\right]$, we may write the ensemble average of $A(\mathbf{r})$ as $\langle A\rangle(\mathbf{r}) = N\langle A_1\rangle_1(\mathbf{r}|\mathbf{r}_1) + N(N-1)\int_V\int_V P^{(2)}(\mathbf{r}_1,\mathbf{r}_2)\langle A'_1\rangle_2(\mathbf{r}|\mathbf{r}_1,\mathbf{r}_2)\mathrm{d}\mathbf{r}_1\mathrm{d}\mathbf{r}_2$ if the indices are interchangeable with $P^{(2)}(\mathbf{r}_1,\mathbf{r}_2)$ being the probability density function of finding a pair of particles 1 and 2 at $\mathbf{r}_1$ and $\mathbf{r}_2$. Therefore, to evaluate the excess free energy from the fluid phase species, it is convenient to write the concentration fields as $C_i(\mathbf{r},\mathbf{r}_i) = \langle C_i\rangle_1(\mathbf{r}|\mathbf{r}_i) + C'_i(\mathbf{r},\mathbf{r}_i)$ for particle i's oligomers and $C_{\text{s}}(\mathbf{r}) = C_{\text{s,b}}\left[1 + \langle C'_{\text{s}}\rangle_1(\mathbf{r}|\mathbf{r}_i) + C''_s(\mathbf{r})\right]$ for solute concentration. After making use of these expressions, combining the oligomer-configurational entropy with the constant term $NM\ln(N)$ in Eq. 5.4 such that $\sum_{i=1}^{N} C_i\left[\ln C_i + \ln(N)\right] = \left(\sum_{i=1}^{N} C_i\right)\ln\left(\sum_{i=1}^{N} C_i\right)$, neglecting higher order particle correlations, manipulations of ensemble averages, and writing $P^{(2)}(\mathbf{r}_1,\mathbf{r}_2) = g(\mathbf{r}_{\text{p}})/V^2$ and $\ln(1+x) \approx x$ if $|x| \ll 1$, for indistinguishable

particles we arrive at,

$$\begin{aligned}
&\frac{F^{\mathrm{mix}}_{\mathrm{fluid}}}{k_{\mathrm{B}}T} = \left\langle \frac{F_{\mathrm{f}}}{k_{\mathrm{B}}T} \right\rangle \\
&= N \int_V \langle C_1 \rangle_1(\mathbf{r}|\mathbf{0}) \left\{ \ln \left[\frac{n_{\mathrm{b}} M}{1-\phi_{\mathrm{b}}} \Lambda_{\mathrm{o}}^3 \right] + \frac{a^2 \mathbf{r}^2}{4R_{\mathrm{g}}^2} - 1 \right\} \mathrm{d}\mathbf{r} + N \int_V n(\mathbf{r}_{\mathrm{p}}) \int_V \frac{\langle C_1' \rangle_2^2(\mathbf{r}|\mathbf{0}, \mathbf{r}_{\mathrm{p}})}{\langle C_1 \rangle_1(\mathbf{r}|\mathbf{0})} \mathrm{d}\mathbf{r} \mathrm{d}\mathbf{r}_{\mathrm{p}} \\
&+ M_{\mathrm{s}} \left\{ \ln \left[\frac{C_{\mathrm{s,b}}}{1-\phi_{\mathrm{b}}} \Lambda_{\mathrm{s}}^3 \right] - 1 \right\} + N C_{\mathrm{s,b}} \int_V \langle C_{\mathrm{s}}' \rangle_1^2(\mathbf{r}|\mathbf{0}) \mathrm{d}\mathbf{r} \\
&+ \frac{N\chi}{1-\phi_{\mathrm{b}}} \int_V \langle \phi_1 \rangle_1(\mathbf{r}|\mathbf{0}) \langle C_{\mathrm{s}} \rangle_1(\mathbf{r}|\mathbf{0}) \mathrm{d}\mathbf{r} + \frac{N\chi C_{\mathrm{s,b}}}{1-\phi_{\mathrm{b}}} \int_V n(\mathbf{r}_{\mathrm{p}}) \int_V \langle \phi_1' \rangle_2 \langle C_{\mathrm{s}}'' \rangle_2(\mathbf{r}|\mathbf{0}, \mathbf{r}_{\mathrm{p}}) \mathrm{d}\mathbf{r} \mathrm{d}\mathbf{r}_{\mathrm{p}}
\end{aligned} \tag{5.27}$$

and

$$\begin{aligned}
&\frac{F^{\mathrm{L}}_{\mathrm{fluid}}}{k_{\mathrm{B}}T} = \left\langle \frac{F^0_{\mathrm{f}}}{k_{\mathrm{B}}T} \right\rangle \\
&= N \int_V \langle C_1^0 \rangle_1(\mathbf{r}|\mathbf{0}) \left\{ \ln \left[\frac{n_{\mathrm{b}}^0 M}{1-\phi_{\mathrm{b}}^0} \Lambda_{\mathrm{o}}^3 \right] + \frac{a^2 \mathbf{r}^2}{4R_{\mathrm{g}}^2} - 1 \right\} \mathrm{d}\mathbf{r} + N \int_V n^0(\mathbf{r}_{\mathrm{p}}) \int_V \frac{\langle C_1^{0\prime} \rangle_2^2(\mathbf{r}|\mathbf{0}, \mathbf{r}_{\mathrm{p}})}{\langle C_1^0 \rangle_1(\mathbf{r}|\mathbf{0})} \mathrm{d}\mathbf{r} \mathrm{d}\mathbf{r}_{\mathrm{p}}
\end{aligned} \tag{5.28}$$

with $\langle C_1' \rangle_2(\mathbf{r}|\mathbf{0}, \mathbf{r}_{\mathrm{p}}) \approx M \left[\langle \Lambda_1'' \rangle_2(\mathbf{0}|\mathbf{0}, \mathbf{r}_{\mathrm{p}}) + \left(\frac{1}{\gamma_{\mathrm{s}}} - 2\chi v_{\mathrm{o}} \frac{C_{\mathrm{s,b}}}{1-\phi_{\mathrm{b}}} \right) \langle C_{\mathrm{s}}' \rangle_1(\mathbf{r}|\mathbf{r}_{\mathrm{p}}) \right] G(\mathbf{r})$, $\langle C_1^{0\prime} \rangle_2(\mathbf{r}|\mathbf{0}, \mathbf{r}_{\mathrm{p}})$ $\approx M \left[\langle \Lambda_1^{0\prime\prime} \rangle_2(\mathbf{0}|\mathbf{0}, \mathbf{r}_{\mathrm{p}}) + \langle B^{0\prime} \rangle_1(\mathbf{r}|\mathbf{r}_{\mathrm{p}}) \right] G(\mathbf{r})$, and $\langle C_{\mathrm{s}}'' \rangle_2(\mathbf{r}|\mathbf{0}, \mathbf{r}_{\mathrm{p}}) \approx \langle C_{\mathrm{s}}' \rangle_1(\mathbf{r}|\mathbf{r}_{\mathrm{p}})$. $\ln(n_{\mathrm{b}} M)$ and $\ln(n_{\mathrm{b}}^0 M)$ arise from $\sum_{i=1}^N \langle C_i \rangle_1 = n_{\mathrm{b}} M$ and $\sum_{i=1}^N \langle C_i^0 \rangle_1 = n_{\mathrm{b}}^0 M$, the incompressibility of oligomers. Quantities with a superscript "0" are for pure NOHMs liquid defined in Ref. [6]. We can see that in addition to the leading contribution from the concentration fields around each particle, the perturbations to the fields due to interactions between two particles' oligomers are also taken into account in the fluid phase energies.

Substitution of these expressions for free energies into Eqs. 5.24–5.26 finally yields to $O(a^3/R_{\mathrm{g}}^3)$:

$$\ln \frac{f_{\mathrm{s}}^{\mathrm{V}}}{f_{\mathrm{s}}^0} = \ln \frac{m_{\mathrm{s}}\gamma_{\mathrm{s}}}{1+m_{\mathrm{s}}\gamma_{\mathrm{s}}} + \frac{1-\gamma_{\mathrm{s}}}{1+m_{\mathrm{s}}\gamma_{\mathrm{s}}} + \chi \left(\frac{1}{1+m_{\mathrm{s}}\gamma_{\mathrm{s}}} \right)^2 + \Phi_{\mathrm{c}} + \Phi_{\mathrm{f}}, \tag{5.29}$$

where

$$\Phi_{\mathrm{c}} = -\frac{1}{M} \left[\frac{\gamma_{\mathrm{s}}(1-\phi_{\mathrm{b}}^0)}{1+m_{\mathrm{s}}\gamma_{\mathrm{s}}(1-\phi_{\mathrm{b}}^0)} \right] \left\{ 1 + \frac{4-2\phi_{\mathrm{b}}}{(1-\phi_{\mathrm{b}})^3} \left[\frac{\phi_{\mathrm{b}}^0}{1+m_{\mathrm{s}}\gamma_{\mathrm{s}}(1-\phi_{\mathrm{b}}^0)} \right] \right\} \tag{5.30}$$

is the contribution from the cores due to change in the core number density, and

$$\begin{aligned}\Phi_{\mathrm{f}} = & \frac{\partial}{\partial m_{\mathrm{s}}}\left[\frac{a^2\langle r^2\rangle}{4R_{\mathrm{g}}^2}\right] \\ & + n_{\mathrm{b}}\frac{\partial}{\partial m_{\mathrm{s}}}\left[m_{\mathrm{s}}\int_V \langle C_{\mathrm{s}}'\rangle_1^2(\mathbf{r}|\mathbf{0})\mathrm{d}\mathbf{r}\right. \\ & \qquad \left. - \int_V \langle \Lambda_1''\rangle_2^2(\mathbf{0}|\mathbf{0},\mathbf{r}_{\mathrm{p}})\mathrm{d}\mathbf{r}_{\mathrm{p}} + \frac{(1-2\Delta)^2}{\gamma_{\mathrm{s}}^2}\int_V \langle C_{\mathrm{s}}'\rangle_1^2(\mathbf{r}|\mathbf{r}_{\mathrm{p}})\mathrm{d}(\mathbf{r}-\mathbf{r}_{\mathrm{p}})\right] \\ & - \frac{\partial}{\partial m_{\mathrm{s}}}\left[\frac{\Delta}{1-2\Delta}\langle \Lambda_1'\rangle_1\right. \\ & \qquad \left. + \frac{n_{\mathrm{b}}\Delta}{1-2\Delta}\int_V \langle \Lambda_1''\rangle_2^2(\mathbf{0}|\mathbf{0},\mathbf{r}_{\mathrm{p}})\mathrm{d}\mathbf{r}_{\mathrm{p}} - \frac{n_{\mathrm{b}}\Delta(1-2\Delta)}{\gamma_{\mathrm{s}}^2}\int_V \langle C_{\mathrm{s}}'\rangle_1^2(\mathbf{r}|\mathbf{r}_{\mathrm{p}})\mathrm{d}(\mathbf{r}-\mathbf{r}_{\mathrm{p}})\right]\end{aligned} \tag{5.31}$$

arises from the concentration fields and is evaluated numerically. In Eq. 5.31, the first term involves the change in oligomer mean-square distance from the core center, terms in the second square brackets arise from the entropy of the fluid species, and the rest terms in the third square brackets are due to the enthalpic interactions. $\Delta = \chi v_{\mathrm{o}} C_{\mathrm{s,b}}\gamma_{\mathrm{s}}/(1-\phi_{\mathrm{b}})$ as defined in Eq. 5.23. $m_{\mathrm{s}}\gamma_{\mathrm{s}}/(1+m_{\mathrm{s}}\gamma_{\mathrm{s}})$ and $1/(1+m_{\mathrm{s}}\gamma_{\mathrm{s}})$ are the solute volume fraction and oligomer volume fraction in the fluid phase volume, respectively. It is noteworthy that in the absence of Φ_{c} and Φ_{f} Eq. 5.29 is equivalent to the Flory–Huggins model for gas sorption isotherms [7, 22] in polymers and yields the result for the untethered oligomer melt of the same kind and molecular weight as those tethered to the cores. In NOHMs, Φ_{c} adds to the driving force due to mixing the cores and the fluid species and Φ_{f} accounts for the additional driving force or resistance resulting from the tethering of oligomers to the particles and energy penalties arising from the incompressibility of oligomers.

In the limit of infinite dilution such that $m_{\mathrm{s}} \to 0$, $P_{\mathrm{s}} \to 0$, $\hat{\phi}_{\mathrm{s}}^{\mathrm{V}} \to 1$, and the mole fraction of absorbed solute is approximately m_{s}, we may rearrange Eq. 5.29

to $P_s = m_s H$ with H being the Henry's constant expressed as

$$H = \gamma_s f_s^0 \exp\{1 - \gamma_s + \chi + \Phi_c|_{m_s \to 0} + \Phi_f|_{m_s \to 0}\}. \tag{5.32}$$

Again, in the absence of Φ_c and Φ_f, we obtain the Henry's constant for the oligomer melt. Therefore, from Eq. 5.32 we can estimate whether grafting oligomers on the particle surfaces enhances the solute solubility or not by calculating the ratio of $H_{\text{NOHMs}}/H_{\text{melt}} = \exp\{\Phi_c|_{m_s \to 0} + \Phi_f|_{m_s \to 0}\}$ given γ_s and χ for the solute–oligomer pair and geometrical parameters of the NOHMs system such as R_g/a, ϕ_b^0, and the corresponding M. If $H_{\text{NOHMs}}/H_{\text{melt}} < 1$, NOHMs have a stronger physical driving force for capturing the specific solute than the melt.

In Fig. 5.6, we compare $H_{\text{NOHMs}}/H_{\text{melt}}$ for systems with different parameters to gain a broader view of the parameter space. Figure 5.5 already shows that positive interaction parameters lead to a less stretched oligomer configuration or a smaller mean-square distance of the chain while negative interaction parameters result in more stretched oligomers and reduce the chain-configurational entropy. As a result, in Figs. 5.6(a) and 5.6(b), for a given volume ratio γ_s, positive χ generally yields a higher solvent capacity of NOHMs with fixed ϕ_b^0 or R_g/a. At $\chi = 0$, which corresponds to the case where the captured solute has similar chemistry as the monomers, since the oligomers tend to uniformly fill the space, the increase in the interparticle spacing as the solute is absorbed yields a reduced capacity of NOHMs. For a given ϕ_b^0 and γ_s, in Fig. 5.6(a) we observe a stronger enhancement or reduction in the solvent capacity of NOHMs as R_g/a decreases because the solute may release or increase more of the entropic penalties of stiffer oligomers depending on the value of χ. Besides the dominant driving force resulting from the increase in chain conformations, the tethering of chains along with the incompressibility of the system regulate the distribution of fluid species such that on average the captured solute molecules have larger

distance from the monomers and effectively reduce the strength of the enthalpic interaction. Consequently, while in general solutes that interact with oligomers via a positive χ yield less restricted oligomer configurations, at $\chi = 0.5$, the more subtle "regulation effect" combined with the increase in the interparticle spacing eventually leads to a slightly lower capacity of NOHMs compared with the melt.

On the other hand, the mixing entropy of the cores also plays a role. Figure 5.6(b) indicates that when we fix R_g/a and γ_s, increasing ϕ_b^0 always improves the solvent capacity of NOHMs because the added solute increases more of the core entropy at higher core volume fractions. While this effect favors gas capture, its contribution is minor compared with the change in the oligomer-configurational entropy, as evidenced by the weaker variation of the $H_{\text{NOHMs}}/H_{\text{melt}}$ values. Intuitively, at smaller ϕ_b^0 the interparticle spacing is larger and the oligomers are more entropically frustrated which should lead to a higher solvent capacity of NOHMs than the melt. The slight increase in the capacity of NOHMs as ϕ_b^0 increases could be attributed to the fact that the changes in the interparticle spacing and the chain stretching are not very sensitive to the core volume fraction in the range of $\phi_b \geq 0.1$ [19] such that the increase in the core entropy due to mixing becomes a more important factor that determines the solvent capacity. It is expected that if we push the theory to even lower core volume fractions, the relaxation of strongly restricted chain conformations at higher grafting density and larger interparticle spacing combined with the more substantial regulation effect on the fluid species distribution will eventually lead to an increase in the solvent capacity of NOHMs. This increase in the solvent capacity at lower ϕ_b^0 is anticipated to be more pronounced at smaller R_g/a ratios. Finally, Fig. 5.6(c) shows that the entropic driving forces caused by

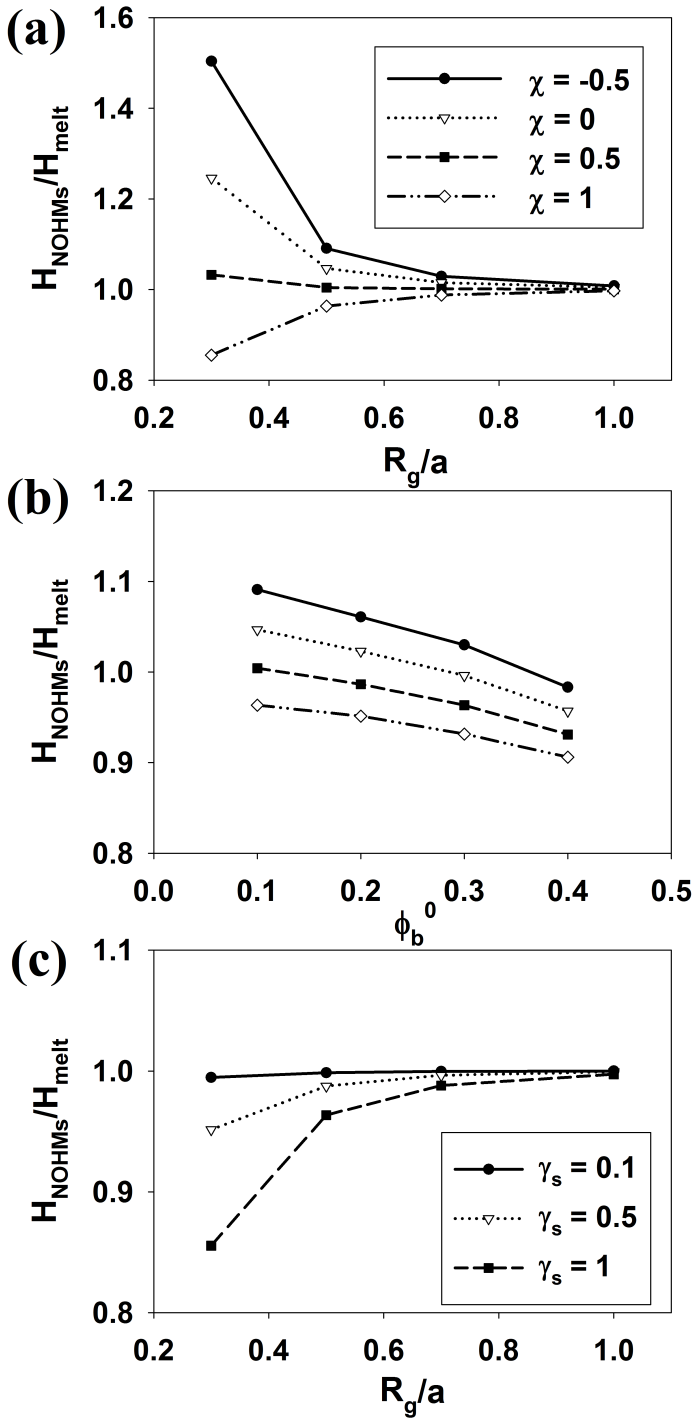

Figure 5.6: (a) The ratio of Henry's constants between NOHMs and unattached melt, $H_{\mathrm{NOHMs}}/H_{\mathrm{melt}}$, as a function of R_{g}/a for different χ at $\phi_{\mathrm{b}}^{0} = 0.1$ and $\gamma_{\mathrm{s}} = 1$. (b) $H_{\mathrm{NOHMs}}/H_{\mathrm{melt}}$ as a function of ϕ_{b}^{0} for different χ at $R_{\mathrm{g}}/a = 0.5$ and $\gamma_{\mathrm{s}} = 1$. The line descriptions are the same as (a). (c) $H_{\mathrm{NOHMs}}/H_{\mathrm{melt}}$ as a function of R_{g}/a for different γ_{s} at $\phi_{\mathrm{b}}^{0} = 0.1$ and $\chi = 1$.

mixing NOHMs and solute are reduced for smaller γ_s because all the above-mentioned effects are weaker for smaller solutes.

With the general effects of different parameters in mind, we start to investigate the solubility of CO_2 in NOHMs. The simplest NOHMs structure consists of silica nanocores and poly(ethylene glycol) (PEG) as the majority of the tethered oligomeric corona [4]. We adopt the interaction parameter data between monomers and gas species from Lin and Freeman [7] for cross-linked poly(ethylene glycol diacrylate) (XLPEGDA) which contains 82% poly(ethylene oxide) (PEO) and was assumed to have similar solubility data as PEG. Following their work, we may write $\chi = \chi_0 + \chi_1/T + \chi_2/(1 + m_s\gamma_s)$, which is dependent on the processing temperature and the amount of solute captured. Specifically, at 308 K $\chi = 0.93$ for CO_2 when $m_s \to 0$ (Table 5.1). After applying the same virial equation of state as theirs for determining the fugacities of solute we may obtain the full sorption isotherm of CO_2 in NOHMs. The volume ratio between CO_2 and the oligomer can be estimated from the molar volumes of the pure CO_2 liquid and the PEG melt. The interaction parameter also depends on the molecular weight of oligomers. Since these quantities depend on the detailed intra-chain excluded volume interactions and the monomer–monomer, solute–solute, and monomer–solute packing conformations, which are not described in our model, to emphasize the space-filling effect explored in the theory, we focus on the condition of $\gamma_s = 1$ in the following comparisons to bring out stronger variations in the sorption isotherm due to R_g/a and ϕ_b^0.

The sorption isotherms of CO_2 in NOHMs and the corresponding PEG melt without particles at 308 K is shown in Fig. 5.7. In Fig. 5.7(a) we first fix $\phi_b^0 = 0.1$ and $\gamma_s = 1$ but change the radius of gyration of the oligomers. Since the pos-

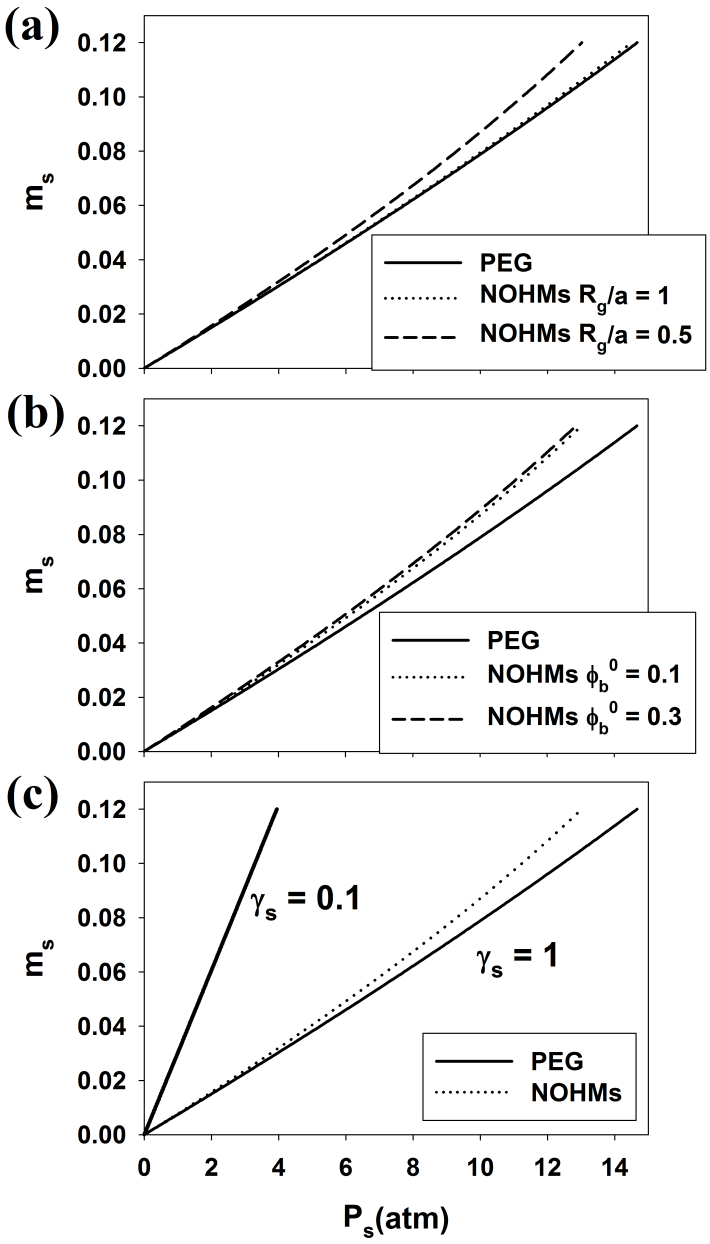

Figure 5.7: (a) Moles CO_2/moles oligomers in PEG-functionalized NOHMs with $\phi_b^0 = 0.1$ and PEG melt at 308 K and $\gamma_s = 1$ as a function of partial pressure of CO_2. (b) Moles CO_2/moles oligomers in PEG-functionalized NOHMs with $R_g/a = 0.5$ and PEG melt at 308 K and $\gamma_s = 1$ as a function of partial pressure of CO_2. (c) Comparison for moles CO_2/moles oligomers in PEG-functionalized NOHMs with $\phi_b^0 = 0.1$ and $R_g/a = 0.5$ and PEG melt at 308 K as a function of partial pressure of CO_2 for $\gamma_s = 1$ and $\gamma_s = 0.1$.

itive interaction parameter makes oligomers retract to reduce the free energy, NOHMs with smaller R_g/a have higher solvent capacity for CO_2 while longer oligomers can easily compromise with the space-filling constraint and yield less tendency to absorb solute. If we fix $R_g/a = 0.5$ and $\gamma_s = 1$ but change the core volume fraction in NOHMs, as shown in Fig. 5.7(b), we find that as indicated in Fig. 5.6(c) the core volume fraction has only moderate effect on the CO_2 capture capacity and NOHMs with higher ϕ_b^0 have slightly CO_2 solubility. Finally, if we fix $R_g/a = 0.5$ and $\phi_b^0 = 0.1$ but change the volume ratio between one CO_2 molecule and one oligomer, Fig. 5.7(c) shows that the entropic driving forces caused by mixing NOHMs and CO_2 are reduced for smaller γ_s, as expected. Therefore the isotherm is very similar to the melt without particles.

Experimental studies have shown that NOHMs with grafted polyethers (containing both ethylene oxide and propylene oxide monomers) which capture CO_2 physically have higher CO_2 solubility compared with the unattached melt [9,23]. If we assume that polyethers have similar enthalpic interaction with CO_2 as PEG, then the predicted favorable trends of CO_2 uptake with NOHMs is consistent with the experimental observation.

5.4.2 Chemisorption

In a recent experimental work of Lin and Park [8], some of the NOHMs systems (NOHM-C-HPE and NOHM-C-MPE in their nomenclature) contained a secondary amine per polyether chain. In this system, CO_2 is not only physically absorbed via the affinity to the ether groups with an interaction parameter χ but also chemically reactive to the secondary amine. We assume a moisture-free

condition for the absorption of CO_2 such that the equilibrium reaction for amine and CO_2 follows [24]

$$2R_1R_2NH + CO_2 \rightleftharpoons R_1R_2NH_2^+ + R_1R_2NCOO^- \tag{5.33}$$

with the equilibrium constant being

$$K_{eq}^* = \frac{[R_1R_2NH_2^+][R_1R_2NCOO^-]}{[R_1R_2NH]^2[CO_2]} \tag{5.34}$$

in the unit of m^3. R_1 and R_2 are two different hydrocarbon groups bonded to the nitrogen, R_1R_2NH is the unreacted oligomers, and the concentration of physically absorbed CO_2 is determined from the gas phase partial pressure of CO_2. The stoichiometry for amine and CO_2 is 2 to 1 and the reaction results in one negatively charge CO_2-bonded polyether ($R_1R_2NCOO^-$) and one positively charged polyether ($R_1R_2NH_2^+$). The charged chains form ionic liquid pairs and the system is electrically neutral as a whole. We treat each oligomer as independently grafted to the core and neglect any change on the translational entropy of the chains due to reaction by assuming that any charged oligomer is easily balanced by a nearby oppositely charged oligomer. To simplify the problem, we also neglect any change on the stiffness of the chains or on the enthalpic affinity of ether groups to CO_2 such that R_g and χ remain the same as unreacted oligomers. Therefore, the only effect of binding CO_2 to the oligomer in our model is to increase the volume of the monomer bead for reacted oligomers by an amount equal to the volume of one CO_2 molecule, as shown in 5.1(d). While chemically bonded CO_2 becomes part of the oligomer, physically absorbed CO_2 is free in space filling the volume not occupied by the cores and oligomers. If we further assume that the volume occupied by a physically absorbed CO_2 is the same as a chemically bonded CO_2, then the change in n_b and ϕ_b due to the total amount of added solute remains the same as the case of physisorption. Therefore in Fig. 5.1(d) the reacted oligomers have bigger beads

than unreacted oligomers with the bead volume being increased by a factor of $1 + \gamma_s$. If $m_s = m_s^f + m_s^{rx}$ is the total moles CO_2/moles oligomer captured with m_s^f being the moles CO_2/moles oligomer that is physically absorbed and m_s^{rx} being the moles CO_2/moles oligomer that is chemically reacted, then on average the volume of one oligomer bead is increased by a factor of $1 + \gamma_s m_s^{rx}$.

We assume that the cores are inert to the absorbed solute therefore we focus on the reaction equilibrium in the fluid phase volume not occupied by the cores. In dimensionless form, let $C_o = \frac{Mn_b}{1-\phi_b}\left(\frac{1}{1+m_s\gamma_s}\right)$ be the total concentration of oligomers in the fluid phase volume with $n_b = \frac{n_b^0}{\left[1+m_s\gamma_s\left(1-\phi_b^0\right)\right]}$ and $\phi_b = \frac{\phi_b^0}{\left[1+m_s\gamma_s\left(1-\phi_b^0\right)\right]}$ from the incompressible condition of fluid phase species, $[CO_2] = C_o m_s^f$ be the concentration of CO_2 solute in equilibrium with the gas phase CO_2 at a given P_s, $[R_1R_2NH] = C_o(1 - 2m_s^{rx})$ be the concentration of oligomers non-reacted with CO_2, $[R_1R_2NCOO^-] = C_o m_s^{rx}$ be the concentration of negatively charged oligomers complexed with CO_2, and $[R_1R_2NH_2^+] = C_o m_s^{rx}$ be the concentration of positively charged oligomers, after substituting these expressions into Eq. 5.34, at quasi-steady state once a local equilibrium is established we may calculate the molar ratio of chemically absorbed CO_2 to oligomers via

$$m_s^{rx} = \frac{\sqrt{C_o m_s^f K_{eq}}}{1 + 2\sqrt{C_o m_s^f K_{eq}}} \tag{5.35}$$

with K_{eq} being K_{eq}^*/a^3. Therefore, the total moles CO_2/moles oligomer in the system is

$$m_s = \frac{\sqrt{\frac{Mn_b}{1-\phi_b}\frac{m_s^f}{1+m_s\gamma_s}K_{eq}}}{1 + 2\sqrt{\frac{Mn_b}{1-\phi_b}\frac{m_s^f}{1+m_s\gamma_s}K_{eq}}} + m_s^f. \tag{5.36}$$

Once m_s^f at a given CO_2 partial pressure is determined, we can calculate the total amount of CO_2 captured.

We use the same approach as shown in section 5.4.1 for relating m_s^f to P_s.

Since the average ratio of the volume occupied by a physically absorbed (free in space) solute to the volume occupied by an oligomer bead varies with the amount of chemically bonded solute, we make the volume of oligomer as a dependent variable of the number of solute molecules in the system. For convenience we define $v_o^{rx} = v_o(1 + \gamma_s m_s^{rx})$ as the new volume of one oligomer bead and $\gamma_s^{rx} = \gamma_s/(1 + \gamma_s m_s^{rx})$ as the new volume ratio of CO_2 to oligomer when the amine-CO_2 reaction is present. The increase in the volume of oligomer bead leads to a decreased effective interaction parameter such that $\chi^{rx} = \chi/(1 + \gamma_s m_s^{rx})$. With all of the field variables $\langle \Lambda_i' \rangle_1$, $\langle \Lambda_i'' \rangle_2$, and $\langle C_s' \rangle_1$ being retaining the same expressions as the case of physisorption, replacing m_s by m_s^f, γ_s by γ_s^{rx}, v_o by v_o^{rx}, and χ by χ^{rx} in the derivation yields

$$\ln \frac{f_s^V}{f_s^0} = \ln \frac{m_s^f \gamma_s^{rx}}{1 + m_s^f \gamma_s^{rx}} + \frac{1 - \gamma_s^{rx}}{1 + m_s^f \gamma_s^{rx}} + \chi^{rx} \left(\frac{1}{1 + m_s^f \gamma_s^{rx}} \right)^2 + \Phi_c^{rx} + \Phi_f^{rx}, \tag{5.37}$$

where $\Phi_c^{rx} = \Phi_c$ and Φ_f^{rx} is of the same form as Φ_f except that the partial derivative is taken with respect to m_s^f and the field variables are defined by the new parameters for chemisorption.

We obtain the information of the chemical equilibrium constant K_{eq}^* from absorption kinetics of CO_2 with liquid-amine-impregnated solid sorbents [12] that have similar reaction mechanism with CO_2 as Eq. 5.33. For NOHMs with a core radius of 5 nm, $K_{eq} \approx 3.8$ at 308 K. Substituting this value into our model with χ being the same as PEG yields isotherms with combined physisorption and chemisorption.

As can be seen from Fig. 5.8, the presence of amines leads to a fast increase of absorption in the start-up region at low partial pressure of CO_2. System with a higher equilibrium constant K_{eq} has a steeper start-up slope and a higher CO_2 capture capacity. The maximum CO_2 loading for chemisorptions is 0.5 moles

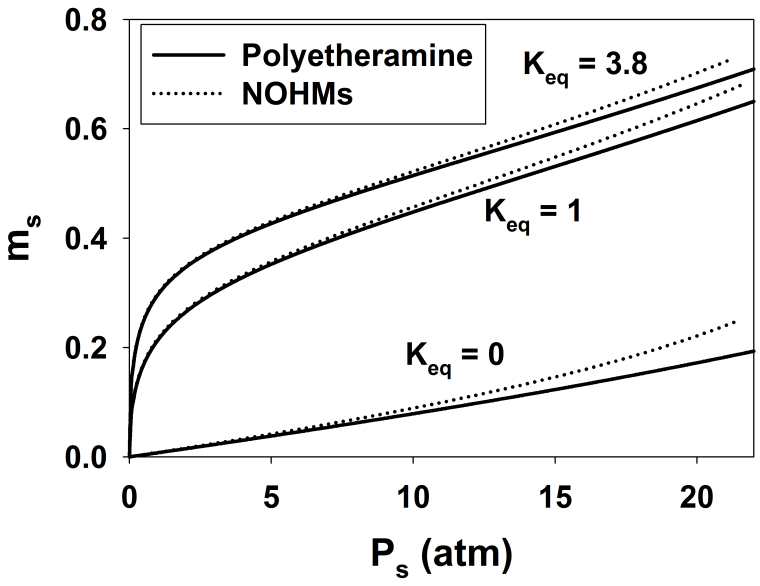

Figure 5.8: Moles CO_2/moles oligomers in polyetheramine-functionalized NOHMs with $\phi_b^0 = 0.3$ and $R_g/a = 0.5$ and polyetheramine melt at 308 K and $\gamma_s = 1$ as a function of partial pressure of CO_2 for various K_{eq}. Result for PEG-functionalized NOHMs with the same ϕ_b^0 and R_g/a is also shown for comparison.

CO_2/moles amines for 2:1 stoichiometry [12]. As amines are consumed (completely reacted with CO_2), CO_2 is absorbed via physisorption such that the amount of CO_2 captured increases further with P_s when $m_s > 0.5$. Compared with the physisorption isotherm for PEG-tethered NOHMs without amines, the capacity difference between NOHMs with and without amines approaches 0.5 at high pressure. The positive value for χ yields more retracted chains as physically absorbed CO_2 can fill the interstices and release the entropic penalty of oligomers. As a result, at high pressure when physisorption dominates NOHMs start to show higher capacity than the unattached oligomer melt. As more CO_2 is chemically absorbed the average monomer size increases and the configurational-entropic effect of tethered oligomers becomes weaker. There-

fore, at small to moderate pressure the chemisorption with higher K_{eq} shows less difference between NOHMs and the melt while eventually at high pressure limit the difference becomes independent of K_{eq}. In our proposed model of one representative bead per chain, each bead can be viewed as a single active site for gas adsorption and once the first adsorption layer is formed by chemical reaction between amines and CO_2, multilayer adsorption can be achieved by physisorption between PEG and CO_2. This mechanism is conceptually equivalent to BET model of adsorption [25].

5.4.3 Ideal Selectivity

For physisorption, the ideal solubility selectivity of a gas pair can be defined by the ratio between the Henry's constants (H) for the pair [16]. For example, selectivity of A over B is defined by H_B/H_A and a higher ratio means that the solvent is more selective of A over B. The thermodynamic driving force that is unique to NOHMs has contributions from the relaxation of entropic frustrations of tethered oligomers as solute fills the interstices and the increase in the translational entropy of cores due to mixing. As discussed in section 5.4.1, since the solute dilutes the system and increases the interparticle spacing, we can benefit from the first contribution if the interaction parameter χ is positive and the chains can retract to decrease the free energy. The first contribution along with the subtle regulation effect that weakens the net enthalpic interaction make NOHMs with stiffer attached oligomers exhibit higher solvent capacity than the melt if the interaction parameter χ is more positive. Therefore, it is expected that NOHMs with a given ϕ_b^0 and R_g/a would be more selective of A over B compared with the melt if $0 < \chi_B < \chi_A$. The enhancement in the selectivity in NOHMs would be

Table 5.1: Interaction Parameters between Gases and Oligomers and Saturation Vapor Fugacities of Gases

	PEG (308 K)[1]		[hmin][Tf_2N] (313 K)	
gas	χ^{∞}[2]	f_s^0 (atm)	χ[3]	f_s^0 (atm)[4]
CO_2	0.93	53	0.43	54
CH_4	1.36	351	0.99	260
C_2H_6	2.04	34		
N_2			0.40	1163
SO_2			−0.25	6

[1] Values are obtained from Ref. [7].

[2] χ^{∞} is the interaction parameter at infinite dilution of solute.

[3] Values are back-calculated from Henry's constants for gases in [hmin][Tf_2N] RTIL reported in Refs. [26–28] given $\gamma_s = 1$.

[4] Values are evaluated with P^{sat} being obtained using Antoine equation coefficients from Ref. [29] and $\hat{\phi}_s^V(T, P^{sat})$ being calculated using Peng-Robinson equation of state [20]. For gas above its critical temperature, the hypothetical P^{sat} is obtained by extrapolating the Antoine equation.

more substantial if R_g/a is smaller at a fixed ϕ_b^0. On the other hand, the contribution from the core entropy due to mixing always adds to the driving force for solute uptake, irrespective of the sign of χ. Therefore, given χ_A, χ_B, and R_g/a in the system, NOHMs with higher ϕ_b^0 would yield a selectivity less different from the melt compared with NOHMs with smaller ϕ_b^0.

Lin and Freeman [7] compared the ideal solubility selectivity of CO_2/CH_4 and CO_2/C_2H_6 gas pairs in XLPEGDA. Adopting their interaction parameters and fugacities for different species into our model for $\gamma_s = 1$ and $T = 308$ K yields the selectivity results for PEG functionalized NOHMs shown in Table 5.2. Based on the physical arguments we have made, Henry's constants for CO_2 in different NOHMs systems are decreased compared with pure PEG melt and the selectivity of CO_2/CH_4 and CO_2/C_2H_6 in NOHMs are also reduced mainly due to the more positive χ for CH_4 and C_2H_6 as summarized in Table 5.1. Specifically, in the systems investigated, more reduction in the selectivity is observed for NOHMs with stiffer oligomeric chains because the system free energy decreases more as CH_4 or C_2H_6 is absorbed. For fixed R_g/a, NOHMs with $\phi_b^0 = 0.3$ has slightly higher CO_2/CH_4 and CO_2/C_2H_6 selectivities than NOHMs with $\phi_b^0 = 0.1$ because the core entropy increases more at higher ϕ_b^0, independent of the variation of chain configurations due to different χ.

Room temperature ionic liquids (RTILs) are nonvolatile and show promising selectivity of CO_2 over other gases [14–16]. Therefore, we are motivated to play with the architecture and chemistry of the oligomers such that the corona on the particle surface forms an array of room-temperature-ionic-liquid pairs. As shown in a recent experimental work [30], the tethered oligomers in nanoparticle hybrids are polyethylene (PE) with an imidazolium-based RTIL

Table 5.2: Ideal Selectivity of CO_2 in PEG-functionalized NOHMs and PEG Melt for $\gamma_s = 1$ at 308 K

Solvent	H_{CO_2} (atm)	H_{CH_4}/H_{CO_2}	$H_{C_2H_4}/H_{CO_2}$
$R_g/a = 0.3, \phi_b^0 = 0.1$	117.90	8.66	1.27
$R_g/a = 0.3, \phi_b^0 = 0.3$	111.52	8.96	1.39
$R_g/a = 0.5, \phi_b^0 = 0.1$	130.59	9.81	1.76
PEG	134.49	10.19	1.93

at the free end. Because the charged pairs are ionically bonded, without loss of generality we may still "lump" the whole chain with ionic-liquid pair into one bead-spring when dealing with the configurational entropy of the oligomer and assume that the tethered RTIL interacts with the solute via the same interaction parameter as the untethered RTIL. For RTILs, the mole fraction of solute accounting for all neutral and ionized species as $P_s \to 0$ is approximately $0.5m_s$ [31]. To compare with the Henry's constant for RTILs reported in literature, given $P_s = m_s H^{IL}$ relationship, we adjust our definition of the Henry's constant and obtain $H^{IL} = 0.5H$ for pure RTILs and RTIL-tethered NOHMs with H being defined in Eq. 5.32. For 1-n-hexyl-3-methylimidazolium bis(trifluoromethylsulfonyl)amide ([hmin][Tf_2N]) functionalized NOHMs, if we consider only the interactions between the tethered ionic pairs and the captured gas species, we obtain the ideal solubility selectivities for different gas species shown in Table 5.3. The input of χ in our calculations shown in Table 5.1 is obtained from H^{IL} values for untethered [hmin][Tf_2N] RTIL at $\gamma_s = 1$.

As can be seen from Table 5.3, compared with [hmin][Tf_2N] RTIL, NOHMs are less selective of CO_2 over CH_4 because χ for CH_4 is more positive than CO_2

while NOHMs are slightly more selective of CO_2 over N_2 due to a slightly less positive χ for N_2 than CO_2. The difference in the CO_2/CH_4 and CO_2/N_2 selectivities between the NOHMs system and RTIL becomes more apparent as the tethered oligomers in NOHMs are more entropically frustrated, as discussed. On the other hand, we obtain higher ratios of $H^{\rm IL}_{\rm SO_2}/H^{\rm IL}_{\rm CO_2}$ for NOHMs relative to pure [hmin][Tf_2N] RTIL because the negative χ between [hmin][Tf_2N] ionic pairs and SO_2 molecules leads to more restricted (stretched) conformations for the oligomers as shown in Fig. 5.5(b) and the incompressibility constraint makes the effective interaction parameter less negative. Therefore NOHMs are generally less subject to poisoning by SO_2 if higher purity of captured CO_2 is desired. Since the core entropy increases more at higher core volume fraction, for fixed $R_{\rm g}/a$, $H^{\rm IL}_{\rm SO_2}/H^{\rm IL}_{\rm CO_2}$ is slightly smaller for NOHMs with $\phi^0_{\rm b} = 0.3$ than $\phi^0_{\rm b} = 0.1$. Note that the enthalpic interaction between [hmin][Tf_2N]–CO_2 pairs is weak enough such that for stiff chains ($R_{\rm g}/a < 1$) the releasing of the spring energy is not substantial at infinite dilution of CO_2 concentration and the observed net increase in the Henry's constants for NOHMs with lower $\phi^0_{\rm b}$ is caused by the less increase in the core entropy.

5.5 Conclusions

We have formulated a density-functional theory for the equilibrium properties of NOHMs–solute mixtures including the configurations of the cores and fluid species and the solvent capacity of NOHMs for different gases. As $R_{\rm g}/a \gg 1$, the simple coarse-grained model of hard cores with attached bead-spring oligomers in the presence of unattached solute beads allows us to derive the solutions for the equilibrium structure of the system and the thermodynamic driving force

Table 5.3: Ideal Selectivity of CO_2 in [hmin][Tf_2N]-functionalized NOHMs and [hmin][Tf_2N] RTIL for $\gamma_s = 1$ at 313 K

Solvent	$H^{IL}_{CO_2}$ (atm)	$H^{IL}_{CH_4}/H^{IL}_{CO_2}$	$H^{IL}_{N_2}/H^{IL}_{CO_2}$	$H^{IL}_{SO_2}/H^{IL}_{CO_2}$
$R_g/a = 0.3, \phi^0_b = 0.1$	44.09	6.82	21.08	0.070
$R_g/a = 0.3, \phi^0_b = 0.3$	40.05	7.13	21.03	0.066
$R_g/a = 0.5, \phi^0_b = 0.1$	42.06	8.03	20.88	0.057
[hmin][Tf_2N]	41.65[1]	8.41[1]	20.82[1]	0.054[2]

[1] Average value obtained from Refs. [26,27].

[2] Value calculated using $H^{IL}_{SO_2}$ from Ref. [28].

for solute uptake semi-analytically. As a result, additional solute molecules not only cooperate with oligomers in filling the interparticle space but also produce more density fluctuations to the system.

One important feature we have found in terms of the equilibrium structure of the NOHMs–solute mixture is that $S(0)$ remains fairly small until there is a large amount of unattached fluid such that the oligomer-functionalized particles are actually dissolved in a sea of unattached solvent. This also indicates that in the presence of a moderate amount of unattached oligomers NOHMs remain a well-dispersed system and do not phase separate and form clusters.

The distributions of cores and fluid species have been utilized to determine the chemical potential and fugacity of the solute in NOHMs. By modeling the oligomer–solute interaction using a mean-field Flory–Huggins parameter, we have demonstrated how the combined effects of changes in oligomer-configurational entropy and enthalpic interactions between oligomers and solute govern the solvent capacity of NOHMs. Solutes with a high affinity for

the oligomers form a nearly uniform mixture causing the oligomers to stretch and reduce their configurational entropy. Solutes with a lower affinity for the oligomers fill the interstitial space, allowing the oligomers to retract and lower their energy. Therefore, the NOHMs configuration reduces the ideal selectivity of the solvent for CO_2 over lower affinity molecules but it also reduces the tendency of the solvent to be poisoned by higher affinity molecules. As a result, PEG-tethered NOHMs possess higher solubility of CO_2 than PEG melt as observed in experiments [9, 23] while the CO_2/CH_4 and CO_2/C_2H_6 solubilities are slightly reduced. On the other hand, while [hmin][Tf_2N]-functionalized NOHMs are less selective of CO_2 over CH_4 than pure [hmin][Tf_2N] RTIL, they are more selective of CO_2 over N_2 and less subject to poisoning by SO_2. The entropic tendency (governed by the geometrical parameters of NOHMs such as R_g/a, ϕ_b^0, and M) and the enthalpic affinity of the oligomers to the solute of interest (determined by the chemistry of the tethered oligomers) work together to achieve a variety of carbon capture operations.

While the theory is valid for $R_g/a \gg 1$, we have the equilibrium structure for stiff chains with $R_g \sim 0.5$ has shown qualitative agreement with molecular dynamics simulations [19]. Therefore, we expect that our calculations for small R_g/a should capture the qualitative trend correctly. It is envisioned that the theory can be modified by applying a more sophisticated model for intrachain configuration and a more detailed treatment of the enthalpic interactions that accounts for the differences in the monomer size and the free volume of oligomers that is available for monomers to pack in. The problem may turn completely computational but the essential physics would not be altered.

BIBLIOGRAPHY

[1] A. B. Bourlinos, R. Herrera, N. Chalkias, D. D. Jiang, Q. Zhang, L. A. Archer, and E. P. Giannelis, Adv. Mater. **17**, 234 (2005).

[2] A. B. Bourlinos, E. P. Giannelis, Q. Zhang, L. A. Archer, G. Floudas, and G. Fytas, Eur. Phys. J. E **20**, 109 (2006).

[3] R. Rodriguez, R. Herrera, L. A. Archer, and E. P. Giannelis, Adv. Mater. **20**, 4353 (2008).

[4] P. Agarwal, H. Qi, and L. A. Archer, Nano Lett. **10**, 111 (2010).

[5] J. L. Nugent, S. S. Moganty, and L. A. Archer, Adv. Mater. **22**, 3677 (2010).

[6] H.-Y. Yu and D. L. Koch, Langmuir **26**, 16801 (2010).

[7] H. Lin and B. D. Freeman, Macromolecules **38**, 8394 (2005).

[8] K.-Y. A. Lin and A.-H. A. Park, Environ. Sci. Technol. **45**, 6633 (2011).

[9] Y. Park, J. Decatur, K.-Y. A. Lin, and A.-H. A. Park, Phys. Chem. Chem. Phys. **13**, 18115 (2011).

[10] J. Gabrielsen, M. L. Michelsen, E. H. Stenby, and G. M. Kontogeorgis, Ind. Eng. Chem. Res. **44**, 3348 (2005).

[11] A. Lawal, M. Wang, P. Stephenson, and H. Yeung, Fuel **88**, 2455 (2009).

[12] E. R. Monazam, L. J. Shadle, and R. Siriwardane, AIChE J. .

[13] G. Qi, Y. Wang, L. Estevez, X. Duan, N. Anako, A.-H. A. Park, W. Li, C. W. Jones, and E. P. Giannelis, Energy Environ. Sci. **4**, 444 (2011).

[14] E. D. Bates, R. D. Mayton, I. Ntai, and J. J. H. Davis, J. Am. Chem. Soc. **124**, 926 (2002).

[15] M. J. Muldoon, S. N. V. K. Aki, J. L. Anderson, J. K. Dixon, and J. F. Brennecke, J. Phys. Chem. B **111**, 9001 (2007).

[16] J. E. Bara, T. K. Carlisle, C. J. Gabriel, D. Camper, A. Finotello, D. L. Gin, and R. D. Noble, Ind. Eng. Chem. Res. **48**, 2739 (2009).

[17] J.-P. Hansen and I. R. McDonald, *Theory of Simple Liquids*, Academic Press, London, 3 edition, 2006.

[18] D. A. McQuarrie, *Statistical Mechanics*, University Science Books, Sausalito, 2000.

[19] A. Chremos, A. Z. Panagiotopoulos, H.-Y. Yu, and D. L. Koch, J. Chem. Phys. **135**, 114901 (2011).

[20] J. M. Prausnitz, R. N. Lichtenthaler, and E. G. de Azevedo, *Molecular Thermodynamics of Fluid-Phase Equilibria*, Prentice Hall, Upper Saddle River, NJ, 3 edition, 1999.

[21] N. F. Carnahan and K. Starling, J. Chem. Phys. **51**, 635 (1969).

[22] T. L. Hill, *An Introduction to Statistical Thermodynamics*, Dover, New York, 1986.

[23] Y. Park, D. shin, Y. N. Jang, and A.-H. A. Park, J. Chem. Eng. Data .

[24] R. A. Khatri, S. S. C. Chuang, Y. Soong, and M. Gray, Energy Fuels **20**, 1514 (2006).

[25] S. Brunauer, P. H. Emmett, and E. Teller, J. Am. Chem. Soc. **60**, 309 (1938).

[26] D. Camper, J. Bara, C. Koval, and R. Noble, Ind. Eng. Chem. Res. **45**, 6279 (2006).

[27] A. Finotello, J. E. Bara, D. Camper, and R. D. Noble, Ind. Eng. Chem. Res. **47**, 3453 (2008).

[28] J. L. Anderson, J. K. Dixon, E. J. Maginn, and J. F. Brennecke, J. Phys. Chem. B **110**, 15059 (2006).

[29] C. L. Yaws, P. K. Narasimhan, and C. Gabbula, *Yaws' Handbook of Antoine Coefficients for Vapor Pressure*, Knovel, 2 edition, 2009.

[30] S. S. Moganty, N. Jayaprakash, J. L. Nugent, J. Shen, and L. A. Archer, Angew. Chem. Int. Ed. **49**, 9158 (2010).

[31] P. Scovazzo, D. Camper, J. Kieft, J. Poshusta, C. Koval, and R. Noble, Ind. Eng. Chem. Res. **43**, 6855 (2004).

CHAPTER 6

PREDICTING DISORDER–ORDER TRANSITION OF SOLVENT-FREE NANOPARTICLE–ORGANIC HYBRID MATERIALS

6.1 Abstract

The transition from disorder to face-centered-cubic solid of solvent-free oligomer-tethered nanoparticles is predicted using a density-functional theory for model hard spheres with tethered bead-spring oligomers. The phase boundary is influenced by the loss of oligomer-configurational entropy in one phase compared with the other. As the ratio of oligomer radius of gyration to particle radius decreases, the phase-boundary volume fraction first decreases then increases. When the particles are localized to ordered phase the cooperation of the oligomers in filling the space is hindered. Therefore stiffer oligomers feel stronger entropic penalty in ordered solid and favor the disordered phase.

6.2 Theory & Results

Disorder–order transitions observed in colloidal suspensions with a solvent at high enough particle number densities are driven by the larger interparticle correlation distance in a localized crystalline structure than a delocalized dense liquid. The unattached, free solvent molecules mediate the particle–particle interactions such that the assumption of pairwise-additive interparticle potential is applicable. Upon increase of particle concentration, for hard spheres computer simulations [1–3] and density-functional theory [4–7] find the liquid–face-

centered-cubic (fcc) transition; for soft spheres interacting via an inverse-power pair potential $u(r) \sim r^{-n}$, when the softness increases or the index n decreases, the liquid–fcc transition becomes the liquid–body-centered-cubic (bcc) transition, as evidenced by experiments [8, 9], computer simulations [10–13], and theories [9, 13–15]. While these studies help understanding the origin of the freezing–melting transitions in soft matter, a prediction of such phase transitions for solvent-free colloidal suspensions is lacking. In this Letter, we use a novel solvent-free nanoparticle fluid, called nanoparticle–organic hybrid materials (NOHMs), as the model system to apply a classical density-functional theory that demonstrates a physical rationalization of the disorder–order transitions in solvent-free "self-suspended" particles in which the fluid is tethered to the core. Since experiments for polymer-grafted particles in a good solvent show fluid–fcc transitions as the effective core-shell volume fraction increases [16,17], in this first attempt, we consider the disordered-liquid–fcc-solid transition by assuming a weak effects of oligomers when the oligomer radius of gyration is much greater than the core radius.

Pure NOHMs contain nanoscale hard cores with radius a surface functionalized by oligomeric chains with radius of gyration R_g in the absence of solvent. Experimental studies have shown that these materials can relax to an equilibrium state and exhibit disordered liquid behavior with the fluidity provided by the tethered hairs [18–22]. The homogeneous mixture of inorganic particles and organic chains without any unattached solvent yields many-body interparticle forces. In addition, the core distributions and the chain configurations are governed by the space-filling requirement for the incompressible oligomers [23]. By applying the coarse-grained model of hard spheres and bead-spring oligomers with one bead per chain tethered to the center of each core via a soft, linear

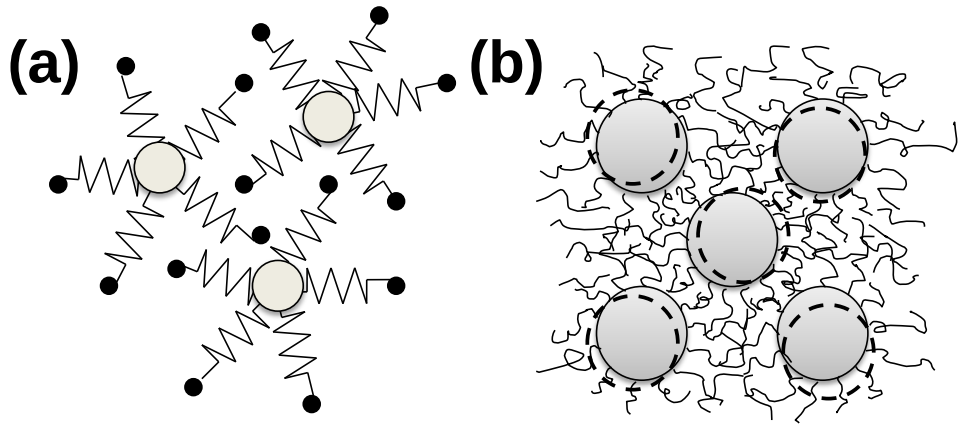

Figure 6.1: (a) Schematic of the proposed coarse-grained model of NOHMs. The big central spheres are the hard cores and the small beads represent the monomers. The monomers are connected to the core with springs and each spring has one monomer. (b) Schematic of fcc-solid NOHMs. The dashed circles around the cores represent small displacements of the cores around the lattice sites determined by the localization parameter α.

spring, as shown in Fig. 6.1(a), for a given configuration of N cores the free energy of the tethered oligomers is directly formulated as

$$\frac{F_{\mathrm{f}}}{k_{\mathrm{B}}T} = \sum_{i=1}^{N} \int_{V} C_i(\mathbf{r}, \mathbf{r}_i) \left[\ln C_i(\mathbf{r}, \mathbf{r}_i) \Lambda_{\mathrm{b}}^3 - 1 \right] + \frac{1}{4R_{\mathrm{g}}^2} (\mathbf{r} - \mathbf{r}_i)^2 \, C_i(\mathbf{r}, \mathbf{r}_i) \mathrm{d}\mathbf{r}, \qquad (6.1)$$

which contains the ideal gas energy for the beads and the excess spring energy for the chain configuration with the spring constant being proportional to $1/R_{\mathrm{g}}^2$. $C_i(\mathbf{r}, \mathbf{r}_i)$ is the concentration field of oligomers at $\mathbf{r}$ attached to particle i at $\mathbf{r}_i$, k_{B} is the Boltzmann constant, T is the temperature, V is the system volume, and Λ_{b} is the thermal de Broglie wavelength of oligomer beads. At equilibrium, $C_i(\mathbf{r}, \mathbf{r}_i)$ corresponds to the minimum of F_{f} subject to $\int_V C_i(\mathbf{r}, \mathbf{r}_i) \mathrm{d}\mathbf{r} = M$ (normalization of oligomer concentration field) and $C(\mathbf{r}) = \sum_{i=1}^{N} C_i(\mathbf{r}, \mathbf{r}_i) = n_{\mathrm{b}} M$ (incompressibility of oligomers) with M being the number of oligomers per core and n_{b} being

the bulk number density of cores [23]. In a solid, each core is localized around its lattice site and we may approximate the average one-body core distribution as a sum of normalized Gaussian spreads around the lattice sites $\{\mathbf{R}_i\}$ written as $n(\mathbf{r}) = \left(\frac{\alpha}{\pi}\right)^{3/2} \sum_{i=1}^{N} e^{-\alpha|\mathbf{r}-\mathbf{R}_i|^2}$ with α being the localization parameter [24], as depicted in Fig. 6.1(b). If we include only the effect of displacing each particle on the oligomer concentration but neglect the coupling between particles, by pre-averaging the total oligomer concentration $C(\mathbf{r})$ over the particle configuration $n(\mathbf{r})$ relative to the lattice structure, the solution of $C_i(\mathbf{r}, \mathbf{r}_i)$ is

$$C_i(\mathbf{r}, \mathbf{r}_i) = \frac{n_\mathrm{b} M e^{-\frac{(\mathbf{r}-\mathbf{r}_i)^2}{4R_\mathrm{g}^2}}}{\sum_{j=1}^{N} e^{-\frac{(\mathbf{r}-\mathbf{r}_j)^2}{4R_\mathrm{g}^2}}} \approx \frac{n_\mathrm{b} M e^{-\frac{(\mathbf{r}-\mathbf{r}_i)^2}{4R_\mathrm{g}^2}}}{\left(\frac{4R_\mathrm{g}^2\alpha}{1+4R_\mathrm{g}^2\alpha}\right)^{\frac{3}{2}} \sum_{j=1}^{N} e^{-\frac{4R_\mathrm{g}^2\alpha}{1+4R_\mathrm{g}^2\alpha}\frac{(\mathbf{r}-\mathbf{R}_j)^2}{4R_\mathrm{g}^2}}}. \tag{6.2}$$

The configurations of cores and oligomers allow us to obtain the information of the system free energy that is essential to determine the thermodynamically stable state of the materials. In both phases (subscripts L for liquid and S for solid) the total Helmholtz free energy per particle is a functional of $n(\mathbf{r})$ written as $\frac{F_{\mathrm{L(S)}}[n(\mathbf{r})]}{Nk_\mathrm{B}T} = f_{\mathrm{L(S)}}[n(\mathbf{r})] = f_{\mathrm{id,L(S)}}[n(\mathbf{r})] + f_{\mathrm{ex,L(S)}}^{\mathrm{HS}}[n(\mathbf{r})] + f_{\mathrm{ex,L(S)}}^{\mathrm{oli}}[n(\mathbf{r})]$ with the ideal gas part being $f_{\mathrm{id,L(S)}} = \left[\ln n(\mathbf{r})\Lambda_\mathrm{p}^3 - 1\right]$, $f_{\mathrm{ex,L(S)}}^{\mathrm{HS}}$ being the excess part contributed from the hard spheres, $f_{\mathrm{ex,L(S)}}^{\mathrm{oli}}$ being the excess part contributed from the oligomers, and Λ_p being the thermal de Broglie wavelength of particles. In a uniform liquid, $n(\mathbf{r}) = n_\mathrm{b}$ in $f_{\mathrm{id,L}}$, $f_{\mathrm{ex,L}}^{\mathrm{HS}}$ is well-described by the Carnahan–Starling equation of state [25], and F_f is smeared out as a mediated interparticle potential averaged over all possible particle configurations such that $f_{\mathrm{ex,L}}^{\mathrm{oli}} = \frac{1}{N}\left\langle \frac{F_\mathrm{f}}{k_\mathrm{B}T} \right\rangle$ with $\langle\rangle$ being the ensemble average. In the solid phase near the freezing transition, $\alpha a^2 > 10$ yields non-overlapping Gaussian spreads associated with the neiboring cores and an analytical approximation for $f_{\mathrm{id,S}}$ is applicable [24]. We apply the modified weighted-density-functional approximation (MWDA) [7] to determine $f_{\mathrm{ex,S}}^{\mathrm{HS}}$

as a function of the weighted density $\hat{n}(n_\mathrm{b},\alpha)$ obtained from self-consistently solving for $\hat{n}(n_\mathrm{b},\alpha) = \left[1 - \frac{1}{2f_{\mathrm{ex,S}}^{\mathrm{HS}\prime}(\hat{n})}\sum_{\mathbf{Q}\neq 0} e^{-\mathbf{Q}^2/2\alpha} c_0^{(2)}(\mathbf{Q};\hat{n})\right]$ with $c_0^{(2)}(\mathbf{Q};\hat{n})$ being the Fourier-space two-body direct correlation function evaluated at the reciprocal-lattice vectors (RLV) $\mathbf{Q}$ and $f_{\mathrm{ex,S}}^{\mathrm{HS}\prime} = \frac{df_{\mathrm{ex,S}}^{\mathrm{HS}}}{d\hat{n}}$. By choosing the uniform-liquid core–core correlations as the solid-state reference using the Percus–Yevick approximation [26, 27], $f_{\mathrm{ex}}^{\mathrm{HS,S}}$ and $c_0^{(2)}(\mathbf{Q};\hat{n})$ can be conveniently determined. $f_{\mathrm{ex,S}}^{\mathrm{oli}}$ for the solid is directly calculated by substituting Eq. (6.2) into Eq. (6.1).

Finally, with the liquid-phase ideal free energy $f^0 = \ln n_\mathrm{b}\Lambda_\mathrm{p}^3 - 1 + M\left[\ln\left(\frac{M\Lambda_\mathrm{b}^3}{R_\mathrm{g}^3}\right) - \frac{3}{2}\ln(4\pi) - 1\right]$ being the universal reference state, given that the ensemble average of a quantity $A(\mathbf{r}) = \sum_i^N \left[\langle A_i\rangle_1(\mathbf{r}|\mathbf{r}_i) + A_i'(\mathbf{r})\right]$ is $\langle A\rangle(\mathbf{r}) = N\langle A_1\rangle_1(\mathbf{r}|\mathbf{r}_1) + Nn_\mathrm{b}\int_V g(\mathbf{r}_{12})\langle A_1'\rangle_2(\mathbf{r}|\mathbf{r}_1,\mathbf{r}_2)\mathrm{d}\mathbf{r}_{12}$ if for any chosen particle 1 we treat other nonchosen particles 2 as indistinguishable with $g(\mathbf{r}_{12})$ being the pair probability, $\mathbf{r}_{12} = \mathbf{r}_2 - \mathbf{r}_1$, and $\langle\rangle_1$, $\langle\rangle_2$ being the conditional ensemble averages given one or two particles fixed, as $R_\mathrm{g} \gg a$ the relative free energy for the equilibrium liquid correct to $O(a^3/R_\mathrm{g}^3)$ is [23]

$$\Delta f_\mathrm{L} = \frac{4\phi_\mathrm{b} - 3\phi_\mathrm{b}^2}{(1-\phi_\mathrm{b})^2} + Mn_\mathrm{b}\left\{-\int_V \langle\Lambda_1''\rangle_2^2(\mathbf{r}_1|\mathbf{r}_1,\mathbf{r}_2)\mathrm{d}\mathbf{r}_{12} + \int_V \langle B'\rangle_1^2(\mathbf{r}|\mathbf{r}_2)\mathrm{d}(\mathbf{r}-\mathbf{r}_2)\right\}, \quad (6.3)$$

where $\langle\Lambda_1''\rangle_2(\mathbf{r}_1|\mathbf{r}_1,\mathbf{r}_2) = -\frac{1}{8\pi^3}\int_{V_k}\frac{\hat{G}(\mathbf{k})^2 S(\mathbf{k})}{n_\mathrm{b}\left[\hat{G}(\mathbf{k})^2-1\right]}e^{i\mathbf{k}\cdot\mathbf{r}_{12}}\mathrm{d}\mathbf{k}$ is the perturbation to the normalization constant of C_1 given that particles 1 and 2 are fixed at $\mathbf{r}_1$ and $\mathbf{r}_2$ and $\langle B'\rangle_1(\mathbf{r}|\mathbf{r}_2) = \frac{1}{8\pi^3}\int_{V_k}\frac{\hat{G}(\mathbf{k})S(\mathbf{k})}{n_\mathrm{b}\left[\hat{G}(\mathbf{k})^2-1\right]}e^{i\mathbf{k}\cdot(\mathbf{r}-\mathbf{r}_2)}\mathrm{d}\mathbf{k}$ is the perturbation to the total C due to particle 2 with $S(\mathbf{k})$ being the static structure factor defined by $S(\mathbf{k}) = 1 + n_\mathrm{b}\int_V [g(\mathbf{r}_{12})-1]e^{-i\mathbf{k}\cdot\mathbf{r}_{12}}\mathrm{d}\mathbf{r}_{12}$ [26], $\hat{G}(\mathbf{k}) = e^{-k^2R_\mathrm{g}^2}$ resulting from the Gaussian spring, k being the wave number, and V_k being all space in $\mathbf{k}$. In solid phase, as $\alpha a^2 > 10$ and $R_\mathrm{g} \gg a$, variations in C_i are on a larger length scale than variations in the mean-square displacement of cores relative to the lattice sites, therefore the rel-

ative free energy in the solid phase has the form

$$\Delta f_{\mathrm{S}} = \left\{\frac{3}{2}\ln\left(\frac{\alpha a^2}{\pi}\right) - \frac{3}{2} - \ln n_{\mathrm{b}} a^3\right\} + \left\{\frac{3}{2}\left[\left(1-\hat{\phi}\right)^{-2} - 1\right] - \ln\left(1-\hat{\phi}\right)\right\} + M\left\{\ln n_{\mathrm{b}} R_{\mathrm{g}}^3 - \frac{3}{2}\ln\left[\frac{\alpha R_{\mathrm{g}}^2}{\pi(1+4R_{\mathrm{g}}^2\alpha)}\right] - n_{\mathrm{b}} R_{\mathrm{g}}^3\left[\frac{\pi(1+4R_{\mathrm{g}}^2\alpha)}{\alpha R_{\mathrm{g}}^2}\right]^{3/2}\left\langle\frac{\ln\left(\sum_{i=1}^{N} G_{\alpha,i}\right)}{\sum_{i=1}^{N} G_{\alpha,i}}\right\rangle_{v_0}\right\}, \tag{6.4}$$

where $G_{\alpha,i} = e^{-\frac{4R_{\mathrm{g}}^2\alpha}{1+4R_{\mathrm{g}}^2\alpha}\frac{(\mathbf{r}-\mathbf{R}_i)^2}{4R_{\mathrm{g}}^2}}$, $\hat{\phi} = \frac{4\pi a^3}{3}\hat{n}$, and $\langle\rangle_{v_0}$ denotes the volume average over the unit cell volume v_0. The three terms in the curly brackets are the contributions from the ideal gas energy, excess energy for hard spheres, and excess energy for oligomers, respectively.

Experimentally, the solvent-free condition of NOHMs is achieved by first chemically grafting the oligomers to the particle surfaces in the presence of solvent and removing the unattached solvent after the reaction is completed. As a result, for fixed oligomer molecular weight when the core volume fraction ϕ_{b} varies we need to change the oligomer surface grafting density [20–22]; for fixed grafting density the oligomer molecular weight is altered with ϕ_{b} [19, 21]. The ratio of oligomer radius of gyration to core radius (or the interparticle spacing) provides us with a measure of the strength of the interaction as characterized by how easily the chains can fill the space. In this Letter, we aim to locate the disordered-liquid–fcc-solid phase boundary of NOHMs for a given R_{g}/a in the system. Therefore we fix the oligomer number density in such a way that $M = 600$ at $\phi_{\mathrm{b}} = 0.15$ and M is proportional to the ratio of the fluid volume to the number of particles, i.e., $\frac{1-\phi_{\mathrm{b}}}{\phi_{\mathrm{b}}}$. The volume ratio between one core and one oligomer in this condition is 106.

The equilibrium crystal free energy corresponds to $\frac{\partial \Delta f_{\mathrm{S}}}{\partial \alpha} = 0$ at $\alpha a^2 > 10$ where Eq. 6.4 is valid. As shown in Fig. 6.2(a) for the system with $R_{\mathrm{g}}/a = 0.5$

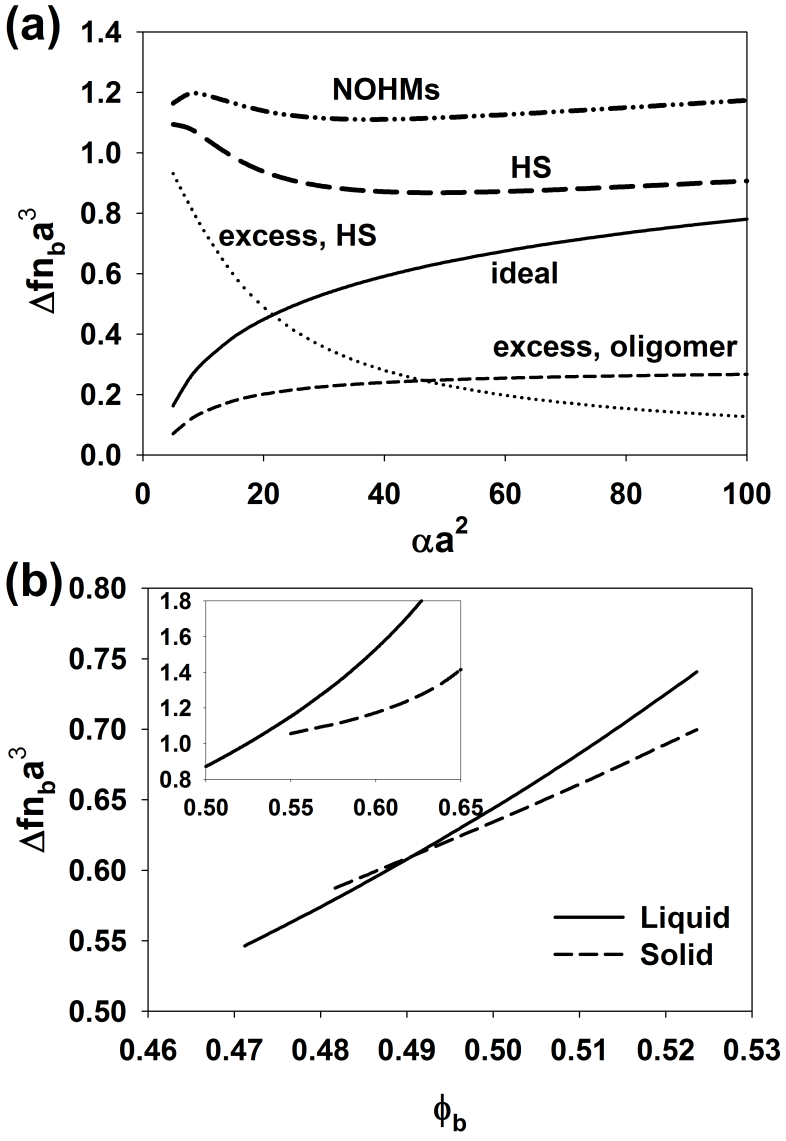

Figure 6.2: (a) Comparison of the scaled relative free energy components per volume $\Delta f n_b a^3$ as a function of the scaled localization parameter αa^2 for NOHMs with $\phi_b = 0.58$ and $R_g/a = 0.5$. The thick dashed-dotted-dotted curve is the scaled total free energy per volume for NOHMs and the thick dashed curve is the corresponding result for hard spheres at the same ϕ_b. (b) Comparison of the scaled relative free energy per volume as a function of ϕ_b for liquid and solid NOHMs with $R_g/a = 0.6$. The inset is the corresponding comparison for NOHMs with $R_g/a = 0.5$, where below $\phi_b \approx 0.55$ a thermodynamically stable fcc solid is unobtainable in the theory.

and $\phi_b = 0.58$, while $f_{id,S}$ increases monotonically with α because the more localized solid the lower the core entropy, $f_{ex,S}^{HS}$ decreases monotonically with α since the localization reduces the chances for direct hard-sphere interactions. This competition between the ideal energy and excess energy yields a free energy minimum that determines the equilibrium solid structure of hard spheres. For NOHMs, on top of the above two contributions, $f_{ex,S}^{oli}$ also increases monotonically with α as a consequence of more disturbed oligomer configuration at strong particle localization. Therefore, in solventless condition the tethered hairs yield some "randomness" to the equilibrium crystal compared with the reference hard-sphere suspension at the same ϕ_b. The thermodynamic stability of the equilibrium solid is determined by comparing Δf_L and Δf_S. Since the particles cannot be separated from their tethered fluid, macroscopic variations in the volume fraction are prohibited and the thermodynamically stable phase observable is the one that has the lower free energy. As demonstrated in Fig. 6.2(b), the crossover point $\phi_{b,c}$ of the two free energies yields the phase boundary of the NOHMs system; above $\phi_{b,c}$ the system is a fcc solid and below $\phi_{b,c}$ a disordered liquid is obtained.

The resulting ϕ_b–R_g/a phase diagram is constructed in Fig. 6.3. We have also applied the same MWDA approach without oligomers to determine the phase diagram for hard spheres. For comparison, the freezing transition point ($\phi_{b,f}$), melting transition point ($\phi_{b,m}$), and crossover point for hard spheres are shown in black curves. $\phi_{b,f}$ and $\phi_{b,m}$ are obtained by a common tangent construction in the $\Delta f n_b a^3$–ϕ_b diagram as Fig. 6.2(b) that satisfies the equal-chemical-potential and equal-pressure criteria [4,5,7]. We find that at large R_g/a, the phase boundary of NOHMs is close to the free energy crossover point of the reference hard spheres because the oligomers can easily fill the space in both ordered and dis-

ordered structures such that $f_{ex,S}^{oli}$ and $f_{ex,L}^{oli}$ only have weak contributions. As R_g/a decreases gradually to 0.6, the crossover point shifts to a lower volume fraction than hard spheres since the particles in a fcc solid are more well spaced than a concentrated liquid such that the oligomers are less frustrated in a crystal and favor the crystalization. However, as we further decrease R_g/a, the lower limit of ϕ_b at which the theory can predict a thermodynamically stable fcc solid with $\alpha a^2 > 10$ is highly increased such that the free energy crossover point is missing. We determine the phase boundary in this case using this lower limit at which Δf_L is slightly greater than Δf_S, as depicted in the inset of Fig. 6.2(b). We conjecture that there could be a minimum of Δf_S at $0 < \alpha a^2 < 10$ that characterizes a weakly localized crystalline solid or a disordered glass. To correctly locate the minimum in this region full expressions for $f_{id,S}$ and $f_{ex,S}^{oli}$ without the pre-averaging are necessary. Qualitatively, when $R_g/a < 0.6$ the phase boundary for disorder–order transition starts to increase and eventually becomes greater than $\phi_{b,c}$ of hard spheres. When $R_g/a = 0.5$ NOHMs can remain in disordered phase at ϕ_b as high as 0.55. It is noteworthy that if we compare the predicted phase boundary of NOHMs with the freezing transition point $\phi_{b,f}$, then at all R_g/a the disorder–order transition of NOHMs occurs at higher volume fractions than hard spheres.

To directly investigate the free energy penalty for the oligomers due to the incompressiblity constraint in the two phases, we also compare the oligomer contributions to Δf_L (the second term in Eq. 6.3) and Δf_S (the third term in Eq. 6.4) as $\alpha \to \infty$ for a perfect fcc crystal at the crossover point of hard spheres. As can be seen from Fig. 6.4, while in both phases the oligomer free energy increases with decreasing R_g/a, the increasing rates are different. Since oligomers tethered to a given core cooperate with other cores' oligomers in filling the space, the phase

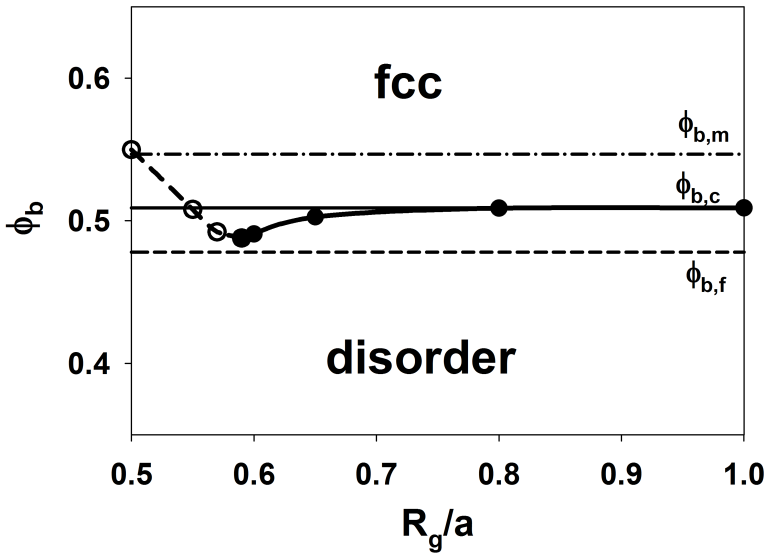

Figure 6.3: The predicted ϕ_b–R_g/a phase diagram of NOHMs with the volume ratio of one core to one oligomer being 106. Above $R_g/a = 0.59$ the thick solid curve with solid symbols is the phase boundary obtained from the free-energy crossover point; below $R_g/a = 0.59$ the thick dashed curve with open symbols is the minimum-accessible fcc-solid volume fraction. The predicted freezing (0.48), crossover (0.51), and melting (0.55) points of hard spheres are shown in thin lines for comparison.

with more nearest neighbors is expected to have less frustrated oligomers at small R_g/a. Therefore it is not surprising that as R_g/a decreases the free energy penalty for oligomers increases faster in solid phase than liquid phase because the number of the nearest Voronoi neighbors for a disordered fluid with a random packing is larger than that for an ordered fcc solid [28, 29]. This result is consistent with the phase diagram we predict and indicates that the localized particle configuration in solid phase hinders the cooperation of oligomers in filling the space therefore at small R_g/a the oligomers favor delocalization of particles.

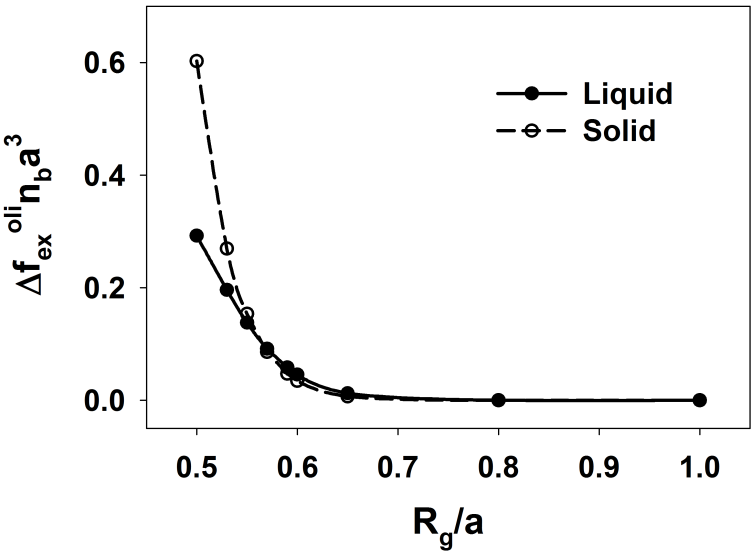

Figure 6.4: The increase in the scaled oligomer free energy per volume $\Delta f_{\rm ex}^{\rm oli} n_{\rm b} a^3$ in liquid and solid NOHMs due to applying the incompressibility constraint as a function of $R_{\rm g}/a$ at $\phi_{\rm b} = 0.51$, the crossover point of hard spheres.

In conclusion, we have applied a density-functional approach to determine the phase boundary of disordered-liquid–fcc solid transition for solvent-free NOHMs. Utilizing the coarse-grained model of hard spheres with center-tethered bead-linear spring oligomers, the free energies of liquid and solid NOHMs are formulated semi-analytically which allows a direct investigation of the entropic penalty of oligomers as a function of the core volume fraction and the ratio of oligomer radius of gyration to core radius when the oligomer number density is fixed. While there is a competition between the changes in oligomer-configurational entropy in the liquid and solid phase relative to an ideal random state as $R_{\rm g}/a$ decreases, the predicted disorder–order transition always occurs at a higher particle volume fraction than the freezing transition point of hard-sphere suspensions because the particle degrees of freedom fa-

cilitate the cooperation of oligomers. This may help explain the experimental observation that pure NOHMs can be disordered soft glasses even when the core volume fraction was close to or higher than the hard-sphere freezing volume fraction [22]. For hard spheres at sufficiently high particle volume fraction the free energy for a fcc crystal is lower than a bcc crystal [30]. Since fcc structure is more close packed than bcc, according to our theory bcc-solid NOHMs would be unfavorable as the entropically frustrated oligomers further increase the free energy. Molecular dynamics (MD) simulations of NOHMs with short tethered chains in the presence of a moderate amount of phantom solvent have exhibited a bcc structure [31]. We conjecture that as the solvent content is further reduced, at equilibrium a transition to a more compact fcc structure may occur due to more stringent space-filling requirement for the oligomers.

BIBLIOGRAPHY

[1] B. J. Alder and T. E. Wainwright, J. Chem. Phys. **27**, 1208 (1957).

[2] W. G. Hoover and F. H. Ree, J. Chem. Phys. **49**, 3609 (1968).

[3] B. J. Alder, W. G. Hoover, and D. A. Young, J. Chem. Phys. **49**, 3688 (1968).

[4] P. Tarazona, Mol. Phys. **52**, 81 (1984).

[5] W. A. Curtin and N. W. Ashcroft, Phys. Rev. A **32**, 2909 (1985).

[6] M. Popović and M. V. Jarić, Phys. Rev. B **38**, 808 (1988).

[7] A. R. Denton and N. W. Ashcroft, Phys. Rev. A **39**, 4701 (1989).

[8] G. A. McConnell, A. P. Gast, J. S. Huang, and S. D. Smith, Phys. Rev. Lett. **71**, 2102 (1993).

[9] G. A. McConnell and A. P. Gast, Phys. Rev. E **54**, 5447 (1996).

[10] W. G. Hoover, D. A. Young, and R. Grover, J. Chem. Phys. **56**, 2207 (1972).

[11] B. B. Laird and A. D. J. Haymet, Mol. Phys. **75**, 71 (1992).

[12] R. Agrawal and D. A. Kofke, Phys. Rev. Lett. **74**, 122 (1995).

[13] B. M. Mladek, D. Gottwald, G. Kahl, M. Neumann, and C. N. Likos, Phys. Rev. Lett. **96**, 045701 (2006).

[14] J. F. Lutsko and M. Baus, J. Phys.: Condens. Matter **3**, 6547 (1991).

[15] D. C. Wang and A. P. Gast, J. Chem. Phys. **110**, 2522 (1999).

[16] K. Ohno, T. Morinaga, S. Takeno, Y. Tsujii, and T. Fukuda, Macromolecules **39**, 1245 (2006).

[17] K. Ohno, T. Morinaga, S. Takeno, Y. Tsujii, and T. Fukuda, Macromolecules **40**, 9143 (2007).

[18] A. B. Bourlinos, R. Herrera, N. Chalkias, D. D. Jiang, Q. Zhang, L. A. Archer, and E. P. Giannelis, Adv. Mater. **17**, 234 (2005).

[19] A. B. Bourlinos, E. P. Giannelis, Q. Zhang, L. A. Archer, G. Floudas, and G. Fytas, Eur. Phys. J. E **20**, 109 (2006).

[20] R. Rodriguez, R. Herrera, L. A. Archer, and E. P. Giannelis, Adv. Mater. **20**, 4353 (2008).

[21] P. Agarwal, H. Qi, and L. A. Archer, Nano Lett. **10**, 111 (2010).

[22] J. L. Nugent, S. S. Moganty, and L. A. Archer, Adv. Mater. **22**, 3677 (2010).

[23] H.-Y. Yu and D. L. Koch, Langmuir **26**, 16801 (2010).

[24] Y. Singh, Phys. Rep. **207**, 351 (1991).

[25] N. F. Carnahan and K. Starling, J. Chem. Phys. **51**, 635 (1969).

[26] J.-P. Hansen and I. R. McDonald, *Theory of Simple Liquids*, Academic Press, London, 3 edition, 2006.

[27] D. A. McQuarrie, *Statistical Mechanics*, University Science Books, Sausalito, 2000.

[28] P. Richard, A. Gervois, L. Oger, and J.-P. Troadec, Europhys. Lett. **48**, 415 (1999).

[29] J. P. Singh, S. D. C. Walsh, and D. L. Koch, In preparation .

[30] W. A. Curtin and K. Runge, Phys. Rev. A **35**, 4755 (1987).

[31] A. Chremos, A. Z. Panagiotopoulos, and D. L. Koch, In preparation .

CHAPTER 7

SELF-DIFFUSION AND LINEAR VISCOELASTICITY OF SOLVENT-FREE NANOPARTICLE–ORGANIC HYBRID MATERIALS

7.1 Abstract

Nanoparticle–organic hybrid materials consist of 10 nm diameter spherical inorganic core particles functionalized with oligomeric organic molecules. Although these systems contain no added solvent, they exhibit fluid behavior with the fluidity provided by the attached oligomers. We solve for the non-equilibrium probability density function for pairs of particles subjected to a weak applied flow without hydrodynamic interactions. The many-body inter-core forces contains the hard sphere contribution and an $O(a^3/R_g^3)$ perturbation from the oligomers when the oligomer radius of gyration R_g is much greater than the core radius a. While the obtained long-time self-diffusivity of the cores and steady low shear viscosity of the system are similar to hard sphere suspensions at higher core volume fraction or longer oligomeric chains, the material exhibits stronger resistance to the motion of core particles as the tethered hairs feel more entropic penalty to fill the space, which agrees qualitatively with experiments and is a unique feature of the solvent-free nanoparticle fluid. The high frequency limit shear modulus is a linear function of $\omega^{1/2}$ and the intercept provides information for many-body forces that show both characteristics of hard and soft potentials. The system is viewed as particles that carry their fluid on their backs.

7.2 Introduction

Solvent-free nanoparticle–organic hybrid materials (NOHMs) contain nanocores self-suspended by the surface-tethered oligomers without any unattached solvent. Experimental studies have demonstrated that solvent-free NOHMs display transport properties and rheological behavior that vary with the core volume fraction, oligomer molecular weight, and/or oligomer surface grafting density [1–4]. The homogeneous mixture of the rigid cores and the soft space-filling tethered oligomeric fluid exhibits both characteristics for polymers and particles. The viscosity and the shear modulus are similar to viscous polymer liquids at small particle contents with longer oligomers; however, these properties also increase with the core volume fraction, a trend seen in particle suspensions. From a theoretical standpoint, the many-body entropic forces among the cores that result from the space-filling constraint on the hairs will give rise to unusual flow properties of NOHMs that are not captured in previous theories and calculations for particles in a solvent with pairwise interparticle potentials and hydrodynamic interactions. Recent equilibrium density-functional theory [5] and molecular dynamics (MD) simulations [6] have shed light on the unique structural properties of solvent-free NOHMs and demonstrated that the core distribution as well as the chain configuration are governed by the constraint that no void spaces are allowed in the suspension. In this work, we aim to develop theoretical predictions to the transport properties of NOHMs by analyzing the interactions of pairs of cores subjected to a many-body potential of mean force derived from the density-functional theory.

In general, there are two ways of evaluating the transport properties of interacting colloids. The first one is from the direct flow calculation [7,8] that is nor-

mally simplified to involve pairs of particles that interact through a mean interparticle potential. The transport coefficients are obtained from the force/stress formulation and the problem is solved in the real space. The second one is application of the mode-coupling theory [9, 10] where the memory function for dynamical couplings is the key to the theory and the problem is formulated in terms of the Fourier-space correlation functions. While the mode-coupling theory with the cage diffusivity evaluated based on a binary collision mechanism has been applied to predict diffusivities and viscosities for hard-sphere colloidal suspensions quite successfully [11–13], the complication introduced by the tethered oligomeric fluid in the absence of unattached solvent makes the short-time cage diffusion deviate from the simple analogy for concentrated molecular hard-sphere fluids developed from the kinetic theory for binary collisions. The cage diffusion depends largely on the preciseness of the description of the pair potential between the colliding pair. To gain a more conceptually visualizable picture for the dynamical behavior of the NOHMs system, in this work we will proceed with the direct flow calculation approach from the statistical mechanical theory for the particle distribution that incorporates many-body interactions and obtain the transport properties using fundamental constitutive relations.

Starting with the Smoluchowski equation, we first derive the evolution equation of any given pair of the NOHMs particles in which the relative particle motion is subjected to a convective applied force, diffusive Brownian forces, and the mean force arising from the total interparticle potential. Since no theory is available to describe the viscous response of a tethered fluid medium and we believe that the interparticle potential forces will play a more important role in controlling the dynamical properties, we neglect the detailed hydrodynamic

interactions among the particles and assume a continuum viscous response for the tethered oligomers with a viscosity η_s. In this fashion, we are still solving for a suspension fluid mechanics problem but the space-filling tethered fluid provides a many-body interparticle force that governs the particle distribution. The model NOHMs suspension considered is the same as the equilibrium density-functional theory of Yu and Koch [5], where the coarse-grained model consists of hard cores and bead-spring oligomers (one bead per spring) tethered to the center of each core. The oligomeric fluid is assumed to be incompressible and prevents the formation of large regions of free volume between the core particles. In the limiting case where the radius of gyration of the oligomers R_g is large compared with the core radius a, each core experiences weak interactions with the many other cores residing in its neighborhood within R_g and the core distribution function can be approximated as a hard-sphere distribution for a given particle number density n_b plus a perturbation correlation from the tethered oligomers that is of $O(1/n_b R_g^3)$ or $O(a^3/R_g^3)$. Under a weak applied force, we determine the long-time self-diffusivity of the cores, low shear rate viscosity, and the linear elastic properties for NOHMs in a quasi-analytical manner based on the evoluton equation for pairs of particles experiencing an intercore potential of mean force derived from the density-functional theory.

In section 7.3 we first present a short derivation for the pair evolution equation and elucidate two flow calculations: the tracer diffusion for obtaining the long-time self-diffusivity of particles (section 7.3.1) and the small amplitude oscillatory shear (section 7.3.2) for the linear viscoelasticic properties of NOHMs. The results and discussion are shown in section 7.4 followed by the conclusions in section 7.5.

7.3 Theory

We summarize briefly the derivation of the evolution equation for the distribution function of a pair of NOHMs particle subjected to interparticle and Brownian forces in the presence of an applied flow but without hydrodynamic interactions. For a monodisperse particle suspension of radius a, the N-particle Smoluchowski equation reads:

$$\frac{\partial P^{(N)}}{\partial t} + \sum_{i=1}^{N} \nabla \cdot \mathbf{j}_i = 0, \tag{7.1}$$

where $P^{(N)}$ is the probability density function of finding N particles and

$$\mathbf{j}_i = P^{(N)} \left[\mathbf{U}_i + \sum_{j=1}^{N} \frac{\mathbf{D}_{ij}}{k_\mathrm{B}T} \cdot \mathbf{F}_j \right] \tag{7.2}$$

is the flux due to the forces acting on each particle and the applied convective flow. The diffusivity tensor is defined by $\mathbf{D}_{ij} = D_0\mathbf{I}$ with $D_0 = \frac{k_\mathrm{B}T}{6\pi\eta_s a}$ being the diffusivity of non-interacting isolated particles and $\mathbf{I}$ being the identity tensor. $\mathbf{U}_i$ is the velocity of each particle due to the applied flow and

$$\mathbf{F}_j = -\nabla_j V_N - k_\mathrm{B}T \nabla_j \ln P^{(N)} \tag{7.3}$$

is the total force exerting on individual particle with V_N being the total interparticle potential. T is the temperature and k_B is the Boltzmann constant.

If we integrate over $N-2$ particles' positions except for particles 1 and 2, apply the divergence theorem along with the conservation of other third particles, and recall the homogeneity of the suspension such that $\nabla_2 = -\nabla_1 = \nabla$, we arrive at the evolution equation for a pair of particles,

$$\frac{\partial P^{(2)}}{\partial t} + \nabla \cdot \left[P^{(2)} \langle \mathbf{U}_{12} \rangle_2 \right] - 2D_0 \nabla \cdot \left[P^{(2)} \nabla \frac{\langle V_N \rangle_2}{k_\mathrm{B}T} + \nabla P^{(2)} \right] = 0, \tag{7.4}$$

where $P^{(2)}$ is the probability density function of finding the two particles, $\mathbf{U}_{12} = \mathbf{U}_2 - \mathbf{U}_1$ is the relative velocity due to the applied flow, and $\langle\rangle_2$ denotes a conditional average given the two particles are fixed. For a given quantity $A\left(\mathbf{r}^N\right)$, $\langle A\rangle_2(\mathbf{r}_1, \mathbf{r}_2) = \int_V \cdots \int_V P^{(N-2)}\left(\mathbf{r}^{N-2}|\mathbf{r}_1, \mathbf{r}_2\right) A\left(\mathbf{r}^N\right) \mathrm{d}\mathbf{r}_3 \cdots \mathrm{d}\mathbf{r}_N$ with $P^{(N-2)}\left(\mathbf{r}^{N-2}|\mathbf{r}_1, \mathbf{r}_2\right)$ being the conditional probability density function of finding $N-2$ particle given that particles 1 and 2 are fixed at $\mathbf{r}_1$ and $\mathbf{r}_2$ and V being the system volume. $\nabla\langle V_N\rangle_2$ is the mean force exerting on particle 1 averaged over non-equilibrium configurations of particles 3 to N. The information of the correlations for non-equilibrium forces relies on a closure approximation that accounts for the coupling and cancellation effects between the equilibrium and non-equilibrium correlations [14, 15]. Since for hard spheres the approximation of the equilibrium mean force gives reasonably close rheological results to experiments [16] and for NOHMs with $R_\mathrm{g}/a \gg 1$ the perturbation to the equilibrium force on the tagged particle 1 due to any third particle's tethered oligomers can be attributed to $O((a^3/R_\mathrm{g}^3)^2)$ contributions [5], in the theoretical framework valid to $O(a^3/R_\mathrm{g}^3)$ correlations we may retain the equilibrium particle correlations but neglect the perturbation in the force from other third particles due to the distortion of the equilibrim structure and simply write $\nabla\langle V_N\rangle_2 \approx \nabla V_\mathrm{mf}$. V_mf is the potential of mean force defined by $V_\mathrm{mf}(\mathbf{r}) = -k_\mathrm{B}T \ln g(\mathbf{r})$ with $g(\mathbf{r})$ being the equilibrium pair probability and $\mathbf{r} = \mathbf{r}_2 - \mathbf{r}_1$.

Equation 7.4 with $\nabla\langle V_N\rangle_2$ being replaced by ∇V_mf should be solved with the no-flux boundary condition at particle contact $r = 2a$

$$\mathbf{n} \cdot \left\{ P^{(2)}\langle \mathbf{U}_{12}\rangle_2 - 2D_0 \left[P^{(2)} \nabla \left(\frac{V_\mathrm{mf}}{k_\mathrm{B}T} \right) + \nabla P^{(2)} \right] \right\} \tag{7.5}$$

with $\mathbf{n}$ being the surface normal vector, and $P^{(2)} \to \frac{1}{V^2}$ at infinite particle separations when the pair decorrelate.

7.3.1 Tracer Diffusion

The long-time self-diffusivity of the suspension $D_s^\infty(\phi_b)$ at a given particle volume fraction ϕ_b relates the mean velocity of a tagged particle to a steady applied force acting on it [7,17]. Here we consider a tagged tracer particle 1 subjected to this "thermodynamic force" $\mathbf{F}_1$ in a sea of force-free untagged particles 2 such that the mean velocity of the tracer particle is $\langle \mathbf{U}_1 \rangle = \frac{D_s^\infty(\phi_b)}{k_B T}\mathbf{F}_1$ on the macroscopic level. As the tracer particle moves under the applied force, it deforms the pair distribution function of the other particles relative to it and results in a relaxation force $\mathbf{F}_{rel}$ from the other particles caused by the deformation [15,18]. Therefore, the total force exerting on the tracer particle is $\mathbf{F}_{tot} = \mathbf{F}_1 + \mathbf{F}_{rel}$ and on the microscopic level $\langle \mathbf{U}_1 \rangle$ is related to $\mathbf{F}_{tot}$ via the Stokes–Einstein relation, $\langle \mathbf{U}_1 \rangle = \frac{D_0}{k_B T}\mathbf{F}_{tot}$, without hydrodynamic interactions. The relative velocity between the tracer particle 1 and a far way non-tracer particle 2 based on the Stokes–Einstein relation is $\langle \mathbf{U}_{12} \rangle_2 = -\frac{D_0}{k_B T}\mathbf{F}_1$. When the time scale $\tau \gg a^2/D_0$, at quasi-steady state the net flux of the tracer particle 1 is zero. If we non-dimensionalize ∇ by the core radius a, Eq. 7.4 becomes

$$Pe\nabla \cdot \left[P^{(2)} \frac{\mathbf{F}_1}{F_1} \right] + \nabla \cdot \left[P^{(2)} \nabla \left(\frac{V_{mf}}{k_B T} \right) + \nabla P^{(2)} \right] = 0, \tag{7.6}$$

where Pe is the Péclet number defined by $Pe = \frac{aF_1}{2k_B T}$.

Since the thermodynamic force is a weak applied force, $Pe \ll 1$ and the non-equilibrium pair probability can be written as a regular perturbation to the equilibrium distribution function

$$P^{(2)}(r) = \frac{1}{V^2} g(r) \left[1 + Pe \frac{\mathbf{r} \cdot \mathbf{F}_1}{r F_1} Q(r) + O(Pe^2) \right] \tag{7.7}$$

with Q being an $O(1)$ scaler function. Substituting Eq. 7.7 into Eq. 7.6 yields an $O(1)$ equation for equilibrium distribution function and an $O(Pe)$ equation that

reads with $s = r/a$

$$\frac{1}{s^2}\frac{d}{ds}\left(s^2\frac{dQ}{ds}\right) - \frac{d}{ds}\left(\frac{V_{\mathrm{mf}}}{k_{\mathrm{B}}T}\right)\frac{dQ}{ds} - \frac{2Q}{s^2} = \frac{d}{ds}\left(\frac{V_{\mathrm{mf}}}{k_{\mathrm{B}}T}\right) \tag{7.8}$$

satisfying the boundary conditions $\frac{dQ}{ds} = -1$ at $s = 2$ and $Q \to 0$ as $s \to \infty$. Solving for Eq. 7.8 numerically with the potential of mean force for a given NOHMs system as input, we obtain the perturbed pair distribution function under weak deformation from the equilibrium structure.

The relaxation force exerting on the tracer particle is calculated from averaging the interparticle forces between the tracer and indistinguishable non-tracer particles,

$$\begin{aligned}\mathbf{F}_{\mathrm{rel}} &= \int_V \cdots \int_V P^{(N-1)}\left(\mathbf{r}^{N-1}|\mathbf{r}_1\right)(-\nabla_1 V_N)\,\mathrm{d}\mathbf{r}_2 \cdots \mathrm{d}\mathbf{r}_N \\ &= (N-1)\int_V P^{(1)}(\mathbf{r}_2|\mathbf{r}_1)\nabla\langle V_N\rangle_2 \mathrm{d}\mathbf{r}_2 \\ &\approx n_{\mathrm{b}}\int_V g(\mathbf{r})\frac{aQ(\mathbf{r})}{2r^2}\frac{d}{dr}\left(\frac{V_{\mathrm{mf}}}{k_{\mathrm{B}}T}\right)\mathbf{r}\mathbf{r}\cdot\mathbf{F}_1\mathrm{d}\mathbf{r},\end{aligned} \tag{7.9}$$

where $P^{(N-1)}(\mathbf{r}^{N-1}|\mathbf{r}_1)$ is the conditional probability density function of finding $N-1$ particles given that there is a particle fixed at $\mathbf{r}_1$ and $P^{(1)}(\mathbf{r}_2|\mathbf{r}_1)$ is the conditional probability density function of finding particle 2 at $\mathbf{r}_2$ given that there is a particle fixed at $\mathbf{r}_1$. We have approximated $\nabla\langle V_N\rangle_2$ as ∇V_{mf} and written $P^{(1)}(\mathbf{r}_2|\mathbf{r}_1) = \frac{1}{V}g(\mathbf{r})\left[1 + Pe\frac{\mathbf{r}\cdot\mathbf{F}_1}{rF_1}Q\right]$ to derive the final expression. The spherically symmetric $g(\mathbf{r})$ does not contribute a net force.

Yu and Koch [5] obtained the equilibrium radial distribution function of the NOHMs system based on the reference hard sphere suspension such that $g(\mathbf{r}) = g_{\mathrm{HS}}(\mathbf{r}) + h_{\mathrm{f}}(\mathbf{r})$ with $g_{\mathrm{HS}}(\mathbf{r})$ being the hard-sphere radial distribution function at the same ϕ_{b} as NOHMs and $h_{\mathrm{f}}(\mathbf{r})$ being the regular perturbation term of $O(a^3/R_{\mathrm{g}}^3)$ contributed from the tethered oligomeric fluid. $g_{\mathrm{HS}}(\mathbf{r})$ was calculated

from solving for the Ornstein–Zernike equation with the Percus–Yevick approximation [10, 19]. Taking into account that for hard spheres $g_{\mathrm{HS}}(\mathbf{r}) = 0$ if $r < 2a$, we may write $g(\mathbf{r}) = \bar{g}(\mathbf{r})H(r - 2a)$ with H being the unit step function enforcing a zero pair probability if $r < 2a$. Finally, writing $\frac{d}{dr}\left(\frac{V_{\mathrm{mf}}}{k_{\mathrm{B}}T}\right) = -\frac{1}{g}\frac{dg}{dr}$ in Eq. 7.9 yields the long-time self-diffusivity of NOHMs in the absence of hydrodynamic interactions correct to $O(\phi_{\mathrm{b}})$:

$$\frac{D_{\mathrm{s}}^{\infty}(\phi_{\mathrm{b}})}{D_0} = \frac{\mathbf{F}_{\mathrm{tot}}}{\mathbf{F}_1} = 1 - \frac{1}{2}\phi_{\mathrm{b}}\left[\int_2^{\infty} \frac{dg(s)}{ds} Q(s)s^2 ds + 4g(2)Q(2)\right], \tag{7.10}$$

where $g(2)$ and $Q(2)$ are evaluated at the contact of the two particles. The relaxation force reduces the mobility of the tracer particle and is driven by the tendency of the system to restore the equilibrium structure.

7.3.2 Small Amplitude Oscillatory Shear

The linear viscoelastic response of a suspension can be obtained by the application of a small amplitude oscillatory shear. In this section, we aim to find the shear viscosity and modulus of NOHMs in the absence of hydrodynamic interactions. Under small amplitude oscillations, the relative velocity between a pair of NOHMs particles due to the imposed time-dependent linear flow is $\mathbf{U}_{12} = \mathbf{E} \cdot \mathbf{r}e^{i\omega t}$, where $\mathbf{E}$ is the rate-of-strain tensor with the magnitude of the shear rate being $\dot{\gamma}$ and ω is the frequency of the oscillations. While $\mathbf{U}_{12}$ considers affine motion of the pair due to the applied shear, the potential force drives a velocity that makes the total relative motion not affine. Similar to section 7.3.1, non-dimensionalizing ∇ by a in Eq. 7.4 yields,

$$\frac{a^2}{D_{12}}\frac{\partial P^{(2)}}{\partial t} + Pe\nabla \cdot \left[P^{(2)}\frac{\mathbf{U}_{12}}{a\dot{\gamma}}\right] - \nabla \cdot \left[P^{(2)}\nabla\left(\frac{V_{\mathrm{mf}}}{k_{\mathrm{B}}T}\right) + \nabla P^{(2)}\right] = 0, \tag{7.11}$$

where $Pe = \frac{\dot{\gamma}a^2}{D_{12}^0} = \frac{3\pi\eta_s a^3\dot{\gamma}}{k_B T}$ and $D_{12}^0 = 2D_0$, the relative diffusivity between particles 1 and 2.

For small amplitude oscillatory shear, the system structure is only perturbed by the weak applied flow by a small amount and we may again write

$$P^{(2)}(r) = \frac{1}{V^2} g(r) \left[1 + Pe \frac{\mathbf{r} \cdot \mathbf{E} \cdot \mathbf{r}}{r^2 \dot{\gamma}} e^{i\omega t} f(r, \omega) + O(Pe^2) \right] \tag{7.12}$$

with f being an $O(1)$ scalar function. After substituting Eq. 7.12 into Eq. 7.6 we obtain the following $O(Pe)$ equation:

$$i\omega \frac{a^2}{D_{12}^0} f - \frac{1}{s^2} \frac{d}{ds} s^2 \frac{df}{ds} + \frac{d}{ds} \left(\frac{V_{\text{mf}}}{k_B T} \right) \frac{df}{ds} + \frac{6f}{s^2} = s \frac{d}{ds} \left(\frac{V_{\text{mf}}}{k_B T} \right) \tag{7.13}$$

with the boundary conditions $\frac{df}{ds} = 2$ at $s = 2$ and $f \to 0$ as $s \to \infty$. We write $\alpha = \omega a^2 / D_{12}^0$ as a dimensionless number defined by the oscillatory frequency, which is analogous to Pe defined by the shear rate. With V_{mf} being the input from the equilibrium theory of Yu and Koch [5], we can solve for Eq. 7.13 numerically for arbitrary finite oscillatory frequency and obtain the non-equilibrium pair distribution function $P^{(2)}$.

For rigid particles in the absence of inertia, the bulk stress is related to the time-dependent rate-of-strain tensor such that [16, 20–22]

$$\boldsymbol{\Sigma} = -\langle p \rangle \mathbf{I} + 2\eta_s \mathbf{E} e^{i\omega t} + \frac{1}{V} \sum_{i=1}^{N} \mathbf{S}_i^H + \frac{1}{V} \sum_{i=1}^{N} \mathbf{S}_i^T \tag{7.14}$$

$$= -\langle p \rangle \mathbf{I} + 2 \left[\eta'(\omega) - i \frac{G'(\omega)}{\omega} \right] \mathbf{E} e^{i\omega t}, \tag{7.15}$$

where $\langle p \rangle$ is the isotropic pressure, $\mathbf{S}_i^H$ and $\mathbf{S}_i^T$ are particle stresslets that are hydrodynamic and thermodynamic in origin, respectively. η' is the suspension shear viscosity that is in-phase with the applied oscillations and G' is the suspension shear modulus. We also define the loss modulus $G''(\omega) = \omega\eta'(\omega)$ and

the out-of-phase viscosity $\eta''(\omega) = G'(\omega)/\omega$. In the absence of hydrodynamic interactions, the hydrodynamic stress is [8]

$$\frac{1}{V}\sum_{i=1}^{N}\mathbf{S}_i^H = n_\mathrm{b}\langle\mathbf{S}_i^H\rangle = \frac{20}{3}\pi a^3 n_\mathrm{b}\eta_\mathrm{s}\mathbf{E}e^{i\omega t}. \tag{7.16}$$

The thermodynamic stress results from the interparticle forces $\left(\mathbf{F}_i^\mathrm{P} = -\nabla_i V_N\right)$ among indistinguishable particles and takes the following form:

$$\begin{aligned}\frac{1}{V}\sum_{i=1}^{N}\mathbf{S}_i^T &= -\frac{1}{V}\sum_{i=1}^{N}\mathbf{r}_i\mathbf{F}_i^\mathrm{P} = -n_\mathrm{b}\langle\mathbf{r}_1\mathbf{F}_1^\mathrm{P}\rangle_1 \\ &= n_\mathrm{b}(N-1)\int_V P^{(1)}(\mathbf{r}_2|\mathbf{r}_1)\,\langle(\mathbf{r}_2-\mathbf{r}_1)\nabla_2 V_N\rangle_2\,\mathrm{d}\mathbf{r}_2 \\ &\approx 3\pi n_\mathrm{b}^2\eta_\mathrm{s}a^3 e^{i\omega t}\int_V \mathbf{r}g(\mathbf{r})f(\mathbf{r},\omega)\frac{\mathbf{r}\cdot\mathbf{E}\cdot\mathbf{r}}{r^2}\nabla\left(\frac{V_\mathrm{mf}}{k_\mathrm{B}T}\right)\mathrm{d}\mathbf{r},\end{aligned} \tag{7.17}$$

where $\langle\rangle_1$ denotes the conditional average given one particle is fixed and we have used the same approximations as Eq. 7.9 and chosen any particle as our reference with $\sum_{i=1}^{N}\mathbf{r}_1\mathbf{F}_i^\mathrm{P} = 0$. If we write $f = f_1 + if_2$ and recognize that for hard-sphere distribution function we should include a step function in $g(\mathbf{r})$ as shown in section 7.3.1 since particles do not overlap, we obtain the following shear viscosity and shear modulus for arbitrary oscillatory frequency:

$$\frac{\eta'(\omega)}{\eta_\mathrm{s}} = 1 + \frac{5}{2}\phi_\mathrm{b} - \frac{9}{40}\phi_\mathrm{b}^2\left[\int_2^\infty s^3\frac{dg(s)}{ds}f_1(s,\omega)ds + 8g(2)f_1(2,\omega)\right] \tag{7.18}$$

and

$$\frac{G'(\omega)a^3}{k_\mathrm{B}T} = \frac{3\alpha}{40\pi}\phi_\mathrm{b}^2\left[\int_2^\infty s^3\frac{dg(s)}{ds}f_2(s,\omega)ds + 8g(2)f_2(2,\omega)\right], \tag{7.19}$$

where $\alpha = \omega a^2/D_{12}^0$. Since we neglect the hydrodynamic interactions, the $O(\phi_\mathrm{b})$ contribution to η' is purely due to the hydrodynamic stress for isolated particles and the thermodynamic stress resulting from the potential of mean force only leads to $O(\phi_\mathrm{b}^2)$ contributions to η' and G'. In the absence of hydrodynamic interactions, the second terms in the $O(\phi_\mathrm{b}^2)$ contributions of η' and G' led by the hard-sphere nature of the particles give the collisional contributions and are

equivalent to the direct Brownian contributions to the stress, as indicated by Brady [20].

Here we consider two limiting cases. As $\omega = 0$, $f = f_1$ and $f_2 = 0$, we obtain the steady low shear viscosity η_0 from Eq. 7.18 at zero frequency,

$$\frac{\eta_0}{\eta_s} = 1 + \frac{5}{2}\phi_b - \frac{9}{40}\phi_b^2\left[\int_2^\infty s^3 \frac{dg(s)}{ds} f(s) ds + 8g(2)f(2)\right] \tag{7.20}$$

and $G' \to 0$. The system in this case behaves as a viscous liquid. On the other hand, as $\omega \to \infty$, from Eq. 7.13 we obtain an outer solution

$$f_{out}(s, \alpha) \to -\frac{i}{\alpha} s \frac{d}{ds}\left(\frac{V_{mf}}{k_B T}\right) \tag{7.21}$$

that satisfies the boundary condition at large particle separations, $f_{out}|_{s\to\infty} \to 0$, because the interparticle forces decay to zero. However, $V_{mf} = -k_B T \ln g$ with g being finite at $s = 2$. Therefore this solution fails to satisfy the no-flux boundary condition at $s = 2$. Near particle contact, there will be a boundary layer in which the diffusive flux balances the convective flux resulting from the transient term. From scaling analysis we find that the dimensionless boundary layer thickness δ scales as $\alpha^{-\frac{1}{2}}$ and we may define the boundary layer coordinate as $x = \alpha^{\frac{1}{2}}(s-2)$. To match f_{out} the boundary layer solution should contain $O(\alpha^{-1})$ contributions. Therefore we propose

$$f_{BL}(x, \alpha) = \alpha^{-\frac{1}{2}} f_{BL}^{(1)}(x, \alpha) + \alpha^{-1} f_{BL}^{(2)}(x, \alpha) + O(\alpha^{-\frac{3}{2}}) \tag{7.22}$$

with the boundary condition $\frac{df_{BL}}{dx} = 2$ at $x = 0$. The final solution can be obtained from matched asymptotic solution given $\lim_{x\to\infty} f_{BL}(x, \alpha) = \lim_{s\to 2} f_{out}(s, \alpha)$:

$$f_\infty(s, \alpha) = f_{out}(s, \alpha) + f_{BL}(x, \alpha) - \lim_{s\to 2} f_{out}(s, \alpha), \tag{7.23}$$

which is a uniformly valid approximation. Substituting Eq. 7.22 into Eq. 7.13 yields

$$\alpha^{-\frac{1}{2}} f_{BL}^{(1)} = \frac{1}{\sqrt{2\alpha}}(i-1)e^{-\sqrt{\alpha i}(s-2)}, \tag{7.24}$$

equivalent to the solution found by Brady [20] and Lionberger and Russel [21] for hard spheres without hydrodynamic interactions. We proceed to $O(\alpha^{-1})$ contributions and derive

$$\alpha^{-1} f_{\mathrm{BL}}^{(2)} = -\frac{1}{\sqrt{2\alpha}}(i-1)(1+F_0)(s-2)e^{-\sqrt{\alpha i}(s-2)} - \frac{i}{\alpha}(1+F_0)e^{-\sqrt{\alpha i}(s-2)} + i\frac{2F_0}{\alpha} \quad (7.25)$$

with $F_0 = -\frac{d}{ds}\left(\frac{V_{\mathrm{mf}}}{k_{\mathrm{B}}T}\right)|_{s\to 2}$.

Similarly, after some manipulations the high frequency solution can be written as $f_\infty = f_{1,\infty} + i f_{2,\infty}$, where

$$\begin{aligned} f_{1,\infty}(s,\alpha) = &-e^{-\sqrt{\frac{\alpha}{2}}(s-2)}\left[\sqrt{\frac{2}{\alpha}} - \frac{1}{\sqrt{2\alpha}}(1+F_0)(s-2)\right] \\ &\times\left[\cos\left(\sqrt{\frac{\alpha}{2}}(s-2)\right) - \sin\left(\sqrt{\frac{\alpha}{2}}(s-2)\right)\right] \\ &- e^{-\sqrt{\frac{\alpha}{2}}(s-2)}\left[\frac{(1+F_0)}{\alpha}\sin\left(\sqrt{\frac{\alpha}{2}}(s-2)\right)\right] \end{aligned} \quad (7.26)$$

and

$$\begin{aligned} f_{2,\infty}(s,\alpha) = &\, e^{-\sqrt{\frac{\alpha}{2}}(s-2)}\left[\sqrt{\frac{2}{\alpha}} - \frac{1}{\sqrt{2\alpha}}(1+F_0)(s-2)\right] \\ &\times\left[\cos\left(\sqrt{\frac{\alpha}{2}}(s-2)\right) + \sin\left(\sqrt{\frac{\alpha}{2}}(s-2)\right)\right] \\ &- e^{-\sqrt{\frac{\alpha}{2}}(s-2)}\left[\frac{(1+F_0)}{\alpha}\cos\left(\sqrt{\frac{\alpha}{2}}(s-2)\right)\right] - \frac{s}{\alpha}\frac{d}{ds}\left(\frac{V_{\mathrm{mf}}}{k_{\mathrm{B}}T}\right). \end{aligned} \quad (7.27)$$

From Eq. 7.18 we see that at high frequency $f_{1,\infty}$ makes the $O(\phi_{\mathrm{b}}^2)$ thermodynamic contributions decay as $\omega^{-1/2}$, therefore $\frac{\eta'_\infty}{\eta_{\mathrm{s}}} \to 1 + \frac{5}{2}\phi_{\mathrm{b}}$ and contains only the hydrodynamic contributions. The corresponding loss modulus $G'' - \omega\eta'_\infty$ grows as $\omega^{1/2}$ at high frequency. To derive the shear modulus at infinite frequency G'_∞ we evaluate terms for the boundary layer solution and the outer solution separately

in Eq. 7.19 and obtain

$$\begin{aligned}\frac{G'_\infty a^3}{k_B T} &= \frac{3\alpha}{40\pi}\phi_b^2\left[\int_2^\infty s^3\frac{dg}{ds}f_{out}ds + 8g(2)f_{out}(2)\right] \\ &\quad + \frac{3\alpha}{40\pi}\phi_b^2\left\{\int_0^\infty 8\frac{dg}{ds}|_{s=2}\left[f_{BL}(x) - f_{BL}(\infty)\right]\alpha^{-\frac{1}{2}}dx + 8g(2)\left[f_{BL}(2) - f_{out}(2)\right]\right\} \\ &= \frac{3\sqrt{2}}{5\pi}\phi_b^2 g(2)\alpha^{\frac{1}{2}} \\ &\quad + \frac{3}{40\pi}\phi_b^2\left\{\int_2^\infty s^4 g\left[\frac{d}{ds}\left(\frac{V_{mf}}{k_B T}\right)\right]^2 ds + 8g(2)\left[\frac{d}{ds}\left(\frac{V_{mf}}{k_B T}\right)|_{s=2} - 1\right]\right\}. \end{aligned} \tag{7.28}$$

Note that the second term of the outer solution contributions $8g(2)f_{out}(2)$ cancels the boundary layer integral automatically. As $\omega \to \infty$, G' diverges as $\omega^{1/2}$ and η'' decays as $\omega^{-1/2}$. This growing scaling is consistent with experiments [23–25] and Brownian dynamics (BD) simulations [26], and also agrees with the limiting modulus derived from the mode-coupling theory [11, 27] for hard spheres with weak or no hydrodynamic interactions. Our derivation shows that G'_∞ is a linear function of $\omega^{1/2}$ with the slope being determined only by the equilibrium particle radial distribution function at contact. Extropolation of the straight line to $\omega = 0$ yields the intercept determined by the interparticle forces as well as the particle distribution function. This intercept is a signature of the many-body thermodynamic interactions for systems with hard-core-like potentials and was not calculated in previous work. For continuous interparticle potentials that give $\frac{dV_{mf}}{ds}|_{s=2} = 0$, Eq. 7.21 satisfies the no-flux boundary condition at two-particle contact and one obtains

$$\frac{G'_\infty a^3}{k_B T} = \frac{3}{40\pi}\phi_b^2\int_2^\infty s^4 g\left[\frac{d}{ds}\left(\frac{V_{mf}}{k_B T}\right)\right]^2 ds, \tag{7.29}$$

which is exactly the result derived by Russel and Gast [16] in the absence of hydrodynamic interactions.

7.4 Results & Discussion

Section 7.3 provides the formulation of non-equilibrium pair probability problems and transport properties for a given potential of mean force. In this section, we calculate the transport properties with the input of the core radial distribution function obtained from the theory of Yu and Koch [5]. It is noteworthy that although the weak oligomeric-field approximation is valid when $R_g/a \gg 1$, the weak field theory explains many of the trends of the equilibrium structure seen in MD simulations even when R_g/a is as low as 0.54 [6]. Therefore in the following calculations for transport properties we may extrapolate the weak field theory beyond the $R_g/a \gg 1$ regime. To satisfy the incompressibility constraint for the fluid phase oligomers, the number of oligomers per core is changed with the core volume fraction such that the oligomer concentration in each system of NOHMs investigated remains the same. We choose our reference condition to be 600 chains per core at $\phi_b = 0.15$.

Figure 7.1 shows the core radial distribution function and the potential of mean force for NOHMs with different chain lengths at the core volume fraction of 0.2 evaluated from the theory of Yu and Koch [5]. The core radial distribution function for $R_g/a > 1$ generally shows damped peaks characterizing a softened potential among the cores. On the other hand, for $R_g/a < 1$ the stronger entropic frustrations of oligomers due to the space-filling constraint yield a substantial attraction between the neighboring particles relative to the hard spheres. Therefore $g(s)$ at $R_g/a = 0.7$ is more structured with enhanced peaks and a closer distance between the first and the second peaks than hard spheres. The general behavior shown in this figure is true for different core volume fractions. At larger ϕ_b the interparticle spacing is small and the soft oligomers can still

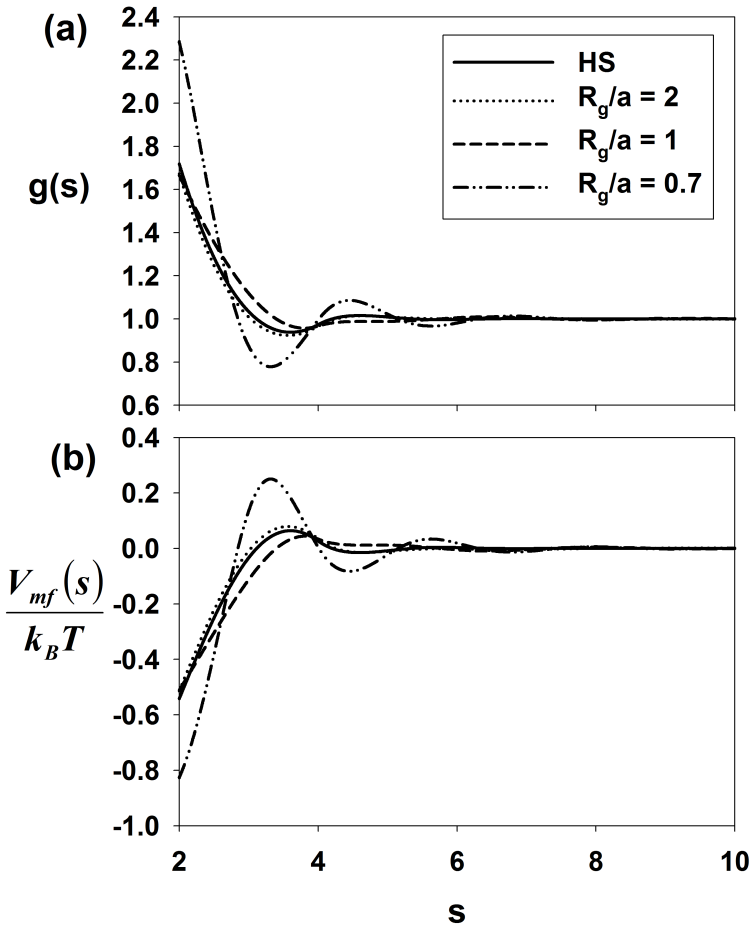

Figure 7.1: (a) Comparison of the radial distribution function g of NOHMs with different R_g/a and hard spheres as a function of the inter-particle distance non-dimensionalized by the core radius, s, at $\phi_b = 0.2$ and (b) the corresponding comparison of the potential of mean force non-dimensionalized by the thermal energy, V_{mf}/k_BT, as a function of s. The line descriptions are the same as (b).

explore the conformational space therefore the changes in $g(s)$ relative to hard spheres are minor. As ϕ_b decreases the variation of $g(s)$ is more apparent since the configuration of tethered oligomers are more restricted to the space-filling constraint.

The long-time self-diffusivity of the NOHMs particles with different chain stiffness and core volume fraction is shown in Fig. 7.2. The current result for hard spheres at different particle volume fraction in the absence of hydrodynamic interactions is equivalent to that predicted by Brady [28], albeit Brady solved for the Smoluchowski equation (Eq. 7.1) in Fourier space using self-intermediate scattering function while we proceed with the interactions of pairs of particles in real space. Since the variations of $g(s)$ and V_{mf} caused by the tethered oligomers are less substantial at moderate to high core volume fraction ($\phi_b > 0.15$), the predicted D_s^∞ for NOHMs is similar to the reference hard sphere suspension at the same ϕ_b. As we decrease ϕ_b, the interparticle spacing increases and the oligomer-mediated potential of mean force exhibits stronger deviation from hard spheres and we start to observe more apparent difference between D_s^∞ for NOHMs and hard spheres. While for hard sphere suspensions the diffusivity increases with decreasing particle concentration due to increasing particle mobility, NOHMs exhibit substantially reduced diffusivity at lower ϕ_b than hard spheres. Eventually when the configuration of the chains is so limited that the oligomers prohibit large displacement of the core D_s^∞ drops drastically. The volume fraction at which this sudden drop in D_s^∞ is observable depends on the stiffness of the chains. As R_g/a decreases this drop occurs at higher ϕ_b because stiffer chains have more difficulty in filling the space.

It is of interest to examine how the core pair probability behaves in the lim-

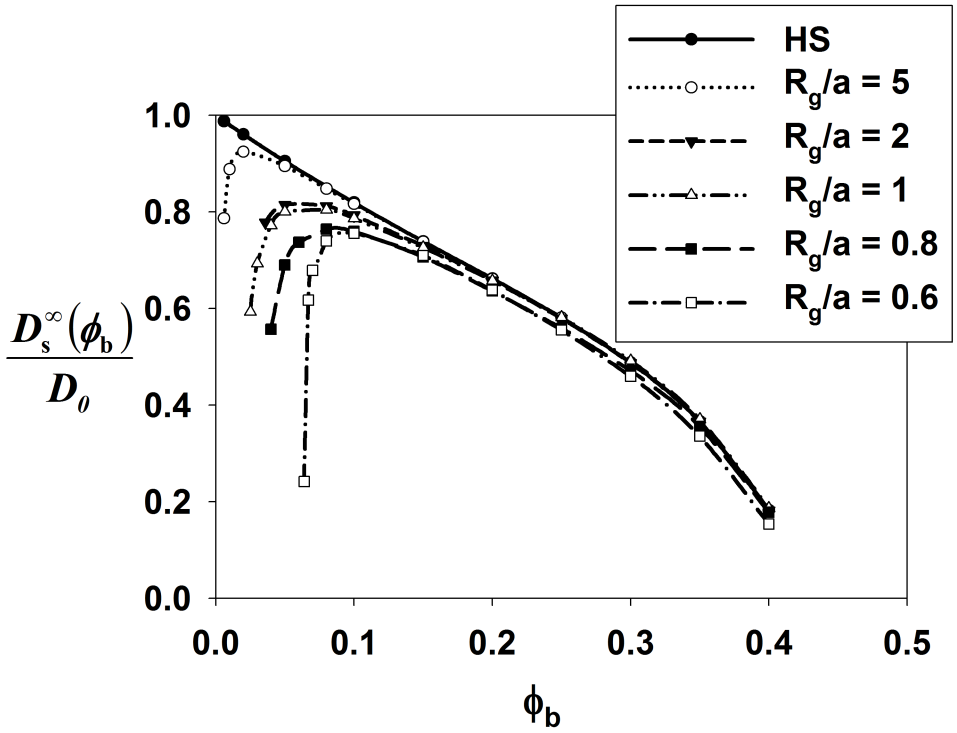

Figure 7.2: The long-time self-diffusivity of the cores D_s^∞ scaled by the Stokes–Einstein diffusivity D_0 for the NOHMs system with different R_g/a and hard spheres as a function of the core volume fraction ϕ_b.

iting condition where the diffusivity decreases drastically. We compare the core radial distribution function at very small ϕ_b for systems with two different R_g/a ratios in Fig. 7.3 and observe two distinct characteristics of the structure. As mentioned above, systems with $R_g/a > 1$ exhibit less structured $g(r)$ than hard spheres. At small ϕ_b, the soft shell provided by the tethered oligomers extends due to more stretched chain configuration. Since the core concentration is dilute, the oligomer grafting density per core is high enough to produce very strong field that excludes the nearest neighbors of each particle from center-to-center separations as close as hard spheres at $r = 2a$. As a result, in Fig. 7.3(a) we obtain $g(r)$ that oscillates on the length scale of R_g with nearly zero probability

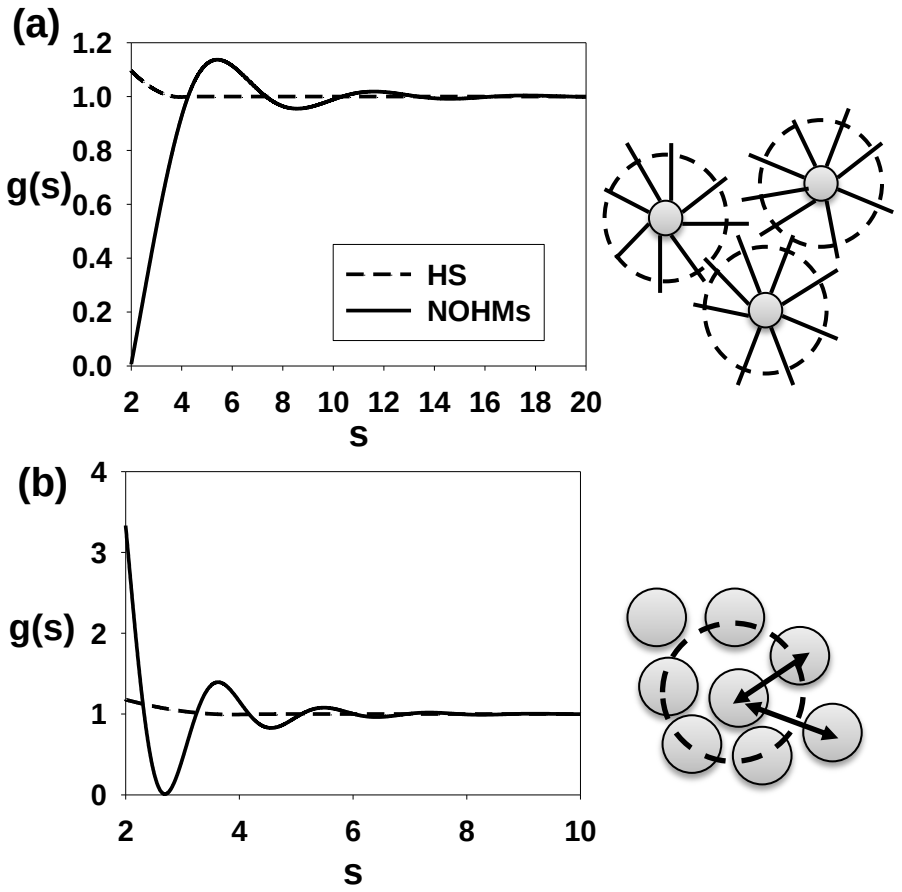

Figure 7.3: (a) The radial distribution function g of NOHMs with $R_g/a = 2$ and hard spheres as a function of the interparticle distance non-dimensionalized by the core radius, s, at $\phi_b = 0.036$. The cartoon shows strongly stretched hairs yielding effectively larger soft particles. (b) Same as (a) for $R_g/a = 0.6$ and $\phi_b = 0.064$. The cartoon shows a shell of neighbors around a chosen particle leading to strong particle interactions.

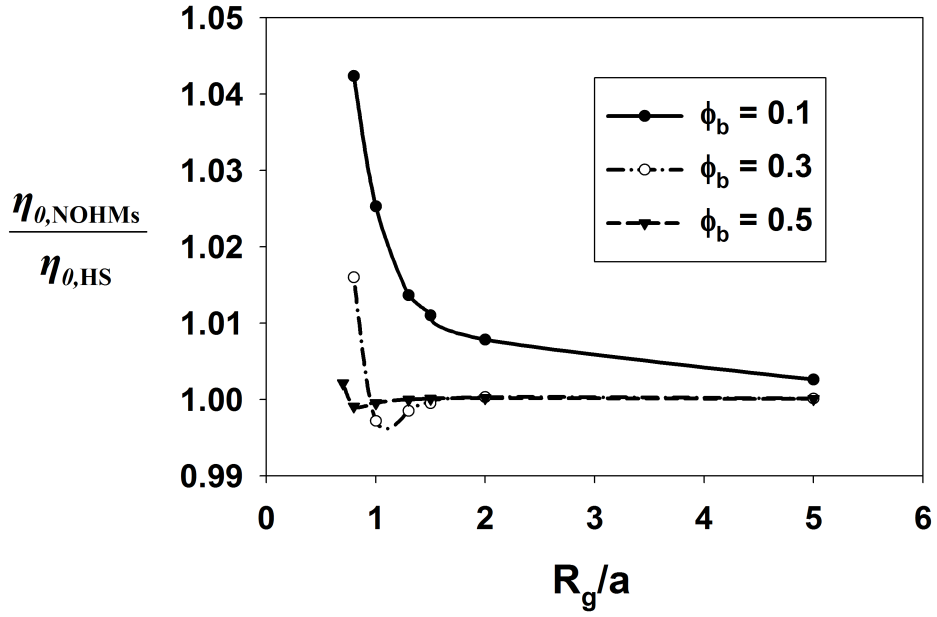

Figure 7.4: Comparison of the steady low shear viscosity for NOHMs $\eta_{0,\mathrm{NOHMs}}$ non-dimensionalized by the steady low shear viscosity for hard spheres $\eta_{0,\mathrm{HS}}$ at a given ϕ_b as a function of R_g/a.

at $r = 2a$, which qualitatively characterizes a suspension of soft particles with a higher effective particle volume fraction than the reference hard sphere solution and the long-time self-diffusivity decreases as expected. On the other hand, for NOHMs with $R_\mathrm{g}/a < 1$, the entropic attraction progresses as interparticle spacing increases. Eventually when the attraction among the cores is strong enough to build up a structured shell of neighbors around each core (or a "cage"), we obtain a highly enhanced first peak followed by a very deep trough in $g(r)$ as shown in Fig. 7.3(b) and the tracer diffusivity is highly reduced.

Equation 7.20 yields the steady low shear viscosity for hard spheres that diverges as ϕ_b approaches the random-close-packing volume fraction $\phi_{\mathrm{b,m}}$, as also predicted by many authors [16, 20, 22, 27]. In Fig. 7.4, we compare the ratio

between the relative viscosity η_0/η_s for NOHMs with a given R_g/a and $\eta_{0,HS}/\eta_s$ for hard spheres in an unattached melt to investigate the viscous response provided solely from the tethered hairs. In general, for a given core volume fraction longer oligomers lead to lower relative viscosity, a trend that is qualitatively consistent with the findings at small *Pe* of Goyal and Escobedo [29] using MD simulations and with experimental observations of Agarwal and Archer [3]. On the other hand, for a given chain length systems with higher core volume fraction show higher relative viscosity but the ratio between NOHMs and hard spheres is lower. These general results agree with the physical argument that when the oligomers feel more entropic frustrations for filling the space the system exhibits slower dynamics. It is noteworthy that at higher ϕ_b there seems to be a transition region near $R_g/a = 1$ at which $\eta_0/\eta_{0,HS}$ shows a minimum and is less than 1. If we estimate the interparticle separation with $n_b^{-1/3}$ we find that the minimum corresponds to the case where $n_b^{-1/3} \approx 2R_g$. Therefore when R_g is comparable with the interparticle spacing the soft shell produced by the oligomers makes the particles more evenly spaced and reduces the resistance. For small enough ϕ_b the particle distribution is sparse enough such that we do not see this minimum.

We may compare the strength of the thermodynamic contributions to the relative viscosity for NOHMs and hard spheres by calculating $K_{\eta_0}(\phi_b) = \frac{\eta_0 - \eta'_\infty}{\eta_s \phi_b^2}$, which is the coefficient of the $O(\phi_b^2)$ term in the relative viscosity. This quantity provides a measure of the thermodynamic effect because the hydrodynamic η'_∞ is excluded. As can be seen from Fig. 7.5, while for higher core volume fraction the hard-sphere interactions dominate the thermodynamic integral such that NOHMs are similar to hard spheres, as ϕ_b decreases the entropic penalty for the oligomers comes into play and the thermodynamic contributions for NOHMs

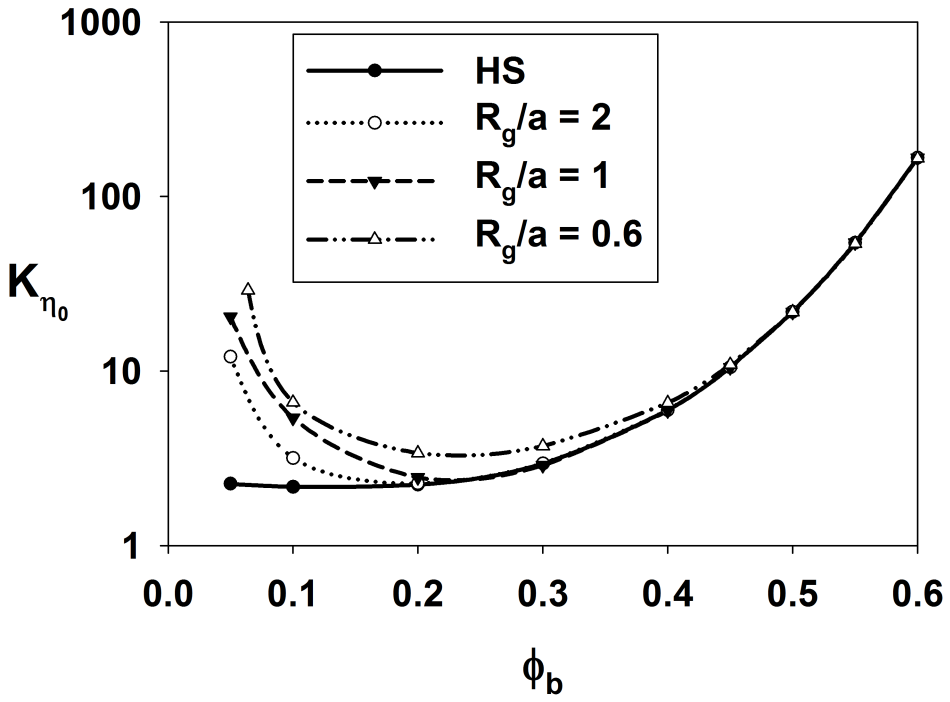

Figure 7.5: Comparison of the $O(\phi_b^2)$ coefficient of the dimensionless steady low shear viscosity η_0/η_s for NOHMs with different R_g/a and hard spheres as a function of ϕ_b.

could be one order of magnitude higher than the reference hard sphere suspension. Therefore, as the strong interparticle forces contribute to the divergence of η_0 as $\phi_b \rightarrow \phi_{b,m}$ for typical hard spheres in a solvent, the unique entropic forces from the tethered oligomeric fluid in NOHMs yield a different mechanism responsible for the increase in the viscous response at lower ϕ_b.

At finite oscillatory frequency ω, the scaled complex viscosity $(\eta' - i\eta'')$ provides us with the information of the dynamic response. As shown in Fig. 7.6 at a given ϕ_b, compared with the hard spheres, the scaled η' and η'' are shifted to lower frequencies for NOHMs with $R_g/a > 1$ but to higher frequencies for NOHMs with $R_g/a < 1$. If we examine Eqs. 7.18 and 7.19 carefully, we find

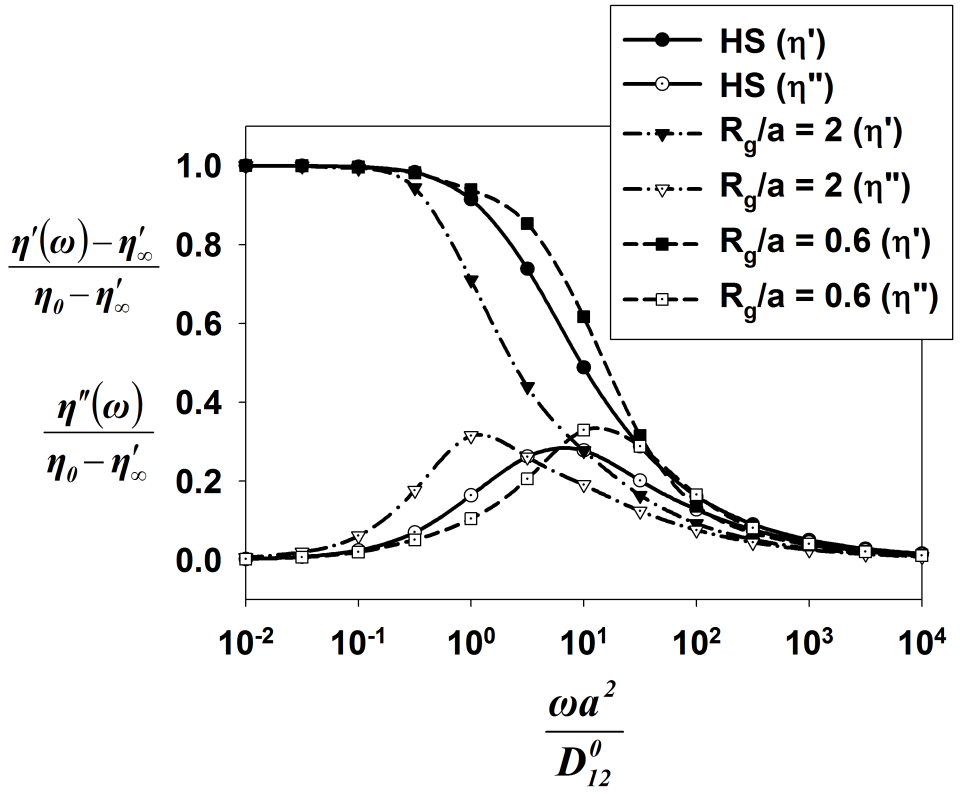

Figure 7.6: Comparison of the scaled complex viscosity ($\frac{\eta'(\omega)-\eta'_\infty}{\eta_0-\eta'_\infty}$ and $\frac{\eta''(\omega)}{\eta_0-\eta'_\infty}$) for NOHMs with different R_g/a and hard spheres at $\phi_b = 0.1$.

that in $O(\phi_b^2)$ contributions the second term resulting from the contact value of the distribution function is more important than the first force integral term when the system is close to hard spheres. In the specific case we present here, NOHMs with longer tethered oligomers are closer to hard sphere suspensions with smaller values of $g(2)f_1(2,\omega)$ and $g(2)f_2(2,\omega)$ than hard spheres, therefore these systems have weaker thermodynamic forces to restore back to the unperturbed equilibrium structure and exhibit a slower relaxation process. Conversely, NOHMs with stiffer chains have comparable contributions from both terms due to stronger many-body interactions at $s > 2$. Therefore the more substantial thermodynamic restoration forces lead to a smaller relaxation time as

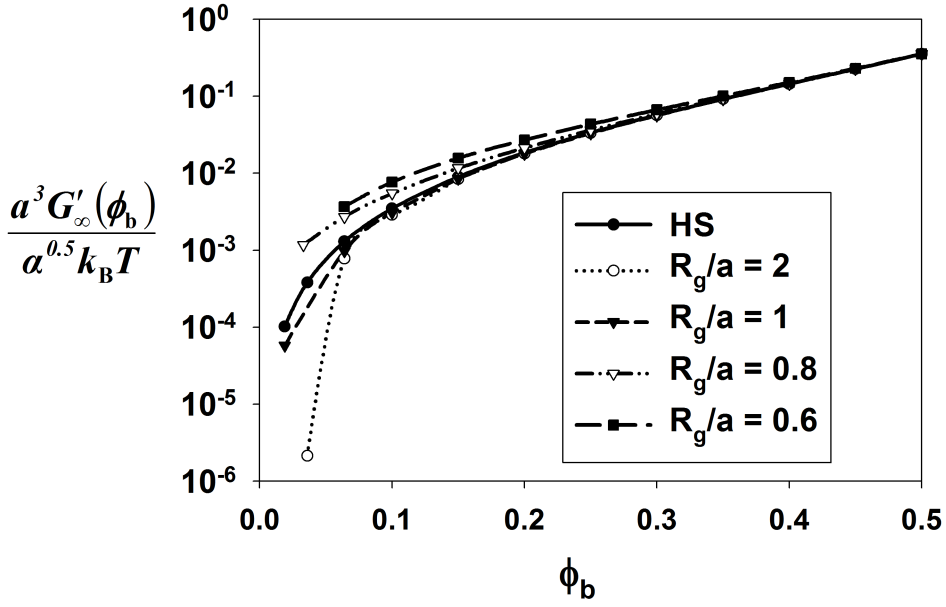

Figure 7.7: The reduced infinite frequency shear modulus $\frac{a^3 G'_\infty}{\alpha^{0.5} k_B T}$ for NOHMs with different R_g/a and hard spheres as a function of ϕ_b.

R_g/a is small. In fact, experimental observations show that NOHMs have much longer relaxation times than hard spheres [3]. It is expected that if the approximation of $R_g \gg a$ is relaxed then more strongly interacting particles would lead to slower dynamics than our current predictions.

Finally, since G' grows as $\omega^{1/2}$ at high frequency, we compare the reduced shear modulus $\frac{a^3 G'_\infty}{\alpha^{0.5} k_B T}$ of NOHMs with hard spheres in Fig. 7.7. From Eq. 7.28, when the dimensionless frequency α is high $\frac{a^3 G'_\infty}{\alpha^{0.5} k_B T} \rightarrow \frac{3\sqrt{2}}{5\pi} \phi_b^2 g(2)$, therefore the reduced shear modulus at high frequency provides us with the contact value of the core radial distribution function. Consequently, for a given chain length the reduced shear modulus increases with the core volume fraction; for a given core volume fraction, compared with hard spheres, NOHMs with $R_g/a > 1$ yields lower modulus while NOHMs with $R_g/a < 1$ exhibits higher modulus.

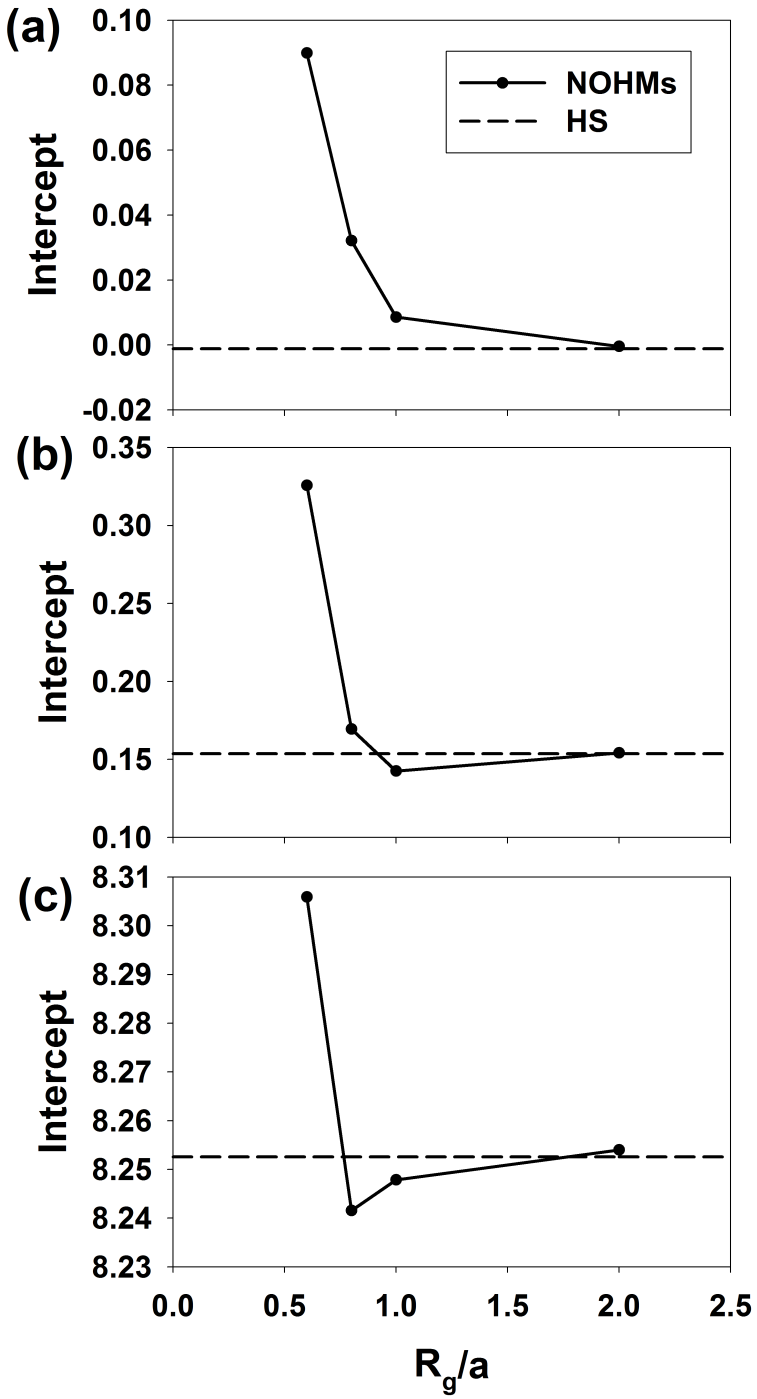

Figure 7.8: (a) The intercept of the straight line of the infinite frequency shear modulus derived in Eq. 7.28 for NOHMs and hard spheres as a function of R_g/a at $\phi_b = 0.1$, (b) $\phi_b = 0.3$, and (c) $\phi_b = 0.5$. The line descriptions for (b) and (c) are the same as (a).

While the slope or growing rate of G'_∞ with respect to $\alpha^{1/2}$ tells us the information of $g(2)$, the intercept may help us understand the importance of many-body interactions. We compare the intercept from Eq. 7.28 for NOHMs and hard spheres in Fig. 7.8. In general, the NOHMs system with a given chain length and the reference hard sphere suspension both show stronger many-body interactions at higher core volume fraction, as characterized by more structured pair probability. For a given core volume fraction, NOHMs with shorter chains also lead to more substantial many-body forces because the oligomers have to cooperate to fill the space and the more stretched stiffer chains result in stronger correlations between the particles. Interestingly, when the interparticle spacing is roughly $2R_g$ at higher ϕ_b, which corresponds to the minimum of $\eta_{0,\mathrm{NOHMs}}/\eta_{0,\mathrm{HS}}$ in Fig. 7.4, we obtain weaker many-body interactions for NOHMs than hard spheres. This observation implies that when the particles are more evenly spaced by the tethered soft shell, the fluidity of the oligomers reduces the direct core–core interactions.

7.5 Conclusions

We have solved for the non-equilibrium pair probability density function for pairs of NOHMs particles subjected to a weak applied force, Brownian forces, and a mean interparticle force obtained from the equilibrium density-functional theory valid in the limit of $R_g/a \gg 1$ in the absence of hydrodynamic interactions. The long-time self-diffusivity is derived when the applied force on a chosen tracer particle is the thermodynamic force while the linear viscoelastic properties are obtained when the small amplitude oscillatory shear is applied to the system. The results demonstrate that the transport properties of solvent-

free NOHMs are governed by the requirement that the tethered oligomeric hairs must fill the interstices. Therefore in general these materials show less resistivity for particle motion when the longer oligomers can more easily fill the interstitial space facilitating relaxation of the cores, a trend which is confirmed by experiments [3] and MD simulations [29].

In the absence of hydrodynamic interactions, the discontinuity of the hard-core potential at two particle contact leads to a shear modulus that diverges as $\omega^{1/2}$ at high applied oscillatory frequency with the growing rate being determined by the core radial distribution function at the closest particle contact. The intercept obtained from extrapolating the linear function of $\omega^{1/2}$ to zero frequency is a function of interparticle forces and particle distribution in the suspension. While our treatment only considers the equilibrium potential of mean force and neglects the coupling effects due to the perturbed force from the third particles, the derivation for G'_∞ is general. Therefore, it is expected that the information regarding the appropriate closure for non-equilibrium many-body interactions can be gained from experimental measurements by comparing the slope and the intercept of the straight line of $G'_\infty = A\omega^{1/2} + B$ at the high frequency limit.

Although the weak field approximation applied in this work captures many of the essential physics of the dynamics of solvent-free nanoparticle suspensions with tethered fluid, it fails to predict the very slow relaxation times observed in experiment. Therefore, a more complete theory that gives a more explicit treatment of the interactions of oligomers of neighboring particles or Brownian Dynamics (BD) simulations that do not rely on the weak field approximation would be desirable.

Since the transport properties are governed by the potential of mean force among the cores, it is anticipated that as another fluid species is present and produces more density fluctuations in the system the weakened interparticle potential will directly decrease the viscosity of the materials. This characteristic might be advantageous to gas absorption such as carbon capture where the fluidity of the system plays an important role in the process.

BIBLIOGRAPHY

[1] A. B. Bourlinos, E. P. Giannelis, Q. Zhang, L. A. Archer, G. Floudas, and G. Fytas, Eur. Phys. J. E **20**, 109 (2006).

[2] R. Rodriguez, R. Herrera, L. A. Archer, and E. P. Giannelis, Adv. Mater. **20**, 4353 (2008).

[3] P. Agarwal, H. Qi, and L. A. Archer, Nano Lett. **10**, 111 (2010).

[4] J. L. Nugent, S. S. Moganty, and L. A. Archer, Adv. Mater. **22**, 3677 (2010).

[5] H.-Y. Yu and D. L. Koch, Langmuir **26**, 16801 (2010).

[6] A. Chremos, A. Z. Panagiotopoulos, H.-Y. Yu, and D. L. Koch, J. Chem. Phys. **135**, 114901 (2011).

[7] G. K. Batchelor, J. Fluid Mech. **74**, 1 (1976).

[8] G. K. Batchelor, J. Fluid Mech. **83**, 97 (1977).

[9] J. P. Boon and S. Yip, *Molecular Hydrodynamics*, McGraw-Hill, New York, 1980.

[10] J.-P. Hansen and I. R. McDonald, *Theory of Simple Liquids*, Academic Press, London, 3 edition, 2006.

[11] R. Verberg, I. M. de Schepper, and E. G. D. Cohen, Phys. Rev. E **55**, 3143 (1997).

[12] E. G. D. Cohen, R. Verberg, and I. M. de Schepper, Physica A **251**, 251 (1998).

[13] R. Verberg, I. M. de Schepper, and E. G. D. Cohen, Phys. Rev. E **61**, 2967 (2000).

[14] N. J. Wagner and W. B. Russel, Physica A **155**, 475 (1989).

[15] R. A. Lionberger and W. B. Russel, J. Chem. Phys. **106**, 402 (1997).

[16] W. B. Russel and A. P. Gast, J. Chem. Phys. **84**, 1815 (1986).

[17] G. K. Batchelor, J. Fluid Mech. **131**, 155 (1983).

[18] H. N. W. Lekkerkerker and J. K. G. Dhont, J. Chem. Phys. **80**, 5790 (1984).

[19] D. A. McQuarrie, *Statistical Mechanics*, University Science Books, Sausalito, 2000.

[20] J. F. Brady, J. Chem. Phys. **99**, 567 (1993).

[21] R. A. Lionberger and W. B. Russel, J. Rheol. **38**, 1885 (1994).

[22] R. A. Lionberger and W. B. Russel, J. Rheol. **41**, 399 (1997).

[23] J. C. van der Werff, C. G. de Kruif, C. Blom, and J. Mellema, Phys. Rev. A **39**, 795 (1989).

[24] T. G. Mason and D. A. Weitz, Phys. Rev. Lett. **75**, 2770 (1995).

[25] G. Fritz, B. J. Maranzano, N. J. Wagner, and N. Willenbacher, J. Non-Newtonian Fluid Mech. **102**, 149 (2002).

[26] D. M. Heyes and P. J. Mitchell, J. Chem. Soc. Faraday Trans. **90**, 1931 (1994).

[27] I. M. de Schepper, H. E. Smorenburg, and E. G. D. Cohen, Phys. Rev. Lett. **70**, 2178 (1993).

[28] J. F. Brady, J. Fluid Mech. **272**, 109 (1994).

[29] S. Goyal and F. A. Escobedo, J. Chem. Phys. **135**, 184902 (2011).